AGU ADVANCING EARTH AND SPACE SCIENCES

Reviews of Geophysics

REVIEW ARTICLE
10.1029/2024RG000843

The El Niño Southern Oscillation (ENSO) Recharge Oscillator Conceptual Model: Achievements and Future Prospects

J. Vialard[1], F.-F. Jin[2,3], M. J. McPhaden[4], A. Fedorov[1,5], W. Cai[6,7,8,9], S.-I. An[10], D. Dommenget[11], X. Fang[12], M. F. Stuecker[3,13], C. Wang[14], A. Wittenberg[15], S. Zhao[2], F. Liu[1], S.-K. Kim[16], Y. Planton[17], T. Geng[6,7], M. Lengaigne[18], A. Capotondi[19], N. Chen[20], L. Geng[2], S. Hu[21], T. Izumo[22], J.-S. Kug[23], J.-J. Luo[24,25], S. McGregor[11,17], B. Pagli[22], P. Priya[11], S. Stevenson[26], and S. Thual[27]

[1]LOCEAN-IPSL, IRD-CNRS-MNHN-Sorbonne Universités, Paris, France, [2]Department of Atmospheric Sciences, SOEST, University of Hawai'i at Mānoa, Honolulu, HI, USA, [3]International Pacific Research Center (IPRC), SOEST, University of Hawai'i at Mānoa, Honolulu, HI, USA, [4]NOAA/PMEL, Seattle, WA, USA, [5]Department of Earth and Planetary Science, Yale University, New Haven, CT, USA, [6]Physical Oceanography Laboratory/Frontiers Science Center for Deep Ocean Multispheres and Earth System/Sanya Oceanographic Institution, Ocean University of China, Qingdao, China, [7]Laoshan Laboratory, Qingdao, China, [8]State Key Laboratory of Marine Environmental Science and College of Ocean and Earth Sciences, Xiamen University, Xiamen, China, [9]State Key Laboratory of Loess and Quaternary Geology, Institute of Earth Environment, Chinese Academy of Sciences, Xi'an, China, [10]Yonsei University, Seoul, Republic of Korea, [11]ARC Centre of Excellence for Climate Extremes, School of Earth, Atmosphere and Environment, Monash University, Melbourne, VIC, Australia, [12]Department of Atmospheric and Oceanic Sciences, Institute of Atmospheric Sciences, Fudan University, Shanghai, China, [13]Department of Oceanography, School of Ocean and Earth Science and Technology (SOEST), University of Hawai'i at Mānoa, Honolulu, HI, USA, [14]State Key Laboratory of Tropical Oceanography, South China Sea Institute of Oceanology, Chinese Academy of Sciences, Guangzhou, China, [15]NOAA Geophysical Fluid Dynamics Laboratory, Princeton, NJ, USA, [16]Irreversible Climate Change Research Center, Yonsei University, Seoul, Republic of Korea, [17]School of Earth Atmosphere and Environment, Monash University, Clayton, VIC, Australia, [18]MARBEC, CNRS, IFREMER, IRD, University of Montpellier, Sète, France, [19]NOAA Physical Sciences Laboratory, University of Colorado Cooperative Institute for Research in Environmental Sciences, Boulder, CO, USA, [20]Department of Mathematics, University of Wisconsin-Madison, Madison, WI, USA, [21]Division of Earth and Climate Sciences, Nicholas School of the Environment, Duke University, Durham, NC, USA, [22]UMR 241 SECOPOL (ex-EIO), IRD-IFREMER-ILM, Université de la Polynésie Française, Tahiti, French Polynesia, [23]School of Earth and Environmental Sciences, Seoul National University, Seoul, Republic of Korea, [24]Institute for Climate and Application Research (ICAR), Nanjing University of Information Science and Technology, Nanjing, China, [25]SKLLQG, Institute of Earth Environment, Chinese Academy of Sciences, Xi'an, China, [26]Bren School of Environmental Sciences and Management, University of California at Santa Barbara, Santa Barbara, CA, USA, [27]Mercator Ocean International, Toulouse, France

Abstract The recharge oscillator (RO) is a simple mathematical model of the El Niño Southern Oscillation (ENSO). In its original form, it is based on two ordinary differential equations that describe the evolution of equatorial Pacific sea surface temperature and oceanic heat content. These equations make use of physical principles that operate in nature: (a) the air-sea interaction loop known as the Bjerknes feedback, (b) a delayed oceanic feedback arising from the slow oceanic response to winds within the equatorial band, (c) state-dependent stochastic forcing from fast wind variations known as westerly wind bursts (WWBs), and (d) nonlinearities such as those related to deep atmospheric convection and oceanic advection. These elements can be combined at different levels of RO complexity. The RO reproduces ENSO key properties in observations and climate models: its amplitude, dominant timescale, seasonality, and warm/cold phases amplitude asymmetry. We discuss the RO in the context of timely research questions. First, the RO can be extended to account for ENSO pattern diversity (with events that either peak in the central or eastern Pacific). Second, the core RO hypothesis that ENSO is governed by tropical Pacific dynamics is discussed from the perspective of influences from other basins. Finally, we discuss the RO relevance for studying ENSO response to climate change, and underline that accounting for ENSO diversity, nonlinearities, and better links of RO parameters to the long term mean state are important research avenues. We end by proposing important RO-based research problems.

Plain Language Summary The El Niño Southern Oscillation (ENSO) is the main driver of Earth's year-to-year climate variations. ENSO arises from air-sea interactions in the tropical Pacific, but influences climate and societies globally. In recent decades, progress in the observing system and in numerical modeling

Key Points:

- The recharge oscillator (RO) simple mathematical model explains most of El Niño Southern Oscillation (ENSO) key properties
- The RO can be extended to account for ENSO pattern diversity (some events peak in the central, others in the eastern equatorial Pacific)
- We propose research avenues for using the RO to address the influence of climate change and other climate modes on ENSO

Correspondence to:
J. Vialard,
jerome.vialard@ird.fr

Citation:
Vialard, J., Jin, F.-F., McPhaden, M. J., Fedorov, A., Cai, W., An, S.-I., et al. (2025). The El Niño Southern Oscillation (ENSO) recharge oscillator conceptual model: Achievements and future prospects. *Reviews of Geophysics*, *63*, e2024RG000843. https://doi.org/10.1029/2024RG000843

Received 24 JUL 2024
Accepted 27 FEB 2025

Author Contributions:
Data curation: S. Zhao, F. Liu, Y. Planton, T. Geng
Formal analysis: S.-K. Kim
Supervision: J. Vialard
Visualization: S. Zhao, F. Liu, M. Lengaigne
Writing – original draft: J. Vialard, M. J. McPhaden, A. Fedorov, S.-I. An, D. Dommenget, X. Fang, M. F. Stuecker, C. Wang, A. Wittenberg
Writing – review & editing: J. Vialard, F.-F. Jin, M. J. McPhaden, A. Fedorov, W. Cai, S.-I. An, D. Dommenget, X. Fang, M. F. Stuecker, C. Wang, A. Wittenberg, S. Zhao, F. Liu, S.-K. Kim, M. Lengaigne, A. Capotondi, N. Chen, L. Geng, J.-S. Kug, J.-J. Luo, B. Pagli, P. Priya, S. Stevenson, S. Thual

yielded a better understanding of the physical processes that govern ENSO. Such understanding can be encapsulated in the recharge oscillator (RO) *conceptual model*, a simple mathematical representation of ENSO fundamental mechanisms, which accounts for ENSO's essential properties: its amplitude, dominant period, tendency to peak at the end of the year, and tendency for larger warm (El Niño) than cold (La Niña) events. We discuss this framework and propose how to adapt it to explore pressing research topics. First, recent research indicates that the RO can be extended to account for the ENSO diverse spatial patterns of ENSO variability, with anomaly centers in either the central or eastern Pacific. Second, we discuss RO applications for studying influences of regions outside the tropical Pacific on ENSO. Finally, we discuss the RO as a tool to understand the ENSO response to climate change. We conclude by compiling important problems related to these challenging topics.

1. Introduction

Why ENSO matters. The El Niño/Southern Oscillation (ENSO) drives the largest fraction of Earth's year-to-year climate variations (Trenberth, 2020). ENSO emerges from the interplay between oceanic and atmospheric dynamics in the tropical Pacific, as originally outlined by Bjerknes (1966, 1969). Teleconnections through the atmosphere transmit ENSO's influences globally (Taschetto et al., 2020). ENSO therefore affects global temperature extremes, droughts and floods, tropical cyclones, marine and terrestrial ecosystems, fisheries, and agriculture. These changes have worldwide societal, economic, and environmental impacts (McPhaden et al., 2006).

Three decades of progress. The far-reaching impacts of ENSO have spurred advances in observing, modeling, and understanding the phenomenon over the past decades. A basin-scale tropical Pacific observing system was initiated in the mid 1980s and completed in the early 1990s (McPhaden et al., 1998; McPhaden, Lee, et al., 2020). Coupled General Circulation Models (CGCMs) now reproduce many aspects of observed ENSO dynamics (Guilyardi et al., 2020), allowing skillful dynamical forecasts up to 1 year ahead (L'Heureux et al., 2020). Such advances have improved the understanding of many aspects of ENSO's complexity (Timmermann et al., 2018), including the discovery that ENSO's seasonal-to-interannual basin-scale dynamics are low-dimensional, that is, they can be usefully characterized using a limited number of parameters. This explains why relatively simple mathematical (or conceptual) models can account both qualitatively and quantitatively for key ENSO properties (see reviews by Neelin et al. (1998), C. Wang (2018), and Jin et al. (2020)).

Challenges and timeliness. Despite this progress, important questions have yet to be addressed. As our planet warms, there is a pressing need to anticipate potential changes in ENSO behavior in a warming world. Early model simulations and projections of the impacts of anthropogenic warming on ENSO yielded diverse outcomes (C. Chen et al., 2017; Collins et al., 2010; Vecchi & Wittenberg, 2010). Subsequent analyses, using refined models capable of replicating the most intense El Niño events, suggest recent (Cai et al., 2023) and future (Cai et al., 2021) increases in the occurrence of extreme ENSO events, with future warm events having a more rapid onset and longer duration (Lopez et al., 2022). Yet, climate model ENSO projections are uncertain (Heede & Fedorov, 2023b; Maher et al., 2022), as they are still impaired by long-standing systematic biases, such as an eastern equatorial Pacific cold tongue that is too cold and extends too far west (Bellenger et al., 2014). Such biases limit the ability of these models to represent key ENSO dynamics (Bayr et al., 2019), and extreme El Niño events (Bayr et al., 2024). Quantitative tools linking the mean state of the tropical Pacific to ENSO characteristics would enhance our understanding of the impacts of model biases and climate change on ENSO. Conceptual models of ENSO can provide such tools.

Brief review of conceptual models. Intermediate coupled models (e.g., Zebiak & Cane, 1987) played an essential role in understanding the ENSO basic dynamics, as reviewed by McCreary and Anderson (1991). This understanding was later encapsulated in simple conceptual models developed in the late 1980s and 1990s. All of these models incorporate the positive feedback proposed by Bjerknes (1966, 1969), wherein equatorial Pacific sea surface temperature (SST) anomalies trigger fast atmospheric and oceanic responses that serve to intensify those SST anomalies over the following months. These models differ, however, in their representation of the delayed negative feedbacks that terminate ENSO events, and can induce transitions between the warm and cold phases of ENSO. The *delayed oscillator* (Battisti & Hirst, 1989; Suarez & Schopf, 1988) emphasizes reflections of

westward-moving near-equatorial oceanic Rossby waves (Equatorial waves are a class of planetary scale wave motions that affect ocean circulation and thermocline depth variations within a few degrees of the equator, and play an important role in understanding ENSO dynamics.) into eastward-moving equatorial Kelvin waves at the western boundary of the Pacific, and the delayed effect of these reflected waves on reversing the temperature anomaly of water that is upwelled into the surface layer of the eastern equatorial Pacific. The seminal work of Wyrtki (1985) and Cane and Zebiak (1985) suggested an important role for the western tropical Pacific subsurface heat content in ENSO phase transitions. Building on that, Jin (1996, 1997a, 1997b) proposed the *recharge oscillator* (hereafter RO), which summarizes the time-integrated effects of the subsurface Kelvin and Rossby wave adjustments as a poleward "discharge" or equatorward "recharge" of subsurface heat content, which then affects the cold tongue SST via vertical and zonal advection. The *advective-reflective oscillator* (Picaut et al., 1997) emphasizes reflections of eastward-moving equatorial Kelvin waves into westward-moving off-equatorial Rossby waves at the eastern boundary, and their effects on near-surface zonal currents in the equatorial central Pacific. The *western Pacific oscillator* (C. Wang et al., 1999; Weisberg & Wang, 1997) highlights the role of wind-forced (rather than reflected) equatorial Kelvin waves in the western Pacific in providing a delayed negative feedback. A unified oscillator incorporating all four of these delayed negative feedbacks was proposed by C. Wang (2001). A formal derivation of the RO, expanding the shallow-water equations in terms of the (small) ratio of the Kelvin wave basin-crossing time to the ENSO period and based on a corresponding integro-differential equation, is provided by Fedorov (2010).

Focus on the RO. In this synthesis, we concentrate on the RO for several reasons. First, it explicitly represents oceanic heat content variations, and captures their observed predictive power of ENSO more than 1 year ahead (e.g., Meinen & McPhaden, 2000). The RO's simple equation also implicitly accounts for oceanic wave reflections that play an important role in both the delayed, and advective-reflective oscillators. The RO has been extended to explicitly include several key ENSO processes (such as nonlinearities, or a representation of random forcing from atmospheric synoptic variability; Jin & An, 1999; Jin et al., 2020), and can quantitatively account for ENSO properties in observations and simulations, as we will showcase in this review. Over the years, the RO has become the leading and simplest unifying conceptual framework to understand ENSO behavior in models and observations.

Purpose. The details of the RO model, and a verification of its core hypotheses, were reviewed by Jin et al. (2020). Here, we remind ENSO basics (Section 2), survey the RO ability to encapsulate ENSO mechanisms (Section 3) and emulate its key properties (Section 4). Based on a detailed literature review, we further discuss desirable RO extensions that are motivated by pressing research questions (Section 5). Section 6 synthesizes this review. Section 7 discusses future RO applications in the form of nine important research questions.

2. ENSO in Observations and Models

2.1. Observed Tropical Pacific Background Climatology

Walker Cell. ENSO variations are conditioned by the background state on which they develop. So, to understand ENSO, we first need to define what we consider to be "normal" in the tropical Pacific (words in italics below refer to Figure 1 sketch). Due to the effect of SST on atmospheric stability (Neelin & Held, 1987), deep atmospheric convection (towering cumulus clouds with heavy precipitation) only occurs above an SST threshold of ∼1°C above the tropical-mean SST (Izumo et al., 2020; Johnson & Xie, 2010), or about 26–28°C over recent decades (Gadgil et al., 1984; Graham & Barnett, 1987). The western equatorial Pacific *warm pool* is climatologically warm (>28°C, Figure 2a), giving rise to ascending motions, deep convection and mid-tropospheric latent heat release. The eastern equatorial *cold tongue* is below the convective threshold (∼24°C, Figures 1 and 2a), leading to subsidence and low clouds that lose heat to space. The easterly low-level *trade winds* (Figure 2a) connect the subsident region in the east to ascending motions in the west, with a westerly return flow in the upper troposphere. This atmospheric circulation cell on the equatorial plane is referred to as the *Walker Cell*, after Sir Gilbert Walker, the early twentieth century meteorologist who discovered the atmospheric signature of ENSO known as the Southern Oscillation (Walker, 1924).

Warm pool and cold tongue. The low level *trade winds* apply a westward force on the upper ocean. As a result, sea level rises in the western Pacific and falls in the eastern Pacific to create a counterbalancing zonal pressure gradient force. Changes in sea level are mirrored in the interior ocean by changes in the depth of the *thermocline*, that is, the sharp vertical temperature gradient that separates the warm surface layer from the cold ocean interior.

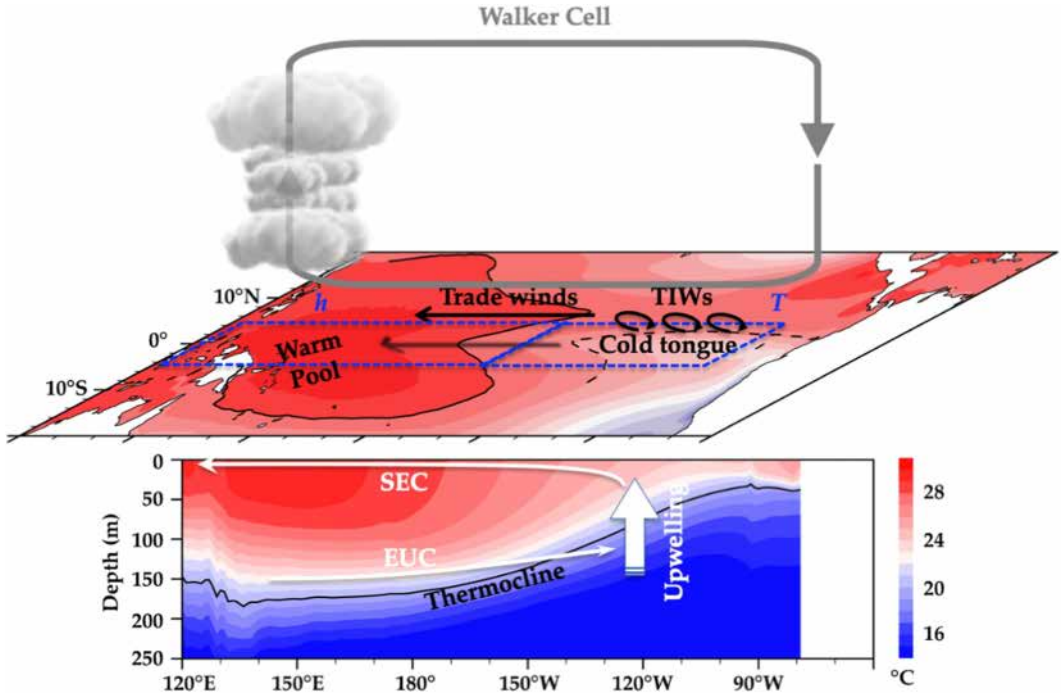

Figure 1. The tropical Pacific mean state. Sketch of the equatorial Pacific "normal" state, over which anomalies associated with ENSO develop. The shading indicates the climatological Sea Surface Temperature (SST) and temperature vertical structure along the equator (ORAS5 data, Zuo et al., 2019; 1958–2020 September–November average). Trade winds are the surface branch of the equatorial plane atmospheric circulation cell known as the Walker cell, and energized by SST contrasts between the eastern Pacific (cold tongue) and western Pacific (Warm pool). The easterly trade winds in return drive upwelling and the cold tongue in the east. The positive feedback loop between the equatorial SST and trade winds is known as the Bjerknes feedback. The dashed lines delineate the western and central Pacific (5°N–5°S, 120°E−150°W) and Niño3 (5°N–5°S, 150°–90°W) averaging regions that are usually used for defining the equatorial Pacific heat content h and surface temperature T variables used in the recharge oscillator, although some other choices (such as the average heat content in the entire equatorial Pacific or the 5°N–5°S, 170°–120°W Niño3.4 region) are sometimes made. The approximate locations for the western Pacific Warm Pool, Eastern equatorial Pacific Cold Tongue and upwelling, region where Tropical Instability Waves (TIWs) occur, thermocline (here the 20°C isotherm), South Equatorial Current (SEC) and Equatorial Undercurrent (EUC) are marked on the Figure. See Section 2.1 for more details on the other elements on this figure.

Thermocline therefore becomes shallower in the east and deepens in the west (Figure 1 vertical section). The deep thermocline in the west results in a subdued cooling of the ocean surface by vertical mixing. The resulting deep warm surface layer is referred to as the western Pacific *warm pool*. Due to the Coriolis force, the easterly trade winds straddling the equator in the eastern Pacific induce poleward-moving surface currents in each hemisphere, which produce a near-equatorial surface divergence that promotes *upwelling* (ascending motion in the upper ocean) to feed that divergence. The shallow thermocline in the eastern Pacific facilitates mixing of upwelled cold thermocline water into the surface layer. This process leads to an SST *cold tongue* that extends from the west coast of South America out to the International Date Line (Figure 1).

Bjerknes feedback. SST contrasts between the cold tongue and warm pool therefore sustain the Walker cell and trade winds, which themselves drive an ocean response that cools the ocean in the east. This positive feedback loop is referred to as the Bjerknes feedback, after Jacob Bjerknes, the Norwegian meteorologist who first described El Niño as a coupled ocean-atmosphere phenomenon (Bjerknes, 1966, 1969). Below, we will see that the Bjerknes feedback is an essential element of ENSO dynamics.

Other important structures. Readers can refer to Trenberth (2020) for a description of other important structures of the tropical Pacific mean state. Here, we only focus on those of relevance for the rest of this review. The westward trade winds drive westward ocean surface flow near the equator in the *South Equatorial Current* (SEC, 20°S–5°N), with a narrow subsurface eastward-flowing current known as the *Equatorial Undercurrent* (EUC, 2°S–2°N) whose core on average slopes upward within the thermocline from ~200 m depth in the west Pacific to

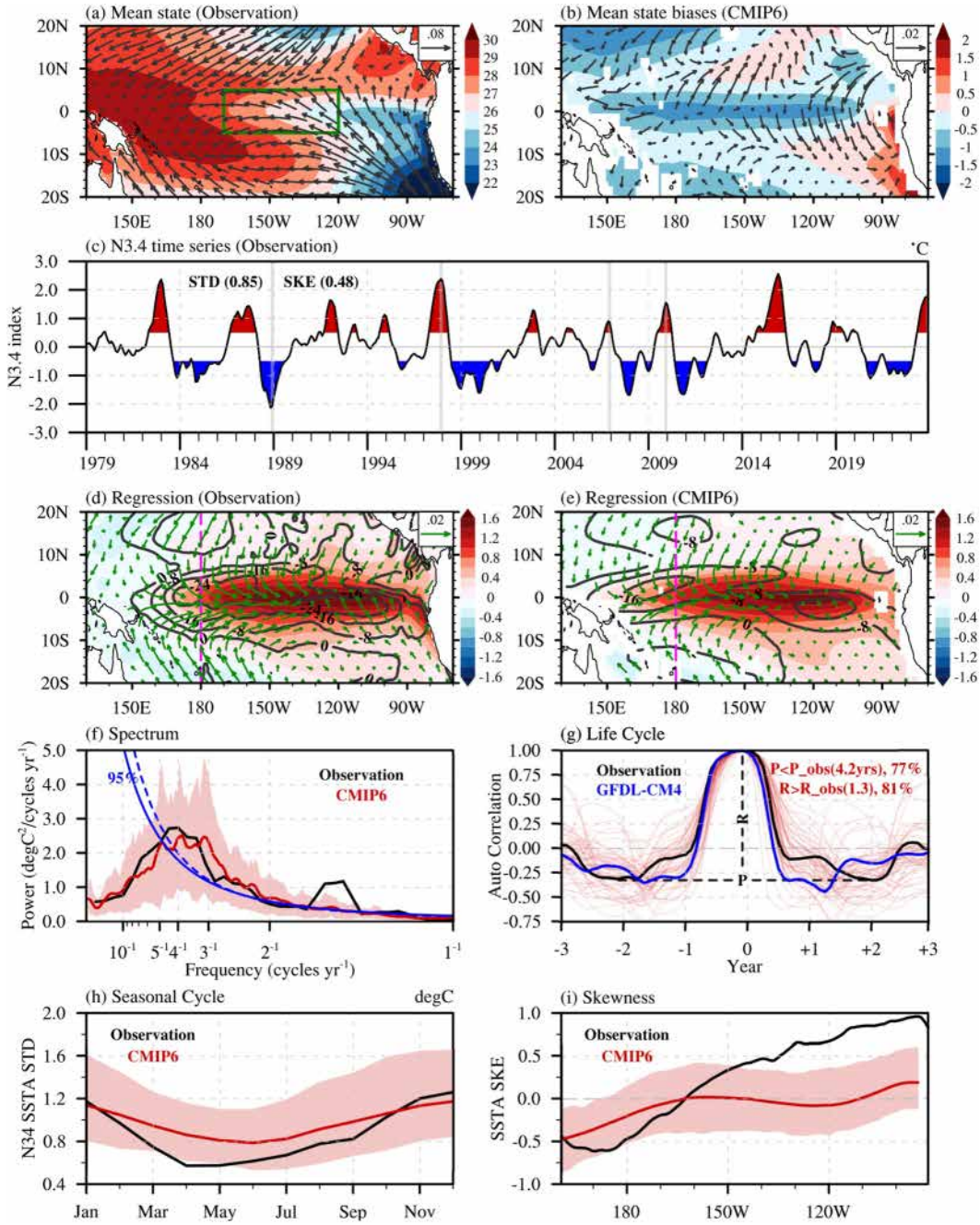

Figure 2. ENSO properties in observations and climate models. (a) Observed SST (shading, °C) and wind stress (vectors, Nm^{-2}) tropical Pacific long-term climatology (1979–2023, HadiSST). (b) Multi model-mean from 57 CMIP6 (Eyring et al., 2016) historical runs minus (a). (c) Times series of observed average Niño3.4 SST anomalies during 1979–2023. (d) Typical ENSO SST (shading, °C), wind stress (Tropflux, vectors, Nm^{-2}) and net heat flux (Tropflux Praveen Kumar et al., 2012, 2013, contours, only negative values, Wm^{-2}) observed spatial pattern (obtained by regressing average November–January (NDJ) anomalies on the normalized NDJ Niño3.4 index). (e) As (d), but for the CMIP6 models ensemble mean. (f) Spectrum of the Niño3.4 indices for observation (black) and CMIP6 models (red with the line indicating the ensemble mean). The dashed and solid blue curves indicate 95% confidence level for observation and CMIP6 models, respectively. (g) ENSO life cycle for observation (black) and CMIP6 models (light red, 1 curve per model), obtained from the lagged auto-correlation of NDJ Niño3.4 index. The dashed lines indicate how the periodicity (P) and regularity (R) metrics are defined for observations following Jiang et al. (2021). P is the time lag of the maximum negative autocorrelation and R is 1 minus the autocorrelation value at this lag. The GFDL-CM4 model (closest model to the median P and R values) is displayed as the blue curve. 81% of the CMIP6 models are more regular, and 77% have a shorter period than observations. (h) Seasonal cycle of Niño3.4 SSTA standard deviation (°C) for observations (black) and CMIP6 models (red). (i) Skewness of 5°S–5°N averaged SST anomalies for observations (black) and CMIP6 models (red). The Niño3.4 region is shown as a green box on (a). The pink lines in panels (d)–(f) indicate the dateline. The light red shadings in panels (f), (h), and (i) denote 10%–90% quartile range for CMIP6.

~70 m in the east. The horizontal shear and density gradients between the cold westward-flowing SEC and the warmer eastward-flowing North Equatorial Countercurrent (NECC, 4°–8°N) further north is dynamically unstable, leading to the formation of eddy-like *tropical instability waves* (*TIWs*; Willett et al., 2006). Those prominent westward-propagating undulations of the SST front at the northern edge of the cold tongue at periods of 20–30 days transport heat from the warm NECC to the cold tongue, and vary at the timescale of ENSO, influencing its heat balance in the near-equatorial region (e.g., An, 2008; Vialard et al., 2001).

2.2. Key Observed ENSO Properties

Amplitude and pattern. Central-eastern Pacific SST (Niño3.4 region, see Figure 2a) displays SST anomalies of up to 2.5°C during El Niño (ENSO warm phase) and −2°C during La Niña (ENSO cold phase, Figure 2c). El Niño events are characterized by a warming and enhanced rainfall over most of the central and eastern equatorial Pacific, as well as westerly wind anomalies over the western Pacific (Figure 2d). The anomalous warming coincides with anomalous surface heat losses to the atmosphere (contours on Figure 2d). It also shifts deep atmospheric convection eastward (westward during cold events), and the associated heat source or sink triggers a planetary-scale atmospheric response that leads to global climatic impacts (e.g., Taschetto et al., 2020).

Timescale and seasonality. The ENSO cycle of warm El Niño and cold La Niña events is irregular (Graham & White, 1988; Vallis, 1986), with a return time of same-polarity events anywhere between one and 7 years. This is further illustrated by the observed spectrum of average Niño3.4 SST anomalies that has a broad peak between roughly 3 and 7 years (Figure 2f) or by the autocorrelation function of Niño3.4 which indicates a dominant periodicity of about 4 years (Figures 2g, Jiang et al., 2021). ENSO events usually start growing in late spring and summer, almost always peak at the end of the calendar year (November through January) and generally terminate in the following spring (Figures 2g and 2h). The system then has a tendency to transition to the opposite phase (see, for example, the warm to cold transitions after the 1982, 1986, 1997, 2010 events, Figure 2c), but can also return to near-neutral conditions (such as after the 2002 El Niño), or stay in the same phase for two or more years (e.g., the 1984–1985, 1998–2000, or 2020–2022 multi-year La Niña events).

Asymmetry. Figure 2c also reveals asymmetries between warm and cold events. El Niño events tend to be stronger than La Niña events (Deser & Wallace, 1987), La Niña events tend to last longer (Ohba & Ueda, 2007), and warm events are more frequently followed by cold events than the opposite (Larkin & Harrison, 2002). As will be seen in Section 4, there are several reasons for this asymmetry but they all involve nonlinearities in the dynamics of ENSO (An, Tziperman, et al., 2020).

Diversity. ENSO exhibits significant diversity in its spatial pattern (e.g., Capotondi et al., 2015, 2020), with sea surface temperature (SST) anomalies peaking in the central Pacific (CP events), eastern Pacific (EP events), or anywhere in between. This diversity is evident in an empirical orthogonal function (EOF) analysis of observed tropical Pacific SST anomalies (Figure 3). The leading EOF mode captures broad central Pacific warming (Figure 3a), while the second mode represents a dipole pattern that modulates the zonal position of the SST maximum (Figure 3b). El Niño events can be classified as either CP-type (e.g., 2009–2010 El Niño, Figure 3g) or EP-type (e.g., the 1997–1998 El Niño, Figure 3d), whereas La Niña events tend to be less variable and predominantly peak in the central Pacific (e.g., 1988–1989, Figure 3e). The relationship between the first and second principal components follows a nonlinear, boomerang-shaped distribution (Figure 3g; Dommenget et al., 2013; Takahashi et al., 2011), indicating that (a) La Niña events (negative PC1, positive PC2) are typically shifted westward relative to El Niño events (Figure 3e) and (b) strong El Niño events (high positive PC1, positive PC2) tend to be EP-type (Figure 3d). Moderate El Niño events such as in 2006–2007, however, do not follow a clearly defined pattern (Figure 3f). There are also notable deviations from this mean relationship. For instance, the 2009–2010 El Niño was a moderate event with a negative PC2 value, making it a clear CP-type event (Figure 3g). Variability in ENSO's spatial pattern, amplitude, and temporal evolution, are collectively referred to as ENSO complexity (Timmermann et al., 2018). In Section 5.1, we review recent studies that reproduce several aspects of ENSO diversity based on the RO framework.

2.3. Observed ENSO Dynamics

Bjerknes feedback. Figure 4a illustrates the trade wind decrease in the western Pacific in response to warm central and eastern Pacific SST anomalies during 1997. Those westerly anomalies excite downwelling equatorially-trapped Kelvin waves which propagate eastward along the equator, crossing the basin in about 45 days

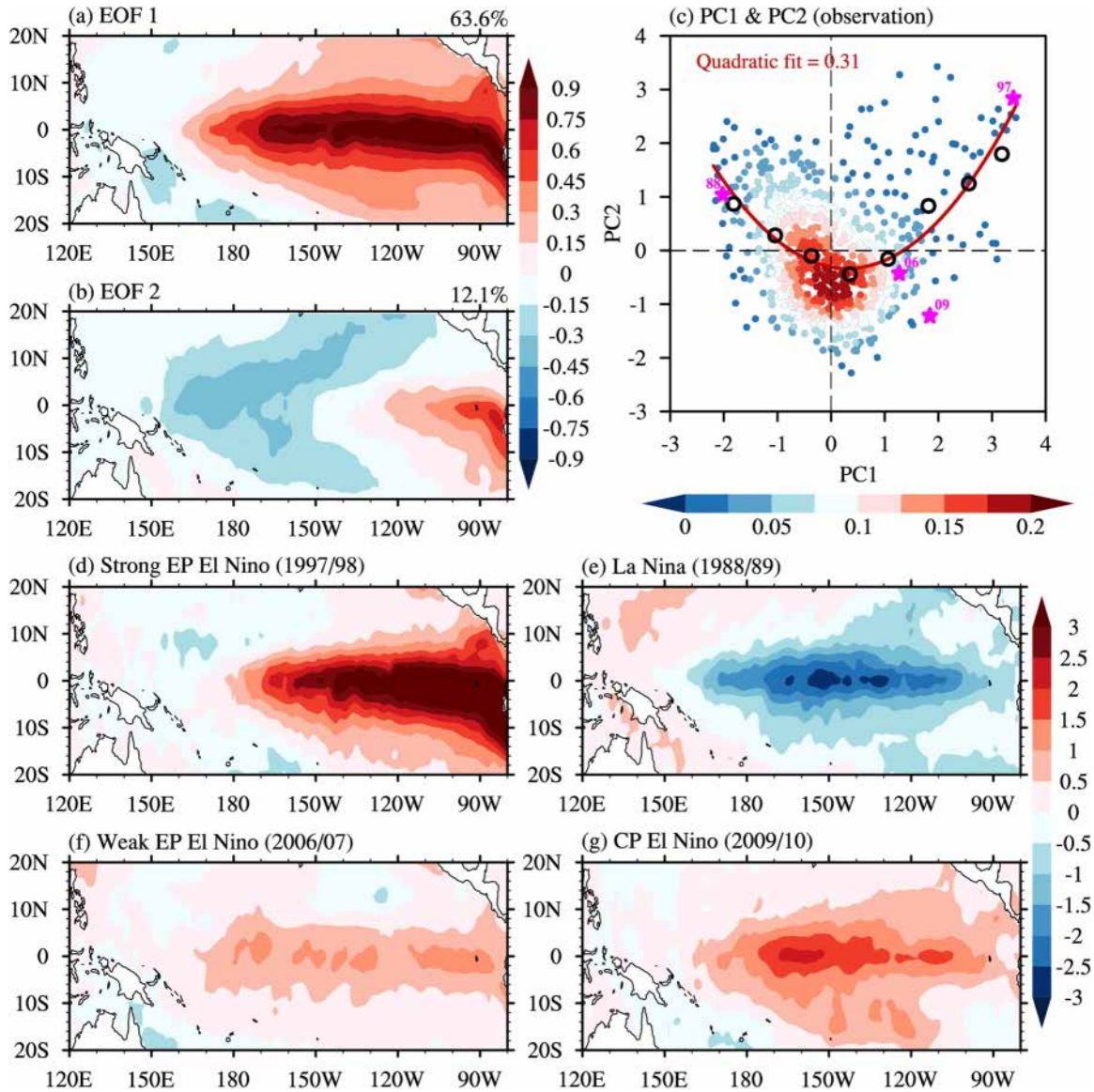

Figure 3. ENSO pattern diversity. Tropical Pacific SST anomalies (HadISST Rayner et al., 2003; 1958–2020, 3-months sliding average) Empirical Orthogonal Functions (EOF) analysis: (a) First and (b) second EOF. The percentage of the total variance explained by each EOF mode is indicated. (c) Scatterplot of the second versus the first normalized principal components (PC1 and PC2, °C). The shading displays a kernel density estimate of the joint PC1, PC2 probability distribution. Circles indicate the PC2 average within 0.75°C PC1 bins, and a quadratic fit to the PC1,PC2 distribution is plotted in red (the quadratic coefficient value is indicated). Purple stars indicate years for which the November–January maps of panels (d)–(g) were plotted. (d)–(g) November to January averages of various years that illustrate the ENSO diversity: (d) 1997–1998 strong EP El Niño, (e) 1988–1989 La Niña, (f) 2006–2007 weak EP El Niño, and (g) 2009–2010 weak CP El Niño event. Note that diversity categories can vary depending on the selected definition.

(Figure 4b). In their wake, they leave eastward current anomalies that push the warm pool edge eastward to the central Pacific, and a depressed thermocline that reduces the upwelling of cool water to the surface in the eastern Pacific cold tongue (Figure 4b). Those two processes warm the cold tongue. The reduced heat gain from the atmosphere (contours on Figure 2d) acts as a thermal damping, but is not sufficient to overcome the effects of ocean dynamics. The cold tongue warming feeds back to the atmosphere, further reducing trade wind strength and allowing El Niño to grow: this is the Bjerknes feedback.

State-dependent WWBs. While there is a clear seasonal envelope of trade winds weakening in the central Pacific, it is punctuated by a series of brief episodes of westerly winds (Figure 4a) lasting a few days to a few weeks, with a zonal span of 1,000–2,000 km. These episodic winds are known as Westerly Wind Events or

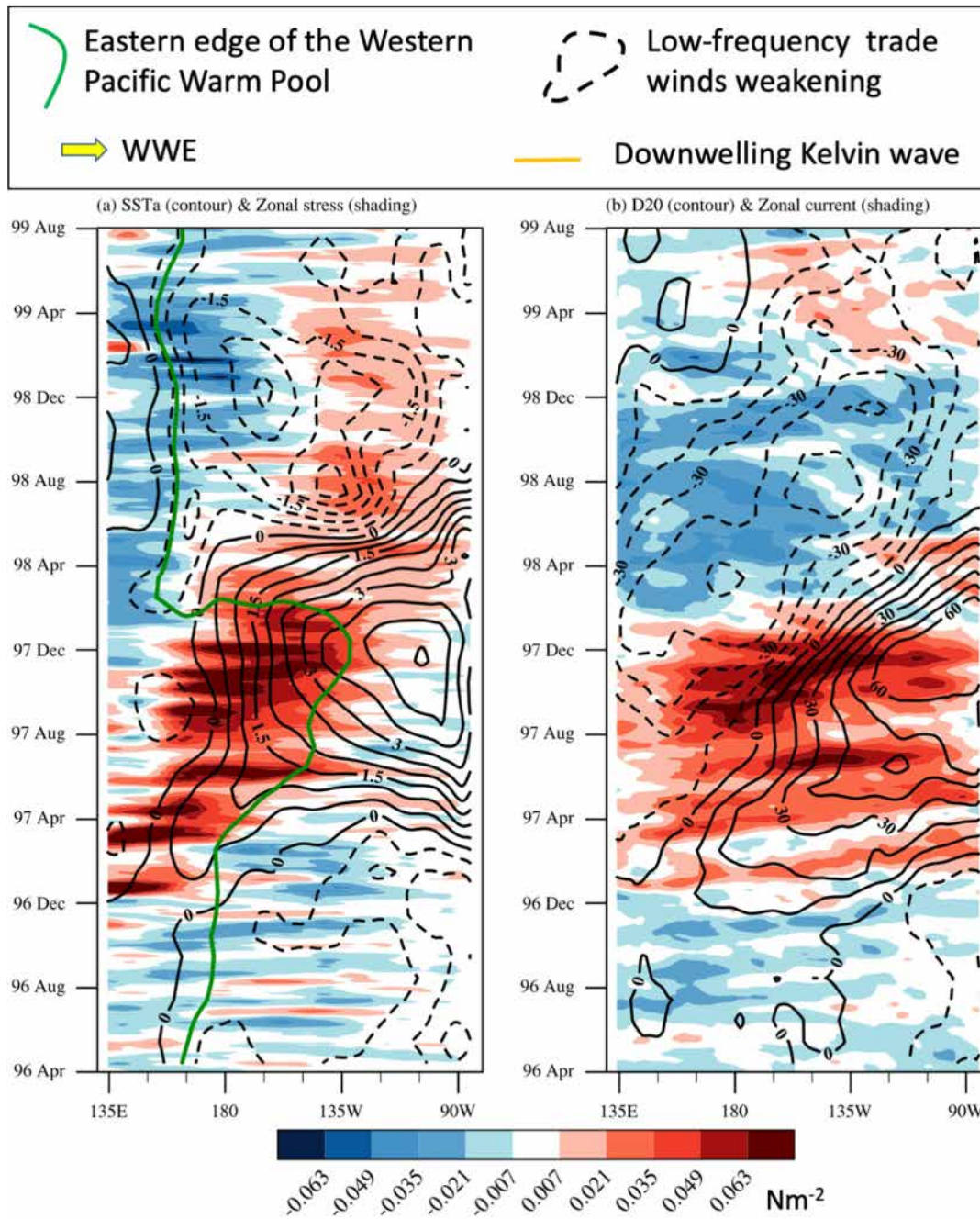

Figure 4. ENSO growth mechanisms, illustrated from the 1997–1998 strong El Niño. Time-longitude sections of 2°S–2°N average anomalous (a) SST (contours, °C) and zonal wind stress (shading, Nm^{-2}), (b) 20°C isotherm depth (D20), a proxy for the equatorial thermocline (contours, m) and 15 m zonal current (shading, ms^{-1}) during the 1997–1998 extreme El Niño event. We use monthly Tropflux (Praveen Kumar et al., 2012, 2013) SST, ORAS5 (Zuo et al., 2019) subsurface temperature, and daily zonal wind stress and Globcurrent (Rio et al., 2014) zonal currents (European Union-Copernicus Marine Service, 2023) anomalies relative to the 1993–2016 climatology. A 3-month (15-day) running filter is applied on SST and D20 (wind stress and current). A 10-degree running average is applied to all fields. The concurrent gradual weakening of the winds, deepening of the thermocline and SST warming during 1997 are manifestations of the Bjerknes feedback.

Bursts (Harrison & Giese, 1991; hereafter WWBs). WWBs are often associated with tropical cyclone formation (Lian et al., 2018; Liang & Fedorov, 2021) and the convective phases of convectively coupled atmospheric Rossby waves and the Madden-Julian Oscillation (Puy et al., 2016). Figure 4 illustrates that December 1996 to March 1997 WWBs played an important role in the development of the 1997–1998 El Niño (McPhaden &

Yu, 1999). WWBs are associated with weather events that are not predictable beyond a couple of weeks, and can be seen as a random forcing at the ENSO timescale, and one of the contributors to ENSO irregularity (An, Kim, & Timmermann, 2020; Harrison & Vecchi, 1997). But while individual WWBs are not predictable, Figure 4a illustrates that they are modulated by ENSO: they can become more frequent and move eastward during warm phases (e.g., Eisenman et al., 2005; Gebbie et al., 2007; Puy et al., 2016). While WWBs occur on a subseasonal time scale and have a strong random component, they provide a critical contribution to the Bjerknes feedback because of their state dependence (S. Yu & Fedorov, 2022).

Tilt and recharge modes. Figure 5 displays an EOF decomposition of interannual thermocline depth anomalies in the tropical Pacific, similar to that in Meinen and McPhaden (2000). The leading mode is associated with a tilt of the equatorial thermocline (Figure 5a), in phase with central Pacific SST anomalies (Figures 5c and 5e). During El Niño, central Pacific wind anomalies force downwelling eastward-propagating Kelvin waves that deepen the eastern Pacific thermocline after about 45 days, and westward-propagating upwelling Rossby waves that lift the thermocline up to the western boundary after about 70 days, that is, almost in phase with SST anomalies at the timescales of ENSO. The second mode is more zonally-uniform in sign (Figure 5b) and is associated with a strong decrease in heat content or discharge during the peak phase of El Niño, and a recharge during the peak phase of La Niña (Figures 5d and 5f). This recharge mode is a consequence of the slower equatorial adjustment (after Kelvin and Rossby waves have had the time to reflect at both boundaries, a time scale of at least 7 months), or equivalently to the poleward Sverdrup transport out of the equatorial band during El Niño, and equatorward transport during La Niña (Jin, 1997a, 1997b). The strong equatorial heat content decline at the end of El Niño and the associated increase in westward currents terminate the zonal and vertical advection anomalies that initiate and drive the event. In many instances the shallowing continues even after the El Niño has ended, producing a large heat content deficit that sets the stage for a follow-on La Niña, as in 1997–1998 (Figure 4b). This slow heat content discharge (it occurs about 8–10 months after the event was initiated) constitutes the delayed negative oceanic dynamical feedback that terminates the event, sometimes inducing a transition to the opposite phase (Clarke, 2014).

Phase transitions are not systematic due to random WWBs. The ∼0.4 correlation coefficient of the recharge mode with the ENSO peak amplitude (Figure 5d) at ∼1 year lead indicates that the western equatorial Pacific oceanic heat content is an ENSO precursor. This was first noted by Wyrtki (1975) and is now used in many statistical forecasts of ENSO since then (e.g., Clarke & Van Gorder, 2003). A buildup of oceanic heat content is however not a sufficient condition for an El Niño to occur, as for instance in 2014 (McPhaden, 2015). This is in part attributable to random differences in WWBs (McPhaden, Santoso, & Cai, 2020; Puy et al., 2019). This stochastic element of wind forcing is hence an important ingredient to encapsulate in an ENSO conceptual model.

2.4. ENSO in Climate Models

Climate models and ENSO. Through explicit representations of oceanic and atmospheric dynamics, and parameterizations of their key physical processes, CGCMs aim to capture the global climate system's rich internal and forced variability, including ENSO. In the 1980s and 1990s, CGCMs were only beginning to crudely simulate ENSO (Delecluse et al., 1998; McPhaden et al., 1998). As the CGCMs' resolutions and parameterizations have improved, their ENSO simulations have become more realistic, with better ENSO amplitudes, spectra, spatio-temporal patterns, seasonal timing, inter-event diversity, physical mechanisms, and global teleconnections (Guilyardi et al., 2020; Planton, Guilyardi, et al., 2021). Some CGCM simulations are now sufficiently realistic to provide close "model-analogs" of observed conditions that, when traced forward in time, yield skillful predictions of ENSO in the real world (Ding et al., 2018). CGCMs can hence be used to generate skillful seasonal forecasts (L'Heureux et al., 2020) and centennial outlooks of ENSO's behavior in a warming world (Cai et al., 2021), and to help understand past ENSO variations, characterize ENSO's internal variability and extremes, and test hypotheses about ENSO.

CMIP6 database. The climate community coordinates multi-model experiments (Model Intercomparison Projects, or MIPs), including future climate projections (ScenarioMIP; O'Neill et al., 2016), which enable much of the research that informs Intergovernmental Panel on Climate Change (IPCC) reports. The most recent coupled ocean-atmosphere MIP is CMIP6 (Eyring et al., 2016). Figure 2 showcases the ability of the CMIP6 historical simulations to reproduce key ENSO features. On average, the CMIP6 models have a reasonable ENSO pattern and amplitude (compare panels d,e), spectrum (compare the red and black spectra on Figure 2f), and tend to peak

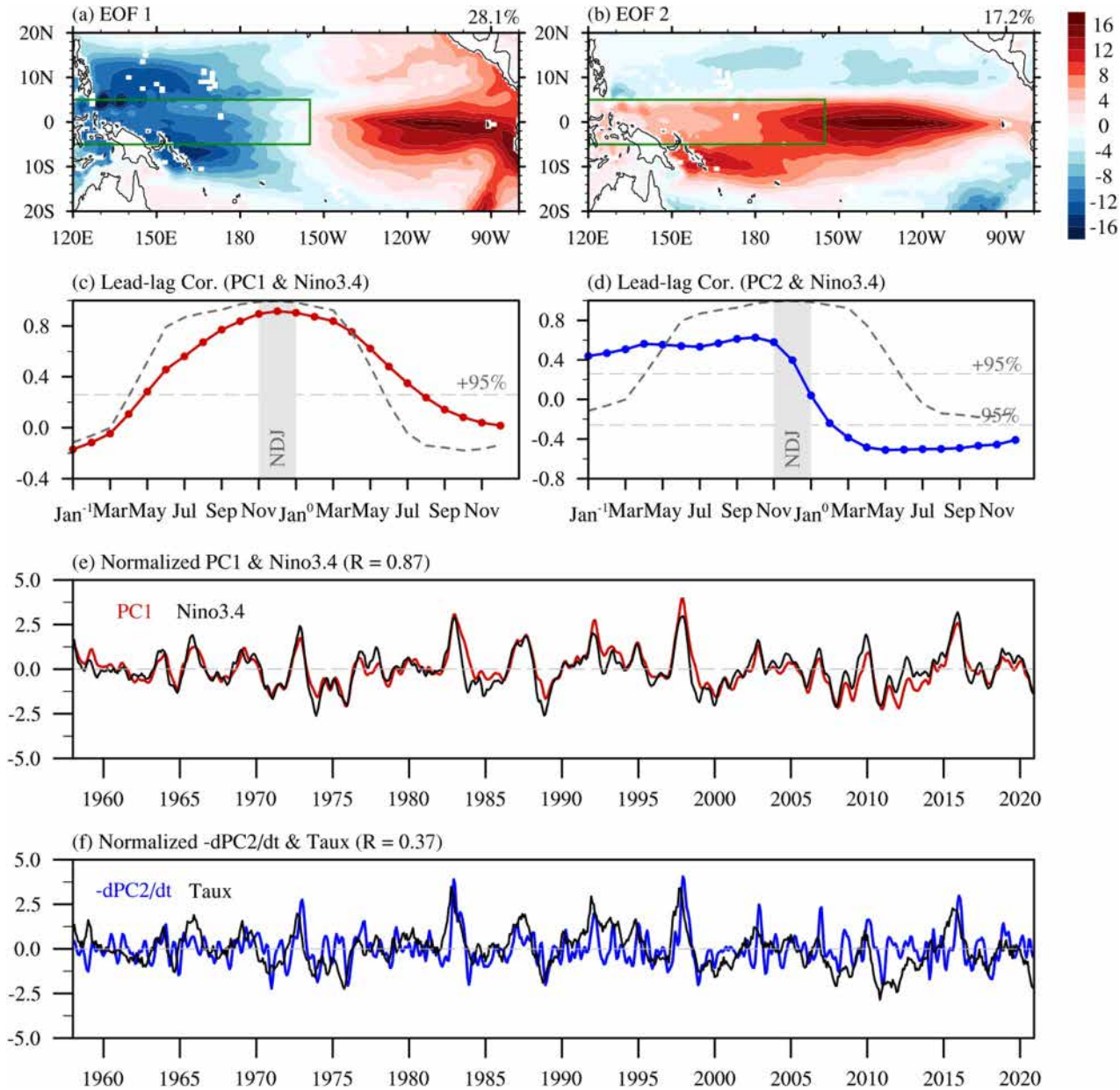

Figure 5. Equatorial heat content discharge/recharge. (a) First and (b) second EOF of the tropical Pacific ORAS5 (Zuo et al., 2019) D20 anomalies (m) over the 1958–2020 period, with % of explained total variance indicated at the top right. The green box delineates the western Pacific (5°N–5°S, 120°–155°W) averaging region. (c)–(d) Lead-lag correlations between the winter (NDJ, gray shading) Niño3.4 index and (c) the first EOF principal component (PC1, red dot curve) and (d) the second EOF principal component (PC2, blue dot curve). The Niño3.4 index lagged autocorrelation is indicated as a gray dashed curve on panels (c) and (d). The light gray horizontal lines indicate the 95% confidence level. (e) Normalized PC1 (red) and Niño3.4indices (black) time series. (f) Normalized –dPC2/dt (blue) and average central Pacific (150°E−130°W, 5°S–5°N) zonal wind stress anomalies (black). The correlation coefficients between the two curves on panels (e) and (f) are indicated on the panel title. A 3-month running average is applied to all the time series in panels (e) and (f).

in winter as observed (black and red seasonally-dependent amplitudes on Figure 2h). Overall this figure indicates that CMIP6 offers a collection of CGCM simulations with diverse yet reasonably realistic representations of ENSO characteristics.

ENSO biases. Many ENSO biases however remain in CGCMs (Guilyardi et al., 2020; Planton, Guilyardi, et al., 2021 for reviews). Although ENSO's amplitude is generally reasonable in CMIP6 (Figures 2d and 2e), some models underestimate and some models overestimate the observed amplitude, offering an opportunity to test the RO's ability to explain what controls ENSO's amplitude (Section 4.1). The ENSO SST warming or cooling

patterns in CMIP6 models tend to be detached from the South American coast, unlike in observations (Figures 2d and 2e). About 80% of the CMIP6 models have a dominant ENSO timescale that is too short, with a median dominant period of 42 months, in contrast to the observed 50 months (Figure 2g). Approximately 80% of the CMIP6 models display a more cyclic behavior than observations, with a median regularity (Regularity is defined in the caption of Figure 2, based on the minimum value of the lagged autocorrelation of the Niño3.4 index. A high regularity indicates a more cyclic behavior (i.e., a stronger tendency for an alternation between opposite ENSO phases)) of 1.5, compared to the observed 1.3 (Figure 2g). Models also have a weaker seasonal decrease in ENSO SST anomaly (SSTA) variability than observed during spring (Figure 2h), that is, their ENSO peaks are not sufficiently synchronized to the end of the calendar year. CGCM ENSO events also tend to be insufficiently skewed toward warm SSTAs in the cold tongue region (Figure 2i). Simulated ENSO SSTA and wind anomaly patterns tend to be displaced too far west (Figures 2d and 2e), and the simulated atmospheric responses of equatorial Pacific deep convection, clouds, rain (e.g., Planton, Guilyardi, et al., 2021), and winds (Figures 2d and 2e) to ENSO events are typically too weak. The thermodynamic damping of ENSO SSTAs by air-sea heat fluxes (mainly from cloud shading and evaporative cooling) also tends to be too weak in CGCMs (Figures 2c and 2d). This already indicates that two important elements in the Bjerknes feedback are too weak: the destabilizing effect of the wind response to a SST change, and the stabilizing effect of the air-sea flux response to this SST change. Finally, most models underestimate the observed ENSO pattern diversity, in particular the inter-event range of longitudes at which SST anomalies peak (Planton, Guilyardi, et al., 2021).

Mean state biases. Many of these CGCM ENSO biases stem from biases in the simulated background climate. Chief among these CGCM climate biases is the "cold tongue bias," associated with a cold tongue (and the associated dry, subsident regime) that is too strong, and extends too far west (e.g., Bayr et al., 2019; Figure 2b). Other common biases include: warm SST biases along the coast of South America (Figure 2b); an excessive "double" ITCZ south of the equator in the east Pacific during boreal spring, with insufficient cross-equatorial southerly winds (Hu & Fedorov, 2018; Figure 2b); a south Pacific convergence zone (SPCZ) in the west Pacific that is too zonally-oriented; and an overly-intense hydrologic cycle (Guilyardi et al., 2020). As discussed in Section 5, these background climate biases affect the balance of terms in the mixed layer heat budget. altering key feedbacks that affect ENSO. Beyond the long-term mean climate, CGCMs also struggle to represent other phenomena that affect ENSO's interactions across time scales—including atmospheric intraseasonal variability (Ahn et al., 2017), oceanic tropical instability waves (TIWs) (Ray et al., 2018; Tian et al., 2019; Wengel et al., 2021), the seasonal cycle (Abellán et al., 2017; Rashid & Hirst, 2016), and modes of decadal variability (McGregor et al., 2018; Power et al., 2017).

RO and CGCMs. Databases like that of CMIP6 offer a great opportunity to test the RO's capacity to reproduce ENSO properties in models. Despite CGCMs' wide utility, they are complex, expensive to run, and can be difficult to understand. Conceptual models like the RO have thus emerged as a useful way to understand ENSO in CGCMs, and help to link CGCM ENSO biases to errors in both the background climate and high-level physical feedbacks and processes. We will demonstrate the RO's capacity to reproduce key ENSO properties in the CMIP6 database in Section 4, and discuss the RO's usefulness for understanding ENSO biases in Section 6.

3. Brief RO Overview

RO derivation. A full RO derivation and description can be found in Jin et al. (2020): we just give an overview here. The recharge oscillator summarizes the evolution of ENSO Sea Surface Temperature to that of a single scalar variable T and that of equatorial heat content anomalies to a second variable h. Jin (1997a) originally used SST anomalies in the eastern Pacific for T and western Pacific heat content anomalies for h (see Figure 1 for the usual definition for those two regions). But other regions of strong ENSO signals are often used such as the 5°N–5°S heat content across the entire Pacific (Burgers et al., 2005) or SST anomalies in the Niño3.4 region (e.g., S. Zhao et al., 2024): we will discuss this in Section 7. In its simplest form, the linear RO (LRO) reduces Equations 1 and 2:

$$\frac{dT}{dt} = RT + F_1 h \tag{1}$$

$$\frac{dh}{dt} = -\varepsilon h - F_2 T \tag{2}$$

Table 1
RO Parameters Naming Conventions and Associated Processes

Parameter	Name	Associated processes
R	Bjerknes feedback	Thermal damping by surface heat fluxes (clouds, evaporation)
		Damping by mean circulation
		Thermocline feedback
		Advective feedbacks
F_1	Delayed oceanic feedback efficiency	Delayed thermocline feedback
		Delayed advective feedback
ε	Basin adjustment	Oceanic waves and efficiency of boundary reflections
F_2	Recharge/discharge efficiency	Sverdrup transport
		Eastern boundary reflection
		Meridional wind structure
$\sigma_{T,h}$	Stochastic forcing amplitude	Westerly-wind burst (WWBs), short-term atmospheric variability unrelated to ENSO and the associated heat and momentum fluxes
B	Stochastic nonlinearity	Westerly-wind bursts modulation by ENSO ("multiplicative noise"): the tendency for more, stronger WWBs during El Niño than during La Niña
	Multiplicative noise efficiency	
b	Deterministic quadratic nonlinearities	Atmosphere
		• Asymmetry in atmospheric convective response to warm versus cold SST anomalies Ocean
		• Tropical Instability Waves (TIWs) • Nonlinear Dynamical Heating • Thermocline feedback nonlinearity
c	Deterministic cubic nonlinearities	?

Note. Various parameters of the RO Equations 4 and 5, the naming conventions used in this paper for each parameter, and the processes underlying the associated term in the equation. Table 2 provides typical values of these parameters when the RO is fitted to observations.

Equation 1 is obtained through a reduction of the oceanic mixed layer heat budget after assuming simple balance relations between T, h, and wind stress, heat fluxes, currents and thermocline depth anomalies (all represented implicitly). Equation 2 for h is obtained through a reduction of equatorial wave dynamics (e.g., Jin, 1997b; Fedorov, 2010; Table 1 for parameter names and associated physical processes). As we will detail below, parameters in Equations 1 and 2 can either be obtained from a fit to observed time series of T, h, or through an analytical theory. Jin (1997a, 1997b) and Jin and An (1999) demonstrated that the LRO implicitly represents the Delayed Oscillator (Battisti & Hirst, 1989; Suarez & Schopf, 1988) and advective-reflective oscillator (Picaut et al., 1997) key mechanisms.

Bjerknes feedback. In Equation 1, R represents the Bjerknes feedback loop by which SST anomalies can grow. A positive (negative) R implies an exponential growth (decay) of T. Jin et al. (2020) derived an analytical expression for R that is briefly discussed below. Here, we will just briefly summarize the essential physics encapsulated in R, which involve a balance between processes that favor a *growth* and processes that favor a *decay* of T (Figure 6; in the rest of the paragraph we describe what happens during an El Niño, but symmetric processes are at work during La Niña). R implicitly includes the following positive feedbacks: the thermocline, Ekman and advective feedbacks (e.g., Jin & Neelin, 1993), respectively associated with remotely and locally-forced downwelling and surface eastward currents, which all induce a warming. The remote component of these mechanisms involve the time it takes for Kelvin wave to propagate between the western and eastern Pacific (about 30–45 days), but is assumed to be instantaneous in the RO. There are two main damping mechanisms that contribute negatively to R: thermodynamic and dynamic damping (e.g., Jin et al., 2006). Thermodynamic damping is associated with air-sea fluxes: a positive T leads to more clouds and reduced downward shortwave radiation, and to more evaporative cooling through Clausius-Clapeyron formula. The resulting negative surface net heat flux anomaly (Figure 2d) damps T. Dynamical damping occurs due to the dissipating effect of the mean circulation on T: vertical advection will for instance tend to cool a surface-focused warm anomaly by bringing subsurface, cooler water.

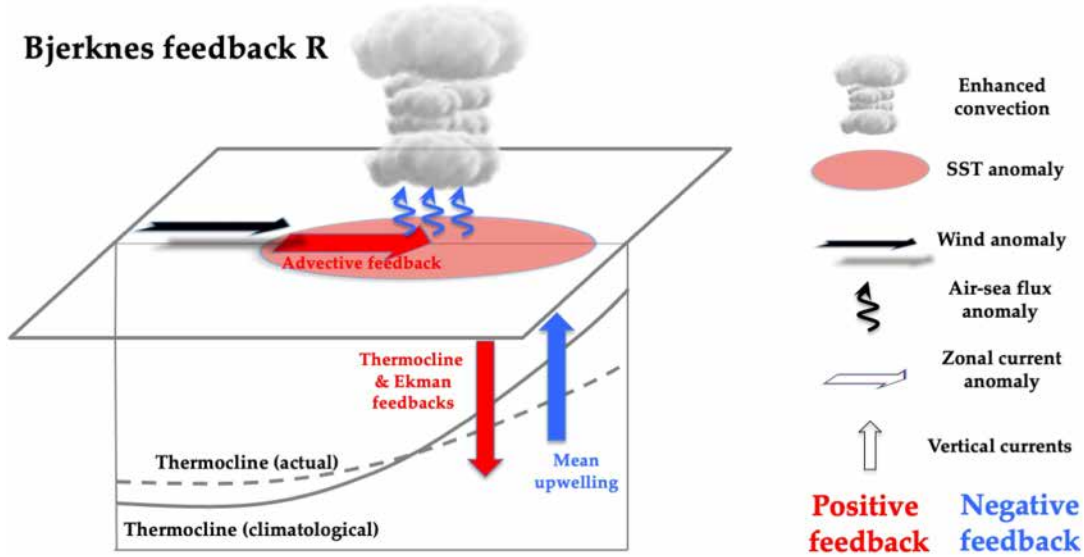

Figure 6. The Bjerknes feedback. Overview of the physical processes involved in the Bjerknes feedback loop, here for the example of a positive SST anomaly. A warm SST anomaly induces enhanced deep atmospheric convection, and westerly wind anomalies through the Gill (1980) response. This leads to negative surface heat flux anomalies (less shortwave, more evaporation), a negative feedback on the SST anomaly. The background circulation also tends to damp the warm anomaly, for instance through the mean upwelling of cold water. On the other hand, the fast oceanic response through downwelling Kelvin waves (assumed to be instantaneous in the RO) is associated with anomalous thermocline deepening in the eastern equatorial Pacific. The associated thermocline feedback favors the development of warm SST anomalies. Wind relaxation along the equator also contributes to surface warming through zonal, meridional and vertical (or Ekman) advection feedbacks. Together, these positive feedbacks control the strength of the Bjerknes feedback. The intensity of both positive and negative feedbacks depend on the background state, and the seasonal cycle leads to a slightly negative R value in spring and early summer. Positive feedbacks take over the thermal damping and damping by the mean circulation from roughly June to December (e.g., Jin et al. (2020)). The overall ENSO stability given by $\frac{R-\varepsilon}{2}$ is usually positive in fall, and weakly negative on annual average (Sections 4.1 and 4.2).

Slow equatorial heat content adjustment. The planetary wave dynamics that govern the equatorial oceanic heat content evolution are complex, as they involve waves that have different meridional structures, propagate both eastward (Kelvin waves) and westward (Rossby), at different phase speeds (Rossby waves are slower than Kelvin waves, with a decreasing phase speed for higher order Rossby meridional modes), and reflect at both boundaries (e.g., Boulanger & Menkès, 1999). Jin (1997b) however demonstrated that these complex dynamics could be approximated by the simple h Equation 2, which can reproduce the observed evolution well (0.89 correlation; Jin et al., 2020), with an ε^{-1} adjustment timescale of ∼8–10 months. The $-F_2 T$ term represents the effect of the Sverdrup transport on h: for a positive T, this leads to a discharge (i.e., $dh/dt < 0$), and induces negative h at the El Niño peak (a recharged h after La Niña).

Delayed oceanic feedback. In a similar spirit to that of the delayed oscillator model (Battisti & Hirst, 1989; Suarez & Schopf, 1988), this negative h feedbacks on T through the $F_1 h$ term in Equation 1, favoring its transition to the opposite phase. This represents the effect of a h on SST, which is mediated by Rossby wave reflections at the eastern boundary, inducing equatorial westward currents and upwelling in the following months. In the RO, those processes are implicit: they are assumed to be instantaneous, and accounted for by simple balance relations between h and central-eastern Pacific currents and thermocline depth, cooling T through the thermocline (upwelling) and advective (westward currents) feedbacks in relation with a negative h after an El Niño.

Bjerknes-Wyrtki-Jin index. Equations 1 and 2 describe an harmonic oscillator, whose growth rate and period are respectively given by the Bjerknes-Wyrtki-Jin (BWJ) index real and imaginary parts (Equation 3; Jin et al., 2006, 2020; Lu et al., 2018). We will see in Sections 4.1 and 4.2 that the BWJ index is useful to quantify ENSO amplitude and dominant periodicity in observations and climate models.

$$\mathrm{BWJ} = \frac{(R-\varepsilon)}{2} + i\sqrt{F_1 F_2 - \frac{(R+\varepsilon)^2}{4}} \tag{3}$$

Stochastic RO (SRO). Fitting Equations 1 and 2 to observed or CMIP6 model T, h data yields a negative BWJ index real part (i.e., the system is damped, see Section 4.1). A stochastic forcing is therefore required to maintain an oscillation, resulting in a ***stochastic RO*** (SRO, first three terms in Equations 4 and 5). The SRO differs from the RO through additional stochastic forcing terms of σ_T, σ_h amplitude in Equations 4 and 5. Depending on studies, this stochastic forcing is either only added in Equation 4, or in both Equations 4 and 5, and the ξ_T, ξ_h are either white (uncorrelated in time) or red (correlated in time) noises of unit amplitude. This stochastic forcing mainly represents the effect of WWBs, which heavily influence ENSO evolution (Section 2.3), and other synoptic, random (at the ENSO timescale) equatorial Pacific wind stress and heat flux perturbations.

$$\frac{dT}{dt} = RT + F_1 h + \sigma_T \xi_T + \sigma_T \xi_T \, BH(T)\, T + bT^2 + cT^3 \tag{4}$$

$$\frac{dh}{dt} = -\varepsilon h - F_2 T + \sigma_h \xi_h \tag{5}$$

Nonlinear RO (NRO). In Section 2, we discussed the observed tendency for more WWBs during El Niño (see Section 4.4). The $\sigma_T \xi_T BH(T)\, T$ term (where H() is the Heaviside step function) represents this observed WWBs modulation by ENSO, with a larger stochastic forcing amplitude $\sigma_T(1 + BH(T)\, T)$ for positive T ($B > 0$), sometimes referred to as "multiplicative noise," or a stochastic nonlinearity. In addition to this stochastic nonlinearity, deterministic nonlinearities (purple frame) can be introduced. Quadratic nonlinearities (bT^2 term) represent physical processes that favor the growth of El Niño relative to La Niña ($b > 0$), as is the case for the stochastic nonlinearity. The stochastic and quadratic nonlinearities are key to explaining the larger El Niño than La Niña maximum amplitude (Section 4.4). Finally, cubic nonlinearities (cT^3 term) represent saturation effects ($c < 0$), contributing to ENSO amplitude. Those generic quadratic and cubic terms cover various oceanic and atmospheric sources of nonlinearities that will be detailed in Section 4.4. Examples of symmetry breaking nonlinearities include asymmetries in atmospheric convection response to warm versus cold SST anomalies, or nonlinear oceanic advection (advection of temperature anomalies by current anomalies). Overall, the last three terms in Equation 4 transform the LRO or SRO into a nonlinear RO (hereafter, NRO).

Seasonality. ENSO is a highly seasonal phenomenon, and a seasonal cycle *R(t)* (Equation 4) is often assumed to represent ENSO seasonal synchronization:

$$R(t) = R_0 - R_a \sin(\omega_a t - \varphi) \tag{6}$$

In principle, a seasonality could be introduced in more RO parameters (e.g., F_1, F_2), but we will see in Section 4.2 that Equation 6 is sufficient to explain observed ENSO seasonality.

Naming conventions and original RO analyses in this review. In the rest of the paper, the LRO refers to Equations 1 and 2; the SRO refers to the first three terms of Equations 4 and 5; the NRO refers to when any of the remaining terms is included. Finally, we will refer to the *seasonal* LRO, SRO or NRO whenever a seasonal cycle in any of the parameters (such as that of *R(t)* in Equation 6) is included. Figures 8–12 original analyses are performed using parameter values obtained from fitting Equations 4 and 5 to *T, h* time series from observations (values listed in Table 2) or CMIP6 models. These figures captions detail which version of the SRO or NRO model was used.

RO representation of ENSO phase changes. Figure 7 sketch summarizes the oscillatory behavior that underpins the RO formulation. During an El Niño, a positive T anomaly grows through the Bjerknes feedback (RT term). The associated Sverdrup transport out of the equatorial band depletes h through the $-F_2T$ term. The resulting negative F_1h term ($F_1 > 0$, $h < 0$), representing the combined effect of a shallow thermocline and westward currents, makes T decay, eventually terminating the El Niño, leaving the system with a negative h. This initiates a negative T through the F_1h term, which grows through the Bjerknes feedback (RT term), leading to a La Niña peak. The associated Sverdrup transport into the equatorial band leads to a positive h, which favors a positive T,

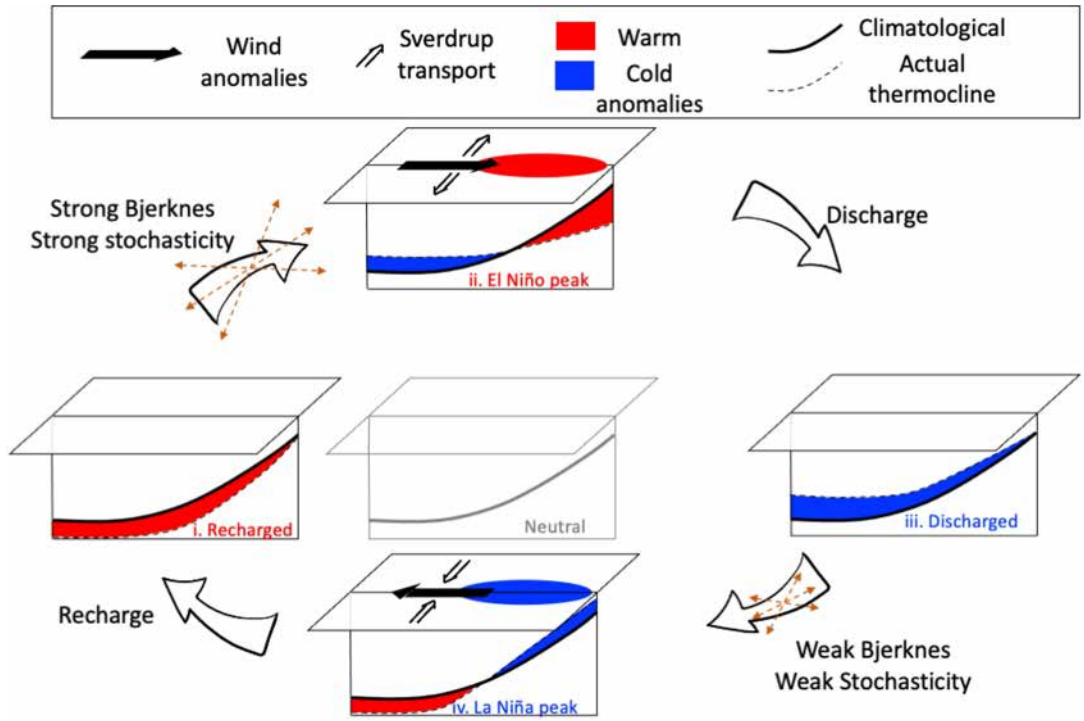

Figure 7. The RO mechanism for ENSO phase transitions. A recharged western Pacific heat content (i), favors the development of warm SST anomalies during summer and fall amplified by the Bjerknes feedback (see Figure 6), and leading to an El Niño peak (ii). Nonlinearities induce more WWBs stochasticity, leading to an uncertain evolution but also favoring the growth of positive T anomalies, possibly leading to stronger warm events than cold events. The westerly stress anomalies lead to a Sverdrup transport out of the equatorial band, inducing a discharge of the western Pacific heat content. The associated delayed advective and thermocline negative feedbacks end the El Niño event, and lead to a discharged state (iii). The transition to La Niña (iv) and to a recharged state (i) again occurs through symmetrical processes, but with less stochasticity due to weakly active WWBs, and symmetry breaking nonlinearity that favor smaller amplitude SST and recharge anomalies during and after La Niña. Stochasticity acts along the entire cycle, making it much more erratic than on this simplified sketch. For instance, stochasticity can represent a series of WWBs, which could lead to an El Niño, even in the absence of an initial positive heat content preconditioning. Stochasticity is enhanced when there are positive SST anomalies, making the evolution of El Niño less predictable than that of La Niña.

re-initiating the cycle. The presence of stochastic forcing of course disrupts this regular cycle, so that the SRO has a slight preference for this succession of phases, but does not always follow it. Finally, the quadratic nonlinearity yields more growth of SST anomalies during El Niño than La Niña, and the multiplicative noise forcing leads to a more uncertain evolution of the system in presence of warm anomalies (cf., Section 4.4).

RO parameters: analytical approach. RO parameters can be obtained in two different manners. Jin et al. (2020) derived analytical formulae for R and F_1 as a function of mean state parameters (such as the temperature horizontal and vertical gradients, mean currents, etc…) and empirical estimates of coupling coefficients (such as the wind stress response per unit of T, the coupling coefficients between currents and h, etc…). This provides, in principle, a theory for linking the properties of the mean state to the Bjerknes feedback strength. Such a theory is necessary to assess the sensitivity of ENSO characteristics to the mean state, important for understanding the effects of model biases, anthropogenic climate change or long-term natural mean state variations. We will come back to this in Sections 5 and 7.

RO parameters: fitting observations or models. However, most studies do not use this analytical theory, which requires accessing three-dimensional observed or model data for computing important mean-state parameters, as well as other data sets (e.g., wind stress, surface currents, heat fluxes, SST) to compute empirical coupling coefficients. Rather, they obtain the RO parameters through a multivariate (and potentially nonlinear) fit of Equations 4 and 5 to time series of T, h. The original results of Figures 8–12 follow this approach, and Table 2 lists typical parameter values obtained when fitting to observed data. Section 4 includes will demonstrate that this

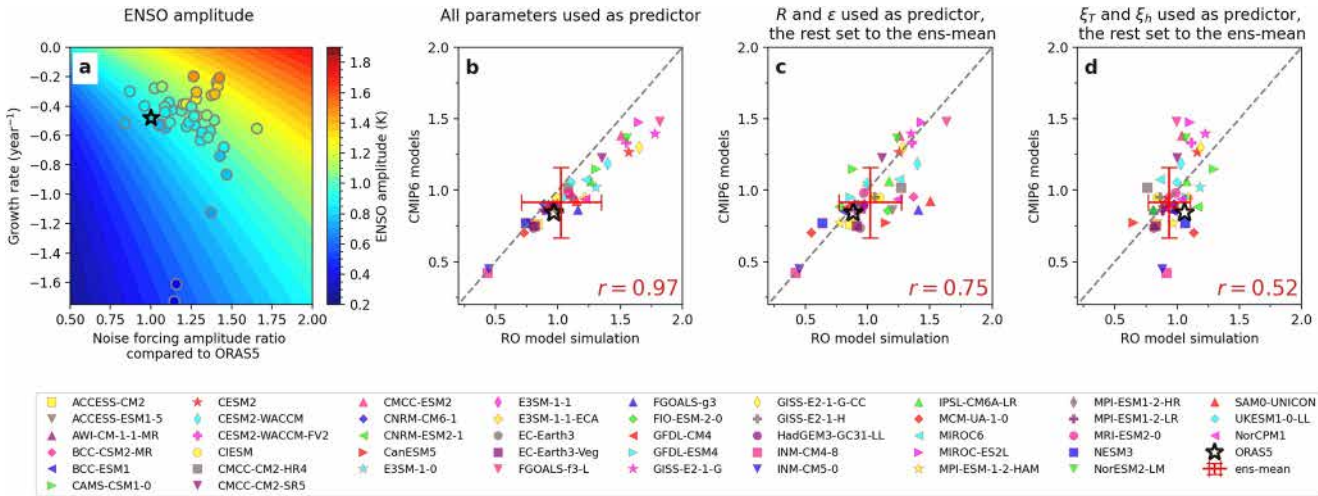

Figure 8. The RO reproduces ENSO amplitude. (a) ENSO amplitude in the NRO (details below), as a function of the growth rate $\frac{R-\varepsilon}{2}$ and noise forcing amplitude (ratio to that of ORAS5 reanalysis) (shading). The NRO parameters were obtained from fits to ORAS5 (*star*, Zuo et al., 2019; see Table 2 for values) or 45 CMIP6 (Eyring et al., 2016) individual models data (*circles*, with the color indicating the ENSO amplitude). (b)–(d) Scatter plots of ENSO amplitude (K) in CMIP6 models and ORAS5 against that from NRO simulations where (b) all NRO parameters, (c) only R and ε, (c) only ξ_T and ξ_h were set to the fitted values, with other parameters set to the ensemble-mean value. Using R, ε, ξ_T, and ξ_h yields a 0.9 correlation with the actual ENSO amplitude (not shown). The CMIP6 ensemble-mean and one standard deviation spread is indicated by the red cross, and the linear correlation coefficient over all CMIP6 models is indicated in the lower right corner of each panel. The RO model used in this figure and in Figures 9–12 original analyses are based on Equations 4 and 5, with h defined from the equatorial average heat content. The stochastic forcing uses red noise for ξ_T; ξ_h, whose amplitude and ∼1 month decorrelation are estimated based on residuals of the fit. This figure is based on the nonlinear RO, with B and b set to zero (i.e., no $R(t)$ seasonal dependency, c only non-zero nonlinear parameter as in Table 2).

approach leads to ENSO characteristics from the RO that match those in observations and climate model control simulations from the CMIP6 project.

4. How Does the RO Account for ENSO Properties in Observations and Climate Models?

4.1. Amplitude

Fitted RO captures ENSO amplitude. The study of Vijayeta and Dommenget (2018) showed that fitting a SRO to observations and CMIP3 and CMIP5 models allows to reproduce their ENSO amplitude. Wengel et al. (2018) further investigated the key controls of ENSO amplitude in 35 CMIP5 models, and demonstrated that the R and ε parameters (that control the overall ENSO stability $(R-\varepsilon)/2$) and stochastic forcing amplitude (σ_T, σ_h) jointly explain more than 80% of the ENSO amplitude variance. Figure 8 displays a similar result to that of Wengel et al. (2018), but here obtained using the NRO model and 45 CMIP6 models. Using fitted values (Figure 8 caption for details) for all the RO parameters allows to explain the observed and CMIP6 ENSO amplitude extremely well ($r = 0.97$, Figure 8b), with a slight overestimation for larger than observed amplitudes. Only retaining fitted value for the overall ENSO stability $(R-\varepsilon)/2$ and noise amplitude respectively explain 50% and 25% of the ENSO amplitude variance individually (Figures 8c and 8d) and 80% together, as in the study of Wengel et al. (2018) (not shown).

Theoretical explanation. Jin et al. (2020) provided a theoretical context to explain those results. They derived an analytical solution for ENSO amplitude in the case of a NRO with no seasonal dependency and $B = 0$ and $b = 0$ (no multiplicative noise, no symmetry-breaking nonlinearity, just a cubic nonlinearity). In this solution, ENSO amplitude is a function of the stability $(R-\varepsilon)/2$, the stochastic forcing amplitude σ_T, σ_h (and/or the noise decorrelation timescale, with longer timescales also increasing ENSO amplitude), and the cubic nonlinearity parameter c. In practice, ENSO amplitude is sensitive to the stability and noise in the vicinity of parameter values derived from observations, but it is weakly sensitive to the cubic nonlinearity parameter c for a stable or marginally stable ENSO (Jin et al., 2020). Physically, this can be understood as follows: the cubic nonlinearity

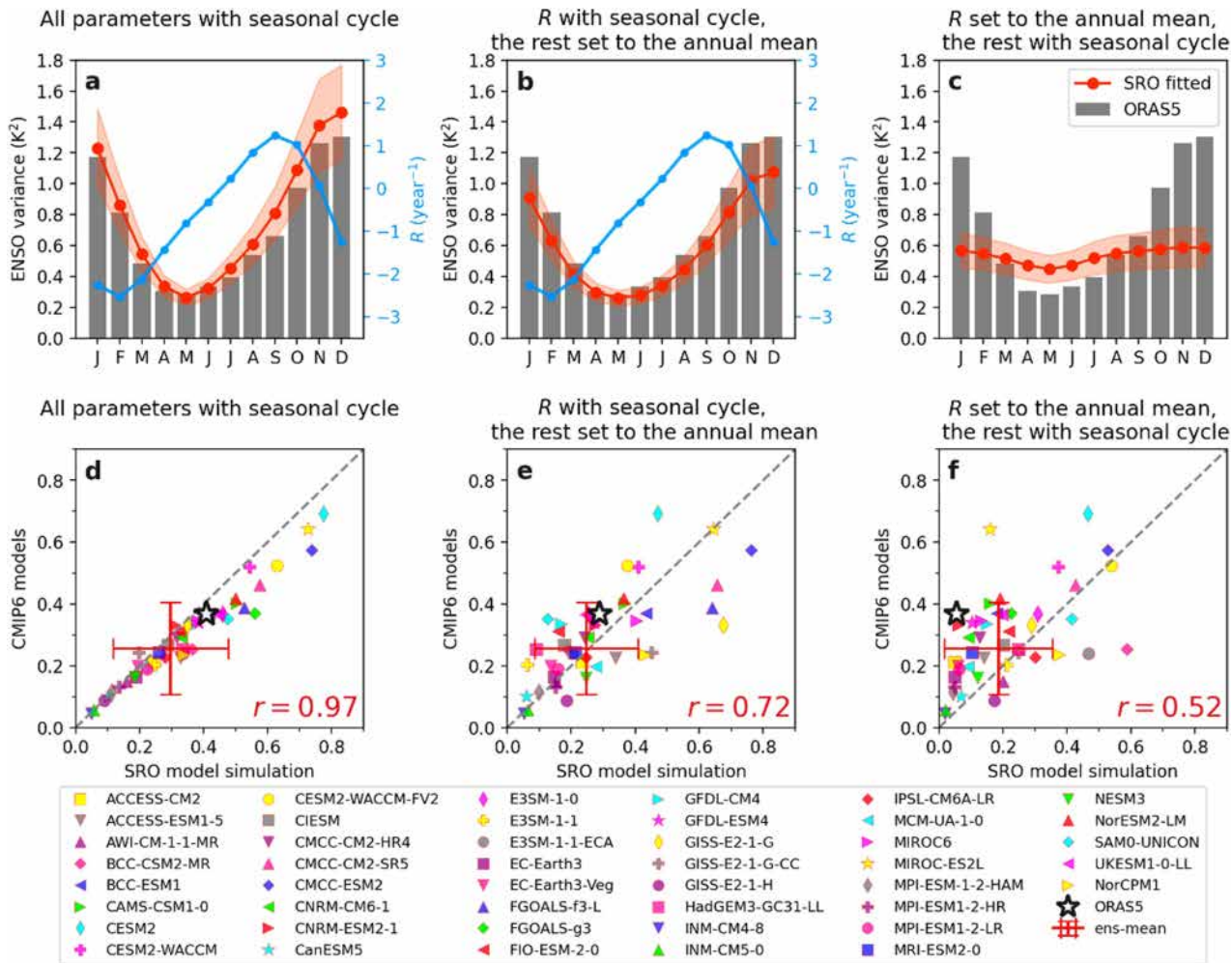

Figure 9. The RO reproduces ENSO seasonality. ENSO variance seasonal cycle in observation (bars) and that obtained from integrating the SRO model with parameters estimated from observed data (red curves): (a) all parameters with seasonal cycle, (b) only R with seasonal cycle and the other parameters set to the annual mean values, (c) R with annual mean, but other parameters with seasonal cycle. The seasonal cycle of R is displayed in blue on panels (a) and (b), with its y-axis also indicated in blue on the right hand side of the panel. The shading indicates the one-standard deviation spread by splitting 3100-yers simulations into 50 ensemble members with the same length of 62 years with observation (1958–2020). (d) Scatter plot of the amplitude of the seasonal cycle of ENSO standard deviation in CMIP6 against that obtained from integrating the NRO fitted to this model. Panel (e) as (d) but with a seasonal cycle in R and other parameters set to their annual-mean values, (f) as (d) but with R set to its annual mean value and the full seasonal cycle for other parameters. The RO models used in Figures 8–12 original analyses are based on Equations 4 and 5, with h defined from the equatorial average heat content. The parameters were obtained from RO fit to ORAS5 or CMIP T, h data (see Table 2 for details and observed coefficient values). The stochastic forcing uses red noise for ξ_T; ξ_h, whose amplitude and ∼1 month decorrelation are estimated based on residuals of the fit. This figure uses the seasonally dependent stochastic RO (i.e., $R(t)$ and $b = B = c = 0$).

acts as a saturation effect and only controls the ENSO amplitude in an unstable case, when a nonlinearity is needed to stop exponential growth. Figure 8a shows that the 45 analyzed CMIP6 models all yield an annual-mean stable growth rate (between −1.6 and −0.2 year^{-1}, with an observed estimate of −0.5), explaining why observed and CMIP6 ENSO amplitude can be accounted for without considering nonlinearities. While one has to bear in mind that the fitted noise can act as a surrogate for incorrectly estimated nonlinearities (such as those associated with the multiplicative noise parameter B), this strong convergence of CMIP6 models and observations suggest that ENSO can be viewed as an asymptotically stable (in an annual-mean sense) system driven by noise, whose amplitude grows with noise and/or when the system is less damped.

Linking amplitude to mean state. While the above results are a testimony of the RO ability to predict ENSO amplitude, they do not link this amplitude to the mean state, as would be needed to understand ENSO amplitude changes in view of natural or anthropogenically-driven multidecadal Pacific variability (e.g., Power et al., 2021). The RO parameters were indeed obtained by a fit to the model and observed data, but not directly estimated based

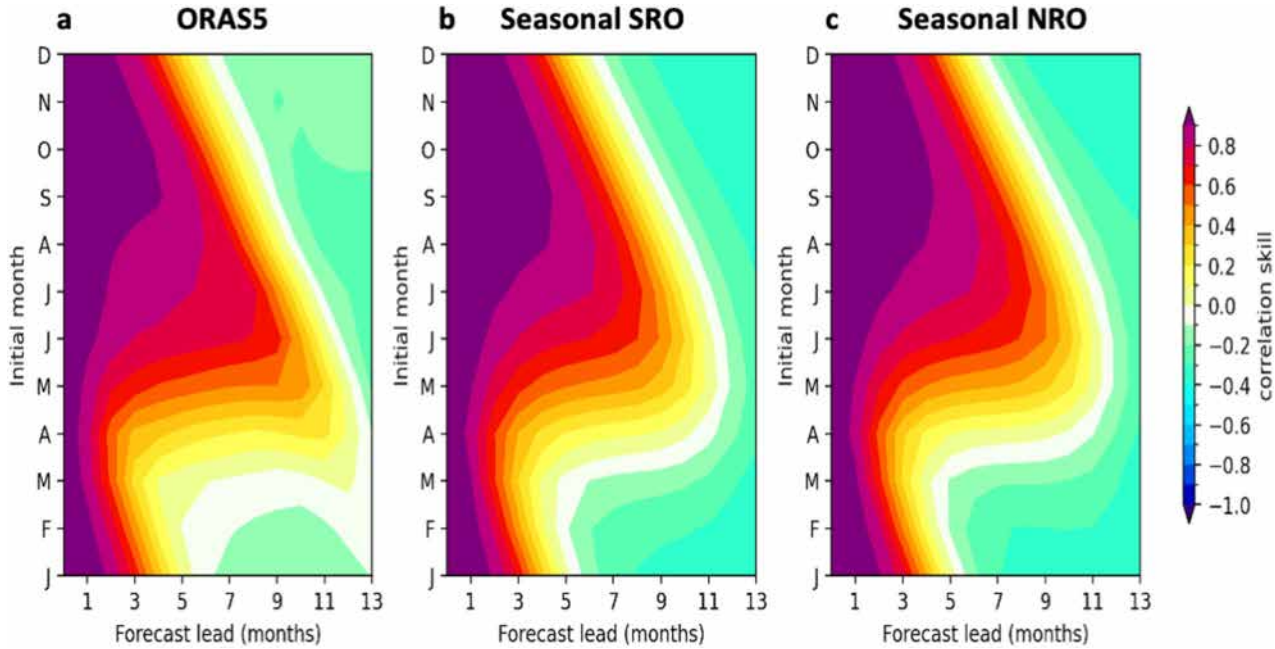

Figure 10. The RO reproduces the ENSO "spring barrier" in predictability. (a)–(c) Persistence of SST anomalies as a function of initial month and forecast lead for ORAS5, and the linear, stochastic, seasonal SRO and nonlinear, stochastic, seasonal NRO fitted to observations. The RO models used in Figures 8–12 original analyses are based on Equations 4 and 5, with h defined from the equatorial average heat content. The parameters were obtained from RO fit to observations or CMIP (see Table 2 for details and observed coefficient values). The stochastic forcing uses red noise for ξ_T; ξ_h, whose amplitude and ~1 month decorrelation are estimated based on residuals of the fit. Panel b is based on the seasonal SRO (i.e., $R(t)$ as on Figure 9 and $b = B = c = 0$) and c on the seasonal NRO (i.e., $R(t)$ as on Figure 9 and b, B, c as in Table 2).

on their mean state. Kim and Jin (2011) and Kim et al. (2014) have used the BWJ index (Jin et al., 2006) to estimate ENSO stability based on key mean state parameters, as well as parameters describing important ENSO feedbacks (e.g., wind stress—SST coupling or surface heat flux—SST coupling) fitted to models. This approach was successful in explaining ENSO amplitude diversity in 12 CMIP3 models (Kim & Jin, 2011), but later failed to

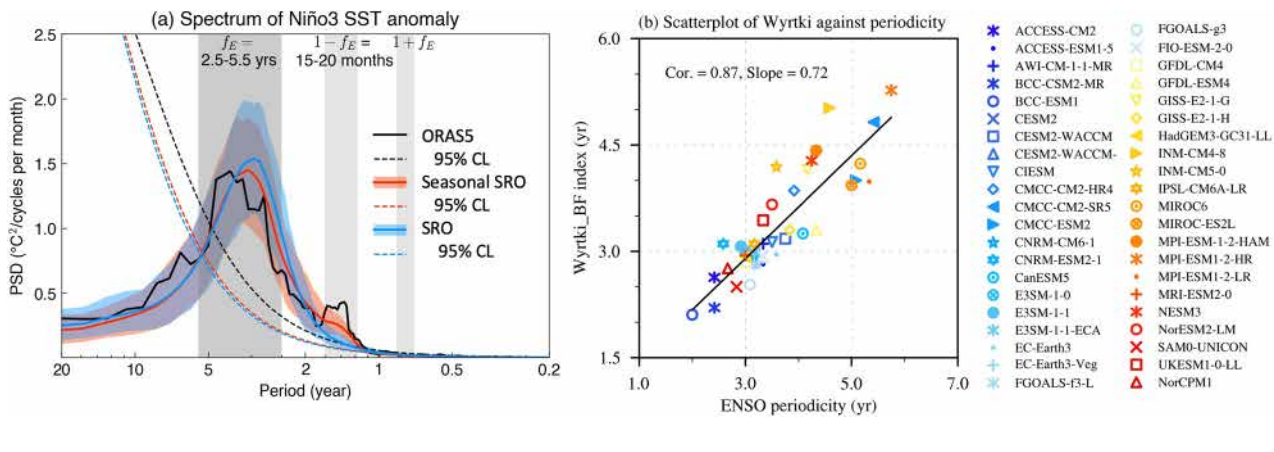

Figure 11. The RO reproduces ENSO dominant timescales. (a) Multi-taper power spectral density (PSD) of the normalized Niño3 indices for ORAS5 (1958–2022, black curve), SRO model (red curve) and seasonal SRO model (blue curve). 100 members (65 year each) are generated based on each model and the shading denotes 10%–90% quartile range. The dashed curves indicate the 95% confidence level (CL) calculated from the 95th percentile of an AR(1) process. The gray shading represents the approximate frequency range of ENSO (f_E) and the near-annual combination tones ($1 - f_E$ and $1 + f_E$), where 1 corresponds to the annual frequency. (b) Scatterplot of the approximate Wyrtki index period $2\pi/(F_1F_2)^{1/2}$ against ENSO periodicity (estimated as on Figure 2g) in 42 CMIP6 historical simulations (1920–1999). The linear regression fit is indicated by the black line (correlation coefficient and slope on the top left). The RO models used in Figures 8–12 original analyses are based on Equations 4 and 5, with h defined from the equatorial average heat content. The parameters were obtained from RO fit to observations or CMIP6 (see Table 2 for details and observed coefficient values). The stochastic forcing uses red noise for ξ_T; ξ_h, whose amplitude and ~1 month decorrelation are estimated based on residuals of the fit. Panel (a) analyses use the SRO ($b = B = c = 0$, with a constant R for the SRO and $R(t)$ as on Figure 9 for the seasonal SRO).

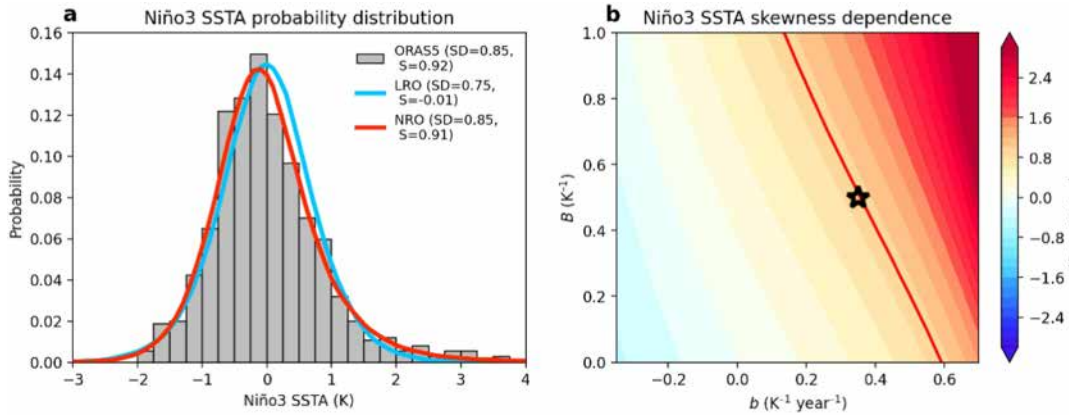

Figure 12. The RO reproduces ENSO amplitude asymmetry. (a) Probability distribution of Nino3 SSTA for the observation (ORAS5, gray bars), and of the T variable from 20,000 years simulations with the stochastic linear (blue) and nonlinear (red) RO models. The standard deviation (SD) and skewness (K) of T are indicated in the legend. (b) T skewness as a function of state-dependent noise forcing amplitude (B) and quadratic nonlinearity (b). The red curve indicates the observed level of skewness. The black star indicates the parameters of the NRO used in panel (a). The RO models used in Figures 8–12 original analyses are based on Equations 4 and 5, with h defined from the equatorial average heat content. The parameters were obtained from a RO fit to observations (see Table 2 for details and coefficient values). The stochastic forcing uses red noise for ξ_T; ξ_h, whose amplitude and ∼1 month decorrelation are estimated based on residuals of the fit. This figure 12 analyses use the SRO ($b = B = c = 0$) and NRO (b, c obtained from the fit as in Table 2); B set to a 0.5 K^{-1} value in order to match the observed ENSO skewness, which compares well with observed estimates of 0.3 from Levine and Jin (2017) or 0.1–0.5 from Kug et al. (2008), with a constant R in both cases.

explain it in 19 CMIP5 models (Kim et al., 2014). While these two studies succeeded in establishing links between the mean state and some of the key ENSO feedbacks (e.g., thermocline feedback), this was insufficient to establish a clear link between mean state and ENSO amplitude changes under the effect of anthropogenic forcing (Kim & Jin, 2011). This points to the need of more research for linking RO parameters with the mean state (Section 7). Another difficulty is that coupled models have biased ENSO dynamics, due to compensating biases in the wind stress-SST coupling and thermodynamical damping by air-sea fluxes, which both tend to be underestimated (H. C. Chen et al., 2021; Kim & Jin, 2011) as a result of the cold tongue bias (Bayr et al., 2019). A lot of CMIP models therefore produce a realistic ENSO amplitude for incorrect reasons.

4.2. Seasonal Synchronization

Recipe to ENSO seasonality in the RO. The variance of observed ENSO SST anomalies exhibits a pronounced seasonal cycle, with peak amplitudes in boreal winter (gray bars on Figures 9a–9c). This fundamental observed ENSO property was first accounted for by including a seasonally-dependent Bjerknes feedback in the delayed oscillator conceptual model (Tziperman et al., 1998). The seasonal synchronization of ENSO can also be reproduced when including a seasonally-modulated Bjerknes feedback $R(t)$ in the recharge oscillator model (Figures 9a and 9b; An & Jin, 2011; H.-C. Chen & Jin, 2020; Dommenget & Yu, 2016; Jin et al., 2020; Kim & An, 2021; Levine & McPhaden, 2015; Stein et al., 2010, 2014). Estimating R from a direct fit of the NRO to observations or from the BWJ approach yields positive (unstable) values from July to November with a peak in September (blue curve in Figure 9a; e.g., H.-C. Chen & Jin, 2020; Jin et al., 2020). Kim and An (2021) provided an approximate analytical solution of the seasonally-dependent ENSO variance, which predicts peak ENSO amplitude ∼3 months after the R maximum, that is, in boreal winter, as observed.

R seasonal modulation mechanisms. The BWJ index allows for a decomposition of seasonal variations of the Bjerknes feedback into contributions from individual oceanic processes (Jin et al., 2020), indicating contributions from many processes, including the thermocline and zonal advective positive feedbacks, dynamical damping by the mean upwelling, or thermodynamical damping (e.g., negative cloud/radiation feedback; Dommenget & Yu, 2016). These represent the combined effects of the seasonal changes in climatological background state (zonal and vertical temperature gradients, vertical velocity), the amplitude of the wind stress response to SST anomalies, and the coupling between this wind stress response and the oceanic (i.e., thermocline tilt) response. Further linking the Bjerknes feedback seasonality to well-identified features of the seasonal cycle such as shifts in

Table 2
Parameter Values for the Original RO Analyses in This Review

Parameters	SRO	NRO
R (year^{-1})	−1.13	−1.13
F_1 (K m^{-1} year^{-1})	0.19	0.19
ε (year^{-1})	0.38	0.38
F_2 (m K^{-1} year^{-1})	17.58	17.58
σ_T (K year^{-1})	2.22	2.22
σ_h (m year^{-1})	14.37	14.37
b (K^{-1} year^{-1})	0.	0.35
c (K^{-1} year^{-1})	0.	−0.04
B (K^{-1})	0.	0.5

Note. Various stochastic RO (SRO) and nonlinear RO (NRO) simulations were used for Figures 8–12 original analyses in this review. This table provides parameter values obtained from a fit to h, T 1958–2020 ORAS5 oceanic reanalysis (Zuo et al., 2019) with h defined as the 5°N–5°S, 120°E–80°W average 20°C isotherm depth anomalies, and T as Niño3 (5°N–5°S, 150°W–90°W) SST anomalies. All parameters but B are obtained from a nonlinear fit of Equations 4 and 5 to these observations. The stochastic forcing uses red noise for ξ_T; ξ_h, whose amplitude and ∼1 month decorrelation timescales (13.27 year^{-1} for T and 10.83 year^{-1} for h) are estimated based on residuals of the fit. B is set to the value for which the T skewness matches the observed value (see Figure 12). SRO simulations set all the values of the nonlinear coefficients b, B, c to zero. NRO simulations use at least one nonzero value for these coefficients. Seasonal SRO or NRO simulations have seasonally varying coefficient values (see, e.g., $R(t)$ as a blue curve on Figures 9a and 9b). A similar procedure is applied to 1958–2020 CMIP6 historical simulations to obtain coefficient values in CMIP6 models.

tropical Convergence zones and the meridional movement of zonal wind anomalies (Abellán & McGregor, 2016; McGregor et al., 2012; Stuecker et al., 2013) has so far proven difficult, probably because the R seasonality is a compound effect of many different processes.

RO reproduces ENSO observed seasonality. Using a SRO, Stein et al. (2010) showed that seasonal variations in F_1 play a much weaker role in the ENSO amplitude seasonality than those in R. Figures 9a–9c confirms this result: the SRO can reproduce the observed seasonality remarkably well when all the fitted parameters are seasonally-dependent (panel a), or when just the R parameter is seasonally dependent (panel b). Including a seasonal dependence in all the parameters but R yields little seasonality in the ENSO variance, underlining the strong role of the Bjerknes feedback R seasonal dependency.

RO reproduces ENSO seasonality in models. Figures 9d–9f further investigates the RO ability to capture the amplitude of the ENSO seasonal cycle in CMIP6 models. Fitting the SRO to individual models allows a very accurate reconstruction of their seasonal amplitude modulation (with an overestimation at larger than observed amplitudes, Figure 9d). Figures 9e and 9f indicate that the R seasonality explains half of the inter-model variance, but that, unlike in observations, parameters other than R also contribute to the diversity in the ENSO amplitude seasonal modulation in models. Previous studies have for instance emphasized the role of the F_2 seasonality in models (Abellán & McGregor, 2016; Izumo et al., 2024; McGregor et al., 2012). This may be due to the fact that models tend to be in a different dynamical regime than observations. Diagnosing CMIP models using the RO framework for instance suggests a too weak zonal advective feedback seasonality, which can further be related to the cold tongue bias (H.-C. Chen & Jin, 2022).

RO reproduces ENSO predictability spring barrier. It is difficult to discuss ENSO seasonality without referring to the "spring barrier" in predictability, that is, the tendency for forecasts that are initiated before boreal spring to display much less skill than those initiated after (e.g., Latif et al., 1998). The lagged autocorrelation of Nino3 SST anomalies as a function of the starting month (Figure 10a) indicates that persistence forecasts initiated before April-May are much less skillful than those initiated after. This skill decrease is less marked, but nonetheless present, when the ocean subsurface heat content is accounted for in initial conditions (e.g., Clarke, 2014; McPhaden, 2003) and in advanced dynamical forecasts (Barnston et al., 2012). Idealized predictability experiments demonstrate that this "spring predictability barrier" is a fundamental characteristic of ENSO, not a property of forecast systems (e.g., Latif et al., 1998). Introducing a Bjerknes feedback seasonal cycle $R(t)$ in the SRO and NRO allows reproducing the spring predictability barrier (Figure 10; Levine & McPhaden, 2015). While Levine and McPhaden (2015) emphasized the role of the multiplicative noise forcing for being able to reproduce the spring predictability barrier best, results here indicate that stochastic nonlinearities are not needed to reproduce this property (Figures 10b and 10c). This difference in results can be attributed to the fact that Levine and McPhaden (2015) did not include a linear stochastic forcing nor a $-\varepsilon h$ term in Equation 5. Overall, the RO can explain the spring barrier as follows: the system is stable and noise-driven before spring, and therefore has a poorly predictable evolution at that time. The shift to unstable conditions in summer and fall allows the growth of initial T, h perturbations to dominate the noise during summer and fall, leading to stronger predictability.

4.3. Dominant Timescale

ENSO timescales. ENSO variations display many characteristic timescales: El Niño events typically last 1 year while La Niña tend to last longer (often two, sometimes 3 years; e.g., Okumura & Deser, 2010); the time interval between two warm events is quite variable and up to around ∼15 years between strong events such as those in 1982–1983, 1997–1998, and 2015–2016 (Figure 2c). As a result, ENSO indices typically display a broad spectrum with enhanced variance in the 3–7 years band (Figure 2f). This broad spectral peak is robust, despite the

large uncertainties in spectra due to the modulation of ENSO at decadal timescales, even with ∼100 years of data (e.g., Wittenberg, 2009).

The RO reproduces the broad ENSO spectrum. Early theoretical debates discussed whether ENSO's broad spectrum was typical of a nonlinear phenomenon in the chaotic regime (e.g., Tziperman et al., 1995; Vallis, 1986), or if ENSO could be explained as a damped oscillator excited by weather noise (e.g., Eisenman et al., 2005; Graham & White, 1988; Harrison & Vecchi, 1997; Kleeman, 2008). Fitting the SRO or NRO to observations (e.g., Jin et al., 2020), CMIP3 and CMIP5 models (e.g., Vijayeta & Dommenget, 2018) or CMIP6 models (Figure 8a) yields a negative annual-mean RO growth rate $(R - \varepsilon)/2$ (Section 4.1, although this growth rate becomes seasonally positive, as discussed in Section 4.2), and allows to reproduce the overall shape of the ENSO spectrum in observations (Figure 11a) and CMIP models (Vijayeta & Dommenget, 2018). Including an annual cycle in the Bjerknes feedback R (Section 4.2) leads to enhanced variance on near-annual periodicities (at about ∼9 and ∼15 months), the combination tones (Stein et al., 2014; Stuecker et al., 2013), as can be seen from a comparison between seasonal and nonseasonal versions of the SRO and observations (Figure 11a).

The Wyrtki index. The RO theory also provides some tools to estimate the dominant ENSO timescale (central periodicity of the ENSO broad spectral peak), from the Wyrki index (BWJ imaginary part, Equation 3), which can be approximated as $T_{\mathrm{BWJ}} = 2\pi/(F_1 F_2)^{1/2}$ (Jin et al., 2020). This period is thus inversely related to the delayed oceanic feedback strength (F_1) and to the recharge-discharge efficiency (F_2), in other words proportional to typical basin-scale ocean dynamics adjustment timescale. Lu et al. (2018) showed that T_{BWJ} computed from fitted RO parameters can explain the diversity of the ENSO dominant period (measured as the ratio of 3–8 to 1–3 years spectral energy) across CMIP5 models and observations. Here, we compare T_{BWJ} to a different metric of the dominant ENSO timescale in CMIP6 models, based on the autocorrelation of the Nino3.4 index (see Figure 2g caption). The relation between ENSO periodicity and T_{BWJ} is much stronger ($R = 0.87$, Figure 10b) than that with simpler parameters such as the mean thermocline depth or various properties of the wind stress coupling with SST ($R < 0.30$; Lu et al., 2018). RO-based diagnostics suggests that climate models have the right ENSO period with wrong dynamics, due compensating errors between a too strong oceanic feedback F_1 and too weak recharge efficiency F_2 (Lu et al., 2018). The RO thus provides useful tools for understanding the controls of ENSO dominant timescales. Yet, T_{BWJ} underestimates the ENSO period in observations and models (slope <1 on Figure 11b, yielding an estimated 3 against 4.2 years dominant timescale for observations).

4.4. Asymmetries

Nonlinear symmetry-breaking processes. ENSO is asymmetrical (An, Tziperman, et al., 2020 for a review): El Niño events tend to be stronger (Deser & Wallace, 1987) and shorter (Ohba & Ueda, 2007) than La Niña events; strong El Niño events often transition into La Niña, while the opposite is less frequent (Larkin & Harrison, 2002). Solutions of the SRO are very symmetrical (compare the 0.91 skewness of the observed Nino3 SST with the −0.01 skewness of the SRO solution on Figures 12a and 12b): nonlinearities are required to break this symmetry (e.g., Jin et al., 2020). Several nonlinearities have been proposed to explain the ENSO asymmetry, some of atmospheric and some of oceanic origin. Atmospheric nonlinearities include the SST threshold for deep convection, which leads to a stronger and eastward-shifted rainfall and wind stress response to positive SST anomalies, relative to negative ones (e.g., Choi et al., 2013; Frauen & Dommenget, 2010; Geng et al., 2019; Hoerling et al., 1997; Kang & Kug, 2002; Srinivas et al., 2024; Takahashi et al., 2019). The second source of atmospheric nonlinearity is stochastic, and associated with the more prevalent and eastward-shifted WWBs in presence of positive SST anomalies (Section 2.3 and, e.g., Capotondi et al., 2018; Eisenman et al., 2005; Kessler et al., 1995; Lengaigne et al., 2004; Planton, Vialard, et al., 2021; Puy et al., 2016). Oceanic nonlinearities include temperature advection, both associated with the low-frequency "Nonlinear Dynamical Heating" (NDH) nonlinear advection terms (e.g., $-u' \partial_x T'$) that enhance the warming during El Niño (e.g., An & Jin, 2004; Jin et al., 2003; W. Wang & McPhaden, 2000) and the thermal damping by TIWs that is weaker during El Niño (e.g., An, 2008; Vialard et al., 2001). A more efficient thermocline feedback during El Niño initially included in the Zebiak and Cane (1987) intermediate model has been proposed to contribute to the genesis of strong events (e.g., Timmermann et al., 2003). Finally, some studies attribute ENSO asymmetry to an enhanced oceanic response to western Pacific wind forcing during El Niño (An & Kim, 2017, 2018; Im et al., 2015). We will come back to these very diverse explanations below.

Stochastic nonlinearities in the RO. As described in Section 3, the nonlinearity associated with WWBs is represented as a state-dependent stochastic forcing in the NRO (orange frame in Equation 4), with B representing the strength of this state-dependency (e.g., Levine & Jin, 2017). Introducing this nonlinear, state-dependent noise forcing in the RO ($B > 0$) leads to larger-amplitude warm events (An, Kim, & Timmermann, 2020; Jin et al., 2007; Levine et al., 2016; Figure 12b).

Deterministic nonlinearities in the RO. Various studies have also used the RO to investigate the effect of deterministic nonlinearities. Frauen and Dommenget (2010) demonstrated that coupling the linear oceanic dynamics of the RO to the nonlinear wind stress response to SST provided by an AGCM was sufficient to reproduce the observed ENSO amplitude asymmetry. Takahashi et al. (2019) showed that changing R from a negative (damping) to zero (neutral) value to represent a less-damped system above the threshold for deep atmospheric convection could allow the RO to reproduce strong El Niño events. An (2008) similarly demonstrated that introducing more damping for negative T (interpreted as the asymmetrical effect of TIWs) leads to larger amplitude El Niño than La Niña. Geng et al. (2019) separately represented oceanic and atmospheric nonlinearities in the RO, by setting different values of R and F_2 depending on the sign of T, and concluded that atmospheric nonlinearities were key to generating ENSO amplitude asymmetry. An, Kim, and Timmermann (2020) and Kim and An. (2020) finally demonstrated that introducing nonlinearities in the RO reproduced the observed amplitude asymmetries, and interpreted those nonlinearities as being caused by NDH.

Ambiguous source of RO deterministic nonlinearities. Overall, most studies indicate that introducing non-linear terms allows the RO to account for the observed stronger El Niño than La Niña events (An, Kim, & Timmermann, 2020; Dommenget & Al-Ansari, 2023; Geng et al., 2019; Kim & An, 2020; compare the NRO to the LRO T skewness on Figure 12a). It is however not easy to attribute the RO deterministic nonlinearity to a single physical cause, because both atmospheric and oceanic processes lead to terms such as the $b\,T^2$ term (Jin et al., 2020), an extra Th term (An, Kim, & Timmermann, 2020; Kim & An, 2020) or a term proportional to h^2 (Geng et al., 2019) in Equation 1. More work is needed to rank the contributions of various atmospheric and oceanic nonlinear processes to the overall nonlinearity, for instance through budget studies in ocean models, as suggested by Jin et al. (2020). A recent study for instance suggests that various sources of oceanic nonlinearities cancel, so that atmospheric ones dominate (F. Liu et al., 2024).

Deterministic versus ***stochastic***. ENSO amplitude increases weakly, but its skewness strongly increases as parameters controlling deterministic and stochastic nonlinearities are increased (An, Kim, & Timmermann, 2020; Jin et al., 2020; Figure 12b), but do deterministic or stochastic nonlinearities contribute most to ENSO asymmetry? Kim and An (2020) found that both contribute, with a stronger role of the deterministic nonlinearity. This is supported by Figure 12b that indicates a stronger sensitivity of the skewness to b than to B in the NRO.

Outlook. Several studies have attributed the more systematic phase transition after El Niño events to asymmetries in the amplitude or meridional structure of the wind anomalies and/or their southward migration during the event decay phase (Choi et al., 2013; Clarke & Zhang, 2019; Geng et al., 2019; Im et al., 2015; McGregor et al., 2012, 2022; Planton et al., 2018). This leads to an observed more efficient discharge after warm than after cold events. Although some aspects of the ENSO asymmetrical phase transitions are reproduced by the NRO (An, Kim, & Timmermann, 2020; Dommenget & Al-Ansari, 2023; Geng et al., 2019), more research is needed to investigate the minimum nonlinear terms and associated processes that would allow to reproduce realistic phase transition asymmetries.

5. Using the RO to Tackle ENSO Pressing Research Topics

5.1. Can the RO Account for ENSO Pattern Diversity?

Geometric approach. The RO uses a single variable T to represent ENSO-related SST variations. As discussed in Section 2, the mean PC1–PC2 relationship in Figure 3c captures key aspects of ENSO diversity, including the westward shift of La Niña events and the tendency for strong El Niño events to be CP-type. Williams and Patricola (2018) showed that the eastern edge of the western Pacific warm pool maps this mean PC1-PC2 relation. Thual and Dewitte (2023) adopted this approach, using a T variable that tracks warm pool displacement rather than temperature anomalies in a fixed region, leading to a similar equation as the RO but with a single quadratic nonlinearity. By applying a simple geometric transformation—shifting the climatological SST profile in response to warm pool displacement—this modified RO successfully reproduces key ENSO diversity features without

requiring an additional variable. However, it underestimates pattern diversity: in their model, the second EOF explains only 3% of SST variance, compared to 12% in observations. This limitation arises because a single T variable captures the mean PC1–PC2 relationship (Figure 3c) but not the full spread around it (e.g., the 2009–2010 CP El Niño, which exhibits a more negative PC2 than expected from the mean relation). Accurately reproducing the full range of ENSO diversity in Figure 3c requires one additional degree of freedom.

RO with 3 variables. Geng et al. (2020) extended the original RO model by adding an equation for SST variations in the central Pacific (T_C) to that of eastern Pacific SST (T_E). They specified a stronger zonal advective feedback in the central Pacific, and stronger thermocline feedback in the eastern Pacific, as suggested by previous work (Kug et al., 2009; Ren & Jin, 2013). Their model also features a wind stress that responds linearly to T_C, but nonlinearly to T_E (due to the SST threshold to trigger deep atmospheric convection) and multiplicative noise forcing that seems to play a significant role in generating ENSO pattern diversity (e.g., Fedorov et al., 2015; Hu et al., 2014). They find that the strength of the deterministic atmospheric nonlinearity plays a key role in controlling both the positive T_E and negative T_C skewness. It also generates a qualitatively similar PC1-PC2 nonlinear relation to that observed (Figure 13b), therefore reproducing observed ENSO spatial pattern asymmetries (eastward shift of the El Niño SST anomalies relative to those during La Niña). While points in the upper right quadrant of Figure 13 are rare, they correspond to extreme El Niño events (such as the 1982, 1997, or 2015 observed ones), which have devastating consequences (Santoso et al., 2017) and therefore are important to describe with the RO.

RO with four or more variables. Fang and Mu (2018) additionally included a fourth, central Pacific zonal current variable in order to explicitly represent the zonal advective feedback in that region. They demonstrate that increasing the strength of the central Pacific zonal advective feedback decreases the ENSO overall amplitude and period, and leads to more CP events. N. Chen et al. (2022) further added both stochastic forcing (including state-dependent forcing) and an additional stochastic equation to represent decadal changes in the strength of the Walker Cell, which in turn modulates the zonal advective feedback strength in the central Pacific. This model reproduces many crucial properties of the observed ENSO pattern diversity, including the T_E and T_C spectrums, occurrence frequency of CP and EP events, and main ENSO asymmetries. As the model of Geng et al. (2020), it generates a similar PC1–PC2 relation to that in observations (Figure 13a), that is, reproduces observed ENSO spatial asymmetries.

Minimal RO for representing diversity? The above RO extensions suggest that it is possible to produce a baseline ENSO pattern diversity without additional degree of freedoms, by using a surface variable that is nonlinearly related to T_E and T_C (Thual & Dewitte, 2023). More observed ENSO diversity features can nonetheless be obtained by adding additional degrees of freedom, yielding a 3 (Geng et al., 2020), 4 (Fang & Mu, 2018) or 6-dimensional (N. Chen et al., 2022) version of the RO. Those exploratory studies can all account for some aspects of ENSO diversity. More research is however needed to determine the requested minimal physics and. The models of Fang and Mu (2018) or N. Chen et al. (2022) both introduced a new prognostic equation for central Pacific currents, while its value is in principle set from the other RO parameters through the near-equatorial semi-geostrophic balance, indicating that such an equation may not be necessary. ENSO diversity has a strong decadal component, with CP or EP-dominated decades (e.g., Capotondi et al., 2020). Geng et al. (2020) and N. Chen et al. (2022) obtained such decadal ENSO diversity variations, respectively by imposing changes in the atmospheric nonlinearity or through an additional Walker Cell stochastic variable. However, such decadal ENSO diversity variations can also be observed in an intermediate coupled model with no prescribed decadal variation in either the atmospheric nonlinearity or the background Walker Cell (Geng & Jin, 2023a, 2023b). In other words, there is currently little consensus on whether ENSO decadal variations occur at random (Wittenberg et al., 2014), involve physical processes internal to the Pacific, or associated with interactions with the extra-tropics or other tropical basins (see Fedorov et al. (2020), Power et al. (2021), and Capotondi et al. (2023) for reviews). Recent studies suggest that the RO can capture aspects of ENSO diversity when the right nonlinearities are introduced, along with, potentially, an additional temperature variable. However, further research is needed to identify the minimal essential physics and assess its ability to explain decadal variations in ENSO diversity.

5.2. The Influence of Regional Processes Outside the Tropical Pacific

Introduction. The RO is derived on the basis that ENSO is primarily governed by dynamics internal to the tropical Pacific. However, previous studies suggested that SST variability outside of the tropical Pacific affects ENSO

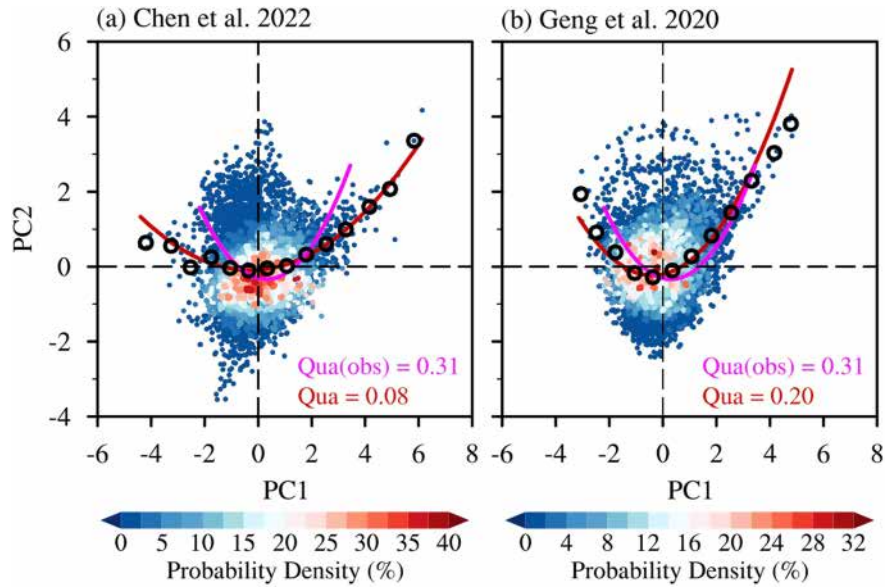

Figure 13. RO extensions can reproduce ENSO pattern diversity. Figure similar to Figure 3c (scatterplot between the first and second normalized principal components PC1 and PC2 of the tropical Pacific SST anomalies sliding 3-month averages), but here for 500-years simulations with two different extensions of the NRO with two SST variables for SST variations T_E in the eastern (Niño3) and T_C in the central-western (Niño4) equatorial Pacific: (a) N. Chen et al. (2022), (b) Geng et al. (2020). Equivalent values to PC1,2 in observations are obtained from a linear combination of their T_E, T_C time series as in Takahashi et al. (2011). The shading displays a kernel density estimate of the joint PC1, PC2 probability distribution. Black hollow circles represent the median PC2 value in 0.75-wide PC1 bins. Quadratic fits to the PC1, PC2 distribution are plotted in red, with the quadratic coefficient value indicated on each panel. The quadratic fit obtained from observed values on Figure 3c is plotted in magenta on both panels.

(see reviews by Cai et al. (2019), C. Wang (2018), and Kug et al. (2020)). These regions outside the tropical Pacific (Figure 14) include the tropical Indian Ocean (e.g., Izumo et al., 2010; Kug et al., 2006; J.-Y. Yu et al., 2002), tropical and subtropical Atlantic (e.g., Ham et al., 2013; C. Wang & Fiedler, 2006) and subtropical-extratropical Pacific (e.g., Vimont et al., 2001). We review the current state of knowledge on this topic under three working hypotheses: (a) ENSO influences other regions, but is not influenced by them; (b) coupled feedbacks between ENSO and other regions contribute to ENSO dynamics, but not to its predictability; (c) other regions can trigger ENSO events and contribute to ENSO predictability.

A null hypothesis. There is an unequivocal influence of ENSO on SST in many regions through atmospheric teleconnections (e.g., Taschetto et al., 2020). Extratropical low-frequency SST variability can largely be explained as being driven by a combination of atmospheric stochastic forcing (i.e., weather; Hasselmann, 1976) and remote ENSO forcing (e.g., Alexander et al., 2002). Much of the statistics of climate variability outside of the tropical Pacific—including their SSTs lead/lag correlations with ENSO—are consistent with the null hypothesis of a one-way forcing of ENSO on other regions (e.g., Jiang et al., 2021; Stuecker, 2018, 2023; Stuecker et al., 2017; W. Zhang et al., 2021). However, SST anomalies in some oceanic regions lead ENSO with correlations that significantly exceed values expected from this null hypothesis (e.g., Jourdain et al., 2016). Several studies also demonstrated a significant influence on ENSO through sensitivity experiments with numerical models (e.g., Dayan et al., 2015; Vimont et al., 2001).

Other regions influence ENSO. A second hypothesis is therefore that ENSO-driven SST signals in regions such as the tropical Indian Ocean (basin-wide warming or cooling that follows ENSO events; e.g., Xie et al., 2009), induce wind signals over the Pacific that feedback on ENSO, affecting its dynamics (e.g., Kug et al., 2006). Several studies using a variety of tools (the RO, observations, a hierarchy of climate models) for instance indicate that the "Indian Ocean capacitor effect" can either damp (e.g., Jansen et al., 2009) or stimulate (e.g., Dommenget & Yu, 2017; Dommenget et al., 2006) variability in the Pacific, and significantly contributes to ENSO phase transition (e.g., Annamalai et al., 2005; Kug & Kang, 2006) by enhancing the delayed negative feedback associated with ocean dynamics (Dommenget & Yu, 2017). The north Pacific Meridional mode

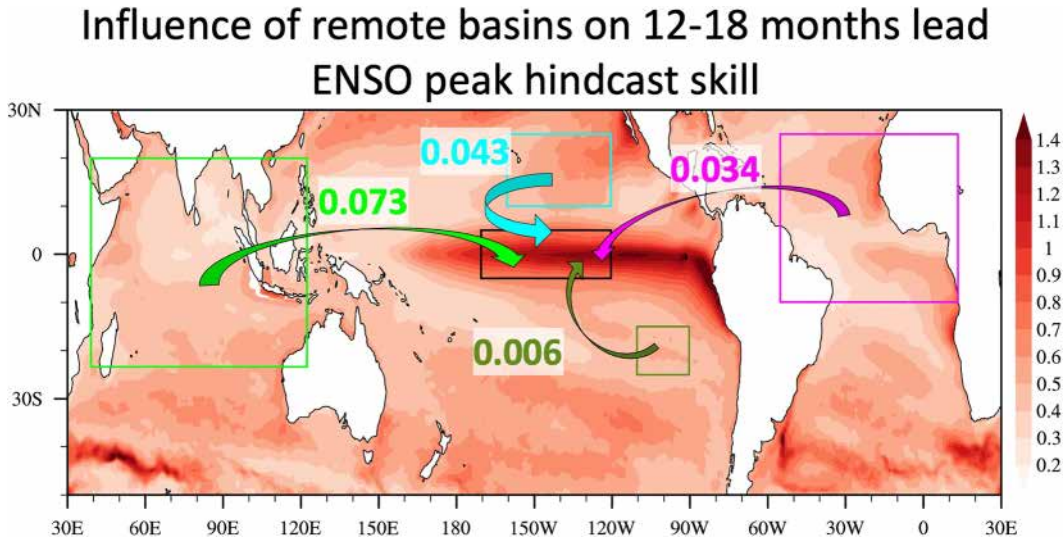

Figure 14. Extended recharge oscillator (XRO) estimate of the influence of remote basins on the 12–18 months lead ENSO peak hindcast skill. Map of the observed standard deviation of SST anomalies since 1980. The frames delineate the tropical Indian Ocean (light green), tropical north Atlantic (magenta), and the center of actions of the North (light blue) and South (dark green) Pacific Meridional Modes (NPMM and SPMM, respectively). The increase in the ENSO peak (Niño3.4 November–January average SST anomalies) 12–18 months lead correlation skill associated with accounting for each mode initial condition is indicated in the same color as the arrow, following the methodology of S. Zhao et al. (2024) and similar to their Figure 3. Higher values of this number indicate that the remote basin has a larger influence on the future evolution of ENSO. It is estimated from a NRO coupled to simple representations of various climate modes in each basin that are driven by stochastic and ENSO remote forcing and are feeding back on ENSO. The Indian Ocean contributes most to the skill increase, followed by the NPMM and tropical North Atlantic. The SPMM has only a weak influence on ENSO predictability. Note that those numbers are indicative, since they vary seasonally and are dependent on the target ENSO phase and RO dynamics details. They however illustrate the usefulness of the RO for studying ENSO interactions with regions outside the tropical Pacific.

(Chiang & Vimont, 2004) interactions with ENSO likewise have systematic impacts on its dynamics (Stuecker, 2018). In such cases, the SST variations in the remote region are caused by ENSO in the first place, and hence do not yield extra predictability (discussion in W. Zhang et al. (2021), Jiang et al. (2021), and Stuecker (2023)). For instance, the Indian Ocean basin mode appears to heavily influence ENSO dynamics but does not contribute to its predictability (Frauen & Dommenget, 2012; Jansen et al., 2009). The last working hypothesis is that climate variability independent of ENSO can induce wind changes over the tropical Pacific through atmospheric teleconnections, which can contribute to the evolution of ENSO events or trigger them (e.g., Ham et al., 2013; Izumo et al., 2010). In that case, an ENSO predictability gain is expected from considering these regions, as could for example, be the case for the tropical Atlantic (e.g., Chikamoto et al., 2020; Frauen & Dommenget, 2012).

The RO perspective. The RO has proven a useful tool for studying basin interactions (e.g., Dommenget & Yu, 2017; Frauen & Dommenget, 2012; Jansen et al., 2009; Jiang et al., 2021; Stuecker, 2023). There is growing evidence that interactions with the Indian Ocean "capacitor effect" can contribute to RO dynamics, that is, that RO parameters are also influenced by the Indian Ocean response to ENSO (Dommenget & Yu, 2017; Frauen & Dommenget, 2012; Jansen et al., 2009). On the other hand, the tropical Atlantic does not seem to contribute strongly to the RO parameters (Dommenget & Yu, 2017; Frauen & Dommenget, 2012; Jansen et al., 2009), but to predictability. The numerous studies that argue for an influence of regions outside the tropical Pacific on ENSO (see reviews by C. Wang (2018); Cai et al. (2019)) provide a strong support for going beyond the "ENSO rules" null hypothesis mentioned above. There is however a lack of consensus on which of the regions on Figure 14 have the strongest influence. A recent RO-based study has however made an important step in that direction (S. Zhao et al., 2024). This study performed ENSO hindcasts with an eXtended RO (XRO) that couples a NRO in the Pacific region with simple representations of climate modes in other regions, which feed back to ENSO. The other modes are modeled as seasonally modulated first order auto-regressive processes driven by a combination of stochastic atmospheric forcing and deterministic remote ENSO forcing (Stuecker et al., 2017). Considering initial

SST conditions from other regions strongly enhances ENSO predictability at lead times beyond 1 year, yielding similar scores to those obtained through deep-learning approaches, and outperforming dynamical models. This approach further allows a quantification of the dominant sources of ENSO predictability outside the tropical Pacific (Figure 14), with a dominant contribution from the tropical Indian Ocean, followed by the North Pacific and the tropical Atlantic. Thus, dynamical ENSO predictability as formulated in the RO is augmented by the relatively slow decay of initial conditions (i.e., damped persistence) of the other climate modes that can energize ENSO in the right seasons. This approach provides an interesting research avenue into climate mode interactions and their impact on seasonal predictability.

5.3. ENSO in a Warmer World

Mean state changes. Understanding how ENSO responds to anthropogenic forcing remains a major research topic. Observations and atmospheric reanalyses indicate a La Niña-like strengthening of the equatorial Pacific zonal SST gradient (i.e., less warming in the east) and Pacific Walker circulation over the last 40 years (e.g., Heede & Fedorov, 2023a; Lee et al., 2022; McGregor et al., 2014; Seager et al., 2022; Watanabe et al., 2024; Wills et al., 2022). In contrast, over the same period, most CMIP historical runs indicate a Walker circulation slowdown (or no change) and enhanced warming in the east (referred to as El Niño-like), which is expected to intensify in the future (Cai et al., 2014, 2015; Heede & Fedorov, 2021; Watanabe et al., 2024; Xie et al., 2010). Even the few models that reproduce the observed cooling trends in the Pacific over the historical period, later produce an "El Niño" like pattern and Walker cell slowdown (e.g., Cai et al., 2021; Gopika et al., 2024; Heede & Fedorov, 2023a). However, there is growing evidence that discrepancies between models and observations are not entirely due to internal variability (e.g., Heede & Fedorov, 2023a; Seager et al., 2022; Wills et al., 2022) and that models might also misrepresent the forced transient response of the tropical Pacific to the rising CO_2 concentrations. The large systematic biases in CMIP models (e.g., Planton, Guilyardi, et al., 2021; Section 2.4) may indeed affect the balance of processes that influence the warming pattern (e.g., Luo et al., 2018). Some processes, such as the less-efficient evaporative cooling feedback over cold water (e.g., Knutson & Manabe, 1995; Xie et al., 2010; L. Zhang & Li, 2014), favor more warming in the east, as seen in models. Other processes, such as the effect of aerosols (Heede & Fedorov, 2021) or the transient ocean thermostat mechanisms (e.g., Clement et al., 1996; Heede et al., 2020) can suppress eastern Pacific warming, as observed (see Watanabe et al.,'s 2024 review). The Bjerknes feedback appears to amplify the response (e.g., Fu & Fedorov, 2023; Knutson & Manabe, 1995; Vecchi et al., 2006), whether it is El Niño or La Niña-like. Overall, there is significant uncertainty regarding future changes in the tropical Pacific zonal SST gradient and circulation (Heede & Fedorov, 2021), but a more robust projected increase in upper-ocean thermal stratification due to surface-enhanced warming (e.g., Carréric et al., 2020). While simple box models can account for some of the CMIP projected changes (Fang et al., 2024; Heede et al., 2020; Z. Liu & Huang, 1997; Sun & Liu, 1996), there is currently no widely-accepted conceptual framework for the tropical Pacific mean state response to climate change.

Observed and projected ENSO changes. Observations and proxy data indicate an increasing ENSO amplitude since the mid twentieth century. The 1980s and 1990s exhibited the largest ENSO amplitude on record, dominated by strong EP events (see Fedorov et al. (2020) or Cai et al. (2021) for a review). After 2000, CP events became dominant, and ENSO average amplitude decreased slightly. These latter changes coincided with a strengthening of the Walker circulation. Earlier studies did not reach a consensus on future changes in modeled ENSO (e.g., Collins et al., 2010), but an increase and eastward shift of the rainfall response to ENSO was still highlighted (Cai et al., 2014). Further accounting for the model-dependent position of the ENSO anomaly position and narrowing CMIP to models that best describe ENSO diversity and/or extreme events yields a robust increase in EP and CP SST variability, and more frequent extreme El Niño and La Niña events in the future (Cai et al., 2021; Fredriksen et al., 2020; Shin et al., 2022). The most recent CMIP6 simulations also suggest that ENSO should become stronger across a broad range of climate scenarios (Cai et al., 2022; Heede & Fedorov, 2023b). Despite this emerging consensus, the above-mentioned uncertainties in the projected mean state changes by climate models, as well as their unrealistic ENSO dynamics linked to mean-state biases (e.g., Bayr et al., 2019; H. C. Chen et al., 2021; Kim & Jin, 2011) still undermines the confidence in those projections.

Processes responsible for ENSO changes. Several studies have investigated the factors responsible for the diversity of the projected ENSO changes in CMIP models. C. Chen et al. (2017) found that changes in the thermocline and advective feedbacks were most associated with ENSO amplitude changes, and interpreted these changes in terms of the mean equatorial upwelling. Zheng et al. (2016) on the other hand found that models

Table 3
Tropical Pacific Response to Anthropogenic Forcing Summary

	Mean state	ENSO
Observed trends since the 1980s	Walker cell intensification Stronger zonal SST gradient	Strong ENSO in the 1980s and 1990s, but weaker ENSO with dominant CP events after year 2000
Climate model projections	Walker cell slowdown Weaker zonal SST gradient	Amplified ENSO with more extreme El Niño and La Niña events
RO	No theory for mean state	RO not successful in explaining ENSO changes across different models
	No complete recipe for RO parameters dependency on mean state	Need for a RO that describes ENSO diversity and incorporates mean state changes

Note. This table summarizes Section 5.3 reviews of the tropical Pacific mean state (left column) and ENSO (right column) response to anthropogenic forcing over recent decades in observations (top row), in climate models future projections (middle row). The bottom row summarizes the current RO status in view of the mean state and ENSO response to anthropogenic forcing.

generating the strongest mean El Niño-like warming pattern produced the most consistent increase in EP SST variability, explaining it by a weakened barrier to deep convection. Heede and Fedorov (2023b) found that the reduction in the mean east-west SST gradient across the Pacific indeed favors a stronger ENSO, which they attribute to the effect of weaker trade winds (e.g., B. Zhao & Fedorov, 2020). Cai et al. (2014) emphasized that this weakened barrier to convection mostly enhances extreme rainfall, not the SST signature of extreme EP events. Several studies suggested that the enhanced vertical stratification due to surface-enhanced mean warming increases air-sea coupling and could be the main factor for the increase in ENSO variability (Cai et al., 2021; Carréric et al., 2020). The theoretical study of Thual et al. (2011) supported the idea that enhanced stratification should lead to a more unstable ENSO. More recently, Stuivenvolt-Allen et al. (2024) found that changes in the spatial structure of ENSO wind stress anomalies with global warming can also contribute to the strengthening of ENSO. The intensification of WWBs is another potential factor (Liang & Fedorov, 2024). Nevertheless, there is still no clear consensus on the processes responsible for the robust future increase in ENSO variability in CMIP models.

Using the RO to tackle ENSO changes. Only a few studies have so far used the RO framework to address ENSO changes under global warming. Dommenget and Vijayeta (2019) explain the average change in ENSO variance in 20 CMIP models by fitting an RO model to present and future simulations, but did not identify a clear dominant feedback that could explain the changes. Kim and Jin (2011) used the BWJ index (Equation 3; Jin et al., 2006, 2020) to explain changes in ENSO amplitude in 12 CMIP3 models. They could explain the amplitude changes in those models, but with a wide variety of processes involved. Heede and Fedorov (2023b) and Ferrett and Collins (2019) on the other hand showed that the BWJ index was not able to predict ENSO amplitude changes in several CMIP6 scenarios. Both studies pointed to the omission of some nonlinearities, such as the convective response to changes in background SST. Heede and Fedorov (2023b) also pointed to the possible effect of future changes in stochastic forcing. Table 3 synthesizes the main points in this section. We will discuss future perspectives for using the RO to investigate the response to climate change in Section 7.

6. Synthesis

Review concept. The key idea of this review is that a conceptual model of ENSO should encapsulate important knowledge about its essential physical processes, and be able to make quantitative prediction about its key properties, how they depend upon the tropical Pacific mean state, and therefore be able to explain the effect of model biases or of our changing climate on ENSO. In this review, we argue that the recharge oscillator is able to perform many of those tasks, and underline how it can be improved to answer today's important research questions.

RO and ENSO recipe. The low dimensionality of ENSO allows the RO to represent the system state with two variables, the central or eastern Pacific surface temperature T, and the oceanic heat content h (usually in the western Pacific, or over the entire equatorial Pacific), which represents the ENSO "memory" associated with slow oceanic dynamics. In its simplest form, the linear RO (LRO) key ingredients are the Bjerknes feedback R

(Figure 6), which represents the tendency of SST anomalies to self-amplify (or decay) through an ocean-atmosphere feedback loop, and the delayed negative feedback associated with oceanic dynamics. The western Pacific heat content indeed decreases (increases) in response to the westerly (easterly) wind anomalies during El Niño (La Niña), and favors a cooling (warming) that eventually switches the system to the opposite phase (Figure 7). Fitting the LRO to observations yields an asymptotically stable system, in which variability can be sustained by adding stochastic forcing, leading to the stochastic RO (SRO). This stochastic forcing represents random atmospheric synoptic perturbations known as Westerly Wind Bursts (WWBs). The last level of complexity involves nonlinearities, yielding the nonlinear RO (NRO). One important nonlinearity relates to the state-dependency of WWBs: they are more numerous and stronger during El Niño than during La Niña, which is often referred to as multiplicative noise. Various other sources of atmospheric or oceanic nonlinearities can be represented as an extra quadratic (i.e., symmetry-breaking) or cubic (i.e., amplitude-limiting) nonlinearity. The RO parameters can be considered as having a seasonal dependency, leading to, for example, a seasonal NRO. The RO parameters can either be obtained by fitting the RO to T and h data, or by using the BWJ index analytical formula (Jin et al., 2020).

Key properties. ENSO core properties include its amplitude, seasonality, dominant timescale, asymmetries, and pattern diversity (some ENSO events have maximum amplitude in the eastern Pacific, and some in the central Pacific). Some forms of the RO can provide quantitative predictions for the first four properties. We tested those quantitative predictions on observations and preindustrial simulations from the CMIP6 database. Fitting the RO to observations and CMIP5/6 models always yields an asymptotically stable system. In this regime, the observed and CMIP6 ENSO amplitudes are mostly controlled by the RO growth rate (BWJ index real part, $(R-\varepsilon)/2$) and by the stochastic forcing amplitude. Fitting a seasonally-dependent Bjerknes feedback $R(t)$ allows the seasonal RO to reproduce the observed peak ENSO amplitude in boreal winter, as well as the observed "spring predictability barrier." It also yields a reasonable estimate of the ENSO amplitude seasonality in models. ENSO has a broad spectral peak in the 3–7 years band. The BWJ imaginary part (whose period can be approximated as $2\pi/(F_1F_2)^{1/2}$) is linearly related to ENSO dominant period in observations and CMIP6 models (with a 30% underestimation). The observed positively skewed T distribution can be reproduced by the nonlinear RO, when considering multiplicative noise and symmetry-breaking nonlinearities. Overall, the literature and analyses in this paper demonstrate that the RO can quantitatively predict the most important ENSO properties in observations and CMIP models.

RO and ENSO pattern diversity. ENSO diversity refers to variations in the location of peak temperature anomalies along the equator, with La Niña events typically shifted westward and strong El Niño events favoring the eastern Pacific (EP type). The RO can account for these features by replacing the T variable with one representing the eastern edge of the western Pacific warm pool (Thual & Dewitte, 2023). However, fully capturing ENSO diversity—such as why moderate El Niño events can be either CP-type (e.g., 2009–2010, Figure 3g) or lack a clear classification (e.g., 2006–2007, Figure 3f)—requires at least two SST variables for western and eastern Pacific anomalies (N. Chen et al., 2022; Geng et al., 2020). In both approaches, introducing a quadratic nonlinearity in the eastern Pacific SST equation plays a key role in enabling shifts between CP and EP events. Further research is needed to identify the minimal model capable of capturing ENSO pattern diversity (as previous studies use between 2 and 5 state variables) and to pinpoint the essential nonlinearity responsible for extreme El Niño events, which Geng et al. (2020) attribute to deep atmospheric convection.

RO and inter-basin interactions. The RO is based on the premises that all the involved dynamics occur within the tropical Pacific. Over the last 10 years, a lot of research has pointed to an influence of other tropical basins and of the midlatitude Pacific on ENSO (see reviews by C. Wang (2018), Cai et al. (2019), and Kug et al. (2020)). The RO has proven a useful tool to study the effect of basin interactions with ENSO. ENSO-driven variability in remote regions (e.g., the average Indian Ocean response to ENSO) drives wind signal over the Pacific that systematically contributes to ENSO dynamics, as revealed from the RO parameter values (e.g., Dommenget & Yu, 2017). Such systematic influences have a weak impact on ENSO predictability. SST variability independent of ENSO can on the other hand influence the ENSO evolution through teleconnections, contributing to its predictability but not to its internal dynamics, as could be the case for the tropical Atlantic (e.g., Frauen & Dommenget, 2012). A recent study further quantifies the influence of individual basins on ENSO, by coupling an NRO in the Pacific with simple representations of SST variability in other basins (S. Zhao et al. (2024)), concluding that the initial SST states of the Indian Ocean, North Pacific, and tropical Atlantic enhance long-range ENSO predictability.

RO and climate change. ENSO response to climate change remains one of the major outstanding research questions of climate sciences, and here we summarize the RO relevance to this question. Our confidence in ENSO future projections is undermined by the conflicting equatorial Pacific long-term trends in observations and models, and by persistent model mean state biases and resulting deficiencies in modeled ENSO dynamics. There is however growing consensus, based on CMIP models, for a future increase by century-end of both CP and EP events' amplitude, associated with more prevalent extreme El Niño and La Niña events (Cai et al., 2021). The mechanism behind this increase is not fully understood, with some studies pointing to the effect of enhanced vertical stratification, which strengthens ocean-atmosphere coupling; and others to the future "El Niño-like" warming pattern characterized by the weakening of the Pacific Walker circulation and trade winds. So far, applying the RO or BWJ index to ENSO change has had limited success in identifying a clear mechanism that would be responsible for the projected change across different models.

7. Way Forward: Nine Important Research Questions About ENSO and the RO

7.1. RO Representation of ENSO

Processes behind RO parameters? The analytical theory for each of the RO parameters summarized by Jin et al. (2020) provides a useful tool for linking these parameters to various physical processes. Yet, some parameters are associated with several distinct physical processes, whose respective contributions are not easily quantified. A good example are quadratic nonlinearities (parameter b), that contribute to ENSO amplitude asymmetry (Section 4.4) and diversity (Section 5.1). Various oceanic and atmospheric processes have been suggested to contribute to those nonlinearities, but their respective contributions are not well identified. As initially suggested by Jin et al. (2020), heat budgets in ocean general circulation models, or sensitivity experiments such as those of Srinivas et al. (2024) and F. Liu et al. (2024) should help to better identify processes associated with various RO parameters.

What choice for h? The initial RO theory (Jin, 1997a, 1997b) and its recent presentation (Jin et al., 2020) specify that the ocean memory parameter h should be the western equatorial Pacific heat content. However, inspired by Meinen and McPhaden (2000), many studies since Burgers et al. (2005) instead fit the RO to time series of the Warm Water Volume (WWV), that is, the oceanic heat content for the entire tropical band. Several studies indicate that this variable contains a fast timescale associated with the Kelvin wave response, that is in principle represented within the Bjerknes feedback term RT (e.g., Izumo et al., 2019; Neske & McGregor, 2018), and can be analytically derived from the RO framework (S. Zhao et al., 2021). Recent work has also suggested other, modified indices for describing ENSO memory, for example, accounting for southwestern equatorial Pacific heat content (Izumo & Colin, 2022), or using the maximum thermal gradient (rather than the 20°C) depth to compute h (Dommenget et al., 2023). Finally, we note that little work has been undertaken since Jin (1997b) for describing the equatorial wave dynamics associated with h adjustment (e.g., respective roles of reflections at both boundaries). We feel that a better understanding of the best choice, timescale and dynamics of the RO h variable is needed.

Minimum RO for diversity and extremes? Some aspects of ENSO diversity (westward shifted La Niña, capacity to produce EP-type extreme events) can be accounted for by introducing a T variable that maps the warm pool displacements. Some other aspects (such as the fact that some moderate El Niño events can either be of the CP or EP type) require additional state variables. In both cases, considering nonlinear processes is important. More research is however needed to develop a minimum model for RO diversity and extremes, with questions such as: (a) whether it can predict the different diversity features in CMIP6 models, (b) what the minimum model required is (models with up to 6-dimensions have been proposed), (c) what the key non-linearities are and how they should be formulated. These are particularly important questions, considering that resolving ENSO diversity is key to understanding ENSO's response to climate change (see below).

Cycle or series of events? Kessler (2002) and Philander and Fedorov (2003) wondered if ENSO was a cycle or a series of events, that is, where its decay time is equivalent (cycle), or much shorter (series of events) than its oscillation timescale. The fundamental idea behind the RO is that of a harmonic oscillator with inherent cyclicity. The idea is supported by a phase-space analysis of ENSO (Dommenget & Al-Ansari, 2023). There are however multiple lines of evidence that stochastic forcing by WWBs play a key role in triggering and/or amplifying ENSO events, which are consistent with the idea that some events are noise-driven rather than the result of cyclicity. Here, we argue that ENSO sometimes displays a cyclic behavior, and sometimes develops under the effect of

noise forcing with little influence from the previous event (Dommenget & Al-Ansari, 2023; Philander & Fedorov, 2003). For instance, extreme El Niño events in the observed record (Figure 2c) are systematically followed by La Niña (often 2-years La Niña). The strong cyclic behavior after strong El Niño could be associated with a more efficient recharge process during the peak of extreme El Niño events (Clarke & Zhang, 2019; Im et al., 2015; McGregor et al., 2022) whose effects can be incorporated in the RO through a nonlinearity in the recharge process.

7.2. Application to Important ENSO Research Questions

RO forecasts? In this review, we evaluated the capacity of the RO to reproduce ENSO key properties, but not its capacity to forecast ENSO. This has so far been done only in a handful of studies (Fang & Chen, 2023; S. Zhao et al., 2024). S. Zhao et al. (2024) in particular demonstrated that the NRO achieves similar scores to those obtained by state-of-the art initialized CGCMs. In the future, we recommend that extensions or refinements to the RO are tested in terms of their hindcast capacity, including for CP and EP events separately for RO versions with more than one SST variable.

Inter-basin interactions? We saw in Section 5.2 that there is ample evidence for other basins influencing ENSO core dynamics and/or contributing to the genesis of ENSO events. Consequently, many climate modes have been proposed to have an influence on ENSO. More quantification of the influences of various climate modes on ENSO are needed, whether they contribute to ENSO predictability (i.e., are independent of ENSO but can contribute to its evolution) or part of ENSO dynamics in a wider sense (i.e., are a response to ENSO that feedbacks on ENSO, with no gain in predictability). The RO has also proven a useful tool to provide a conceptual understanding of basin interactions associated with ENSO (e.g., Dommenget & Yu, 2017; Stuecker, 2023). Such studies need to be encouraged. S. Zhao et al. (2024) for instance demonstrated a clear long-range ENSO forecast skill increase from accounting feedbacks from other basins, with influences from the tropical Indian Ocean, North Pacific and tropical Atlantic ocean.

Multidecadal variability? An issue that has been little discussed so far is tropical Pacific natural multidecadal variability (see reviews by Fedorov et al. (2020), Power et al. (2021), and Capotondi et al. (2023)). This multidecadal variability is seen in many aspects of ENSO, including its amplitude, skewness, pattern diversity, or relation between ocean heat content and El Niño. There are two ways to consider this decadal variability: (a) as being the result of changes in ENSO dynamics associated with the mean state modulation (that mean state modulation being potentially due to long-memory processes such as the oceanic tunnel from mid latitude or influences from other tropical basins e.g., Fedorov et al., 2020); (b) as being the result of stochastic forcing, with no underlying changes in ENSO dynamics or memory effects (e.g., Wittenberg et al., 2014). Kim and An (2020) for instance demonstrated that decadally-varying RO parameters did allow the RO to reproduce observed decadal changes in ENSO amplitude and skewness, providing some support for (a). The NRO with stochastic forcing can on the other hand serve as a good null hypothesis based on (b).

RO parameters from mean state? The analytical theory for the linear RO parameters (Jin et al., 2020) allows linkage between those parameters and the tropical Pacific mean state. It is limited, however, by: (a) the fact that it does not yet account for nonlinearities, and (b) it relies on empirical estimates of some coupling parameters that may themselves depend on the mean state (e.g., coupling between the thermocline depth and surface temperature anomalies, wind stress-SST coupling, etc.). This limits the usefulness of this theory for explaining the effect of model biases or of mean states under different climates on ENSO properties. More work is thus needed on a more complete theory of the RO parameter values and underlying processes.

Cross-breeding with deep learning. Artificial intelligence and deep learning has undergone a fast development in recent years, and has recently been applied quite successfully to ENSO forecasting (e.g., Ham et al., 2019; Mu et al., 2021; R.-H. Zhang et al., 2024). It has also been applied to investigate a minimal RO-based model for reproducing ENSO diversity (Y. Zhang et al., 2024). There is probably a lot of potential for leveraging the power of deep learning approaches to improve the RO or related tools. For instance, these approaches could complement theoretical work for obtaining nonlinear relations between the RO parameters and mean state descriptors based on the large databases provided by CMIP simulations.

ENSO in a warmer world? A key research question about ENSO is its response to climate change (Section 5.3, Table 3). This is a challenging question because of uncertainties in: (a) the tropical Pacific mean state future

evolution; (b) ENSO dynamics; and (c) ENSO projections in climate models. There are several possible RO-based research avenues. Considering ENSO diversity, and more specifically extreme El Niño events, is key for identifying a robust increase in ENSO amplitude in climate models (Cai et al., 2021; Heede & Fedorov, 2023b). This suggests that a RO model that resolves extreme El Niño events and ENSO diversity, and includes the associated nonlinearities would be a better tool to explain the ENSO future evolution in climate models. Another perspective is to investigate the RO sensitivity to two key features of the response to climate change in observations and models: the change in the zonal SST gradient (which decreases in most models, but has increased over the last decades in observations) and the increase in vertical stratification (identified as a key driver by Cai et al. (2021)). A third way forward is to develop tools that can link the RO parameters with the mean state (previous paragraph). The last, most ambitious, goal would be to develop a conceptual model that can also account for the tropical Pacific mean state, and its response to climate change.

7.3. Community RO Model

Technical paper and online code. One of the tasks that the ENSO conceptual model working group will soon undertake is to publish a technical paper on the RO technical implementation and numerics, along with a RO tools distribution in python. This distribution will include the LRO, SRO, and NRO as described in the current article and Jin et al. (2020), including seasonally-dependent versions, and parameter values from fits to various observational products and CMIP6 models. It will also include tools for fitting RO parameters to observed or model data, and some codes for analytical formulae (e.g., ENSO amplitude, period…). This is not a research question, but certainly an important undertaking for fostering a better use of this powerful tool by the community, and for teaching ENSO dynamics.

Data Availability Statement

Analyses and figures in this paper rely on publicly available data sources. They include ORAS5 re-analysis (Copernicus Climate Change Service, Climate Data Store, 2021); Tropflux (Indian National Centre for Ocean Information Services, 2024); HadiSST (Met Office Hadley Centre, 2021), and Globcurrent (European Union-Copernicus Marine Service, 2023) data. We acknowledge the World Climate Research Programme, which, through its Working Group on Coupled Modeling, coordinated and promoted CMIP6. We thank the climate modeling groups for producing and making available their model output, the Earth System Grid Federation (ESGF) for archiving the data and providing access (Program for Climate Model Diagnosis and Intercomparison, Lawrence Livermore National Laboratory, 2024b). Data sets were analyzed using the CLIVAR ENSO metrics package (Planton, Guilyardi, et al., 2021; Program for Climate Model Diagnosis and Intercomparison, Lawrence Livermore National Laboratory, 2024a).

Acknowledgments
Most authors of the review are members of the CLIVAR (Climate and Ocean -Variability, Predictability, and Change) Pacific Region Panel working group on conceptual models of ENSO. This group of ∼20 ENSO experts met through videoconferences in 2021–2022 and during a CLIVAR workshop in Melbourne, Australia in February 2023. This review is one of the achievements of that working group. We acknowledge the logistical and financial support from the CLIVAR International Project Office. JV was supported by the French Agence Nationale pour la Recherche (ANR) ARiSE Grant (ANR-18-CE01-0012). MFS was supported by the NSF Grant AGS-2141728. This is an IPRC publication X and SOEST contribution Y. NC is grateful to acknowledge the support of the Office of Naval Research (ONR) N00014-24-1-2244. AVF was supported by grants from NASA (80NSSC21K0558), NOAA (NA20OAR4310377), DOE (DE-SC0023134), and ANR (ANR-18-MPGA-0001, France). AC was supported by grants from the NOAA Climate Variability and Predictability Program (NA24OARX431C0024-T1-01) and DOE (DE-SC0023228). PMEL contribution no. 5662. SOEST contribution no. 11909. IPRC contribution no. 1635.

References

Abellán, E., & McGregor, S. (2016). The role of the southward wind shift in both the seasonal synchronization and duration of ENSO events. *Climate Dynamics*, *47*(1), 509–527. https://doi.org/10.1007/s00382-015-2853-1

Abellán, E., McGregor, S., & England, M. H. (2017). Analysis of the southward wind shift of ENSO in CMIP5 models. *Journal of Climate*, *30*(7), 2415–2435. https://doi.org/10.1175/JCLI-D-16-0326.1

Ahn, M. S., Kim, D., Sperber, K. R., Kang, I. S., Maloney, E., Waliser, D., & Hendon, H. (2017). MJO simulation in CMIP5 climate models: MJO skill metrics and process-oriented diagnosis. *Climate Dynamics*, *49*(11–12), 4023–4045. https://doi.org/10.1007/s00382-017-3558-4

Alexander, M. A., Bladé, I., Newman, M., Lanzante, J. R., Lau, N., & Scott, J. D. (2002). The atmospheric bridge: The influence of ENSO teleconnections on air–sea interaction over the global oceans. *Journal of Climate*, *15*(16), 2205–2231. https://doi.org/10.1175/1520-0442(2002)015<2205:TABTIO>2.0.CO;2

An, S.-I. (2008). Interannual variations of the tropical ocean instability wave and ENSO. *Journal of Climate*, *21*(15), 3680–3686. https://doi.org/10.1175/2008JCLI1701.1

An, S.-I., & Jin, F.-F. (2004). Nonlinearity and asymmetry of ENSO. *Journal of Climate*, *17*, 2399–2412.

An, S.-I., & Jin, F.-F. (2011). Linear solutions for the frequency and amplitude modulation of ENSO by the annual cycle. *Tellus*, *63A*(2), 238–243. https://doi.org/10.1111/j.1600-0870.2010.00482.x

An, S. I., & Kim, J. W. (2017). Role of nonlinear ocean dynamic response to wind on the asymmetrical transition of El Niño and La Niña. *Geophysical Research Letters*, *44*(1), 393–400. https://doi.org/10.1002/2016gl071971

An, S. I., & Kim, J. W. (2018). ENSO transition asymmetry: Internal and external causes and intermodel diversity. *Geophysical Research Letters*, *45*(10), 5095–5104. https://doi.org/10.1029/2018gl078476

An, S.-I., Kim, S.-K., & Timmermann, A. (2020). Fokker-Planck dynamics of the El Niño-Southern Oscillation. *Scientific Reports*, *10*(1), 16282. https://doi.org/10.1038/s41598-020-73449-7

An, S. I., Tziperman, E., Okumura, Y. M., & Li, T. (2020). ENSO irregularity and asymmetry. *El Niño Southern Oscillation in a Changing Climate*, 153–172. https://doi.org/10.1002/9781119548164.ch7

Annamalai, H., Potemra, J., Murtugudde, R., & McCreary, J. P. (2005). Effect of preconditioning on the extreme climate events in the tropical Indian Ocean. *Journal of Climate*, *18*(17), 3450–3469. https://doi.org/10.1175/jcli3494.1

Barnston, A. G., Tippett, M. K., L'Heureux, M. L., Li, S., & DeWitt, D. G. (2012). Skill of real-time seasonal ENSO model predictions during 2002–11: Is our capability increasing? *Bulletin of the American Meteorological Society*, *93*(5), 631–651. https://doi.org/10.1175/bams-d-11-00111.1

Battisti, D. S., & Hirst, A. C. (1989). Interannual variability in the tropical atmosphere-ocean model: Influence of the basic state, ocean geometry and nonlineary. *Journal of the Atmospheric Sciences*, *45*, 1687–1712.

Bayr, T., Lübbecke, J. F., Vialard, J., & Latif, M. (2024). Equatorial Pacific cold tongue bias degrades simulation of ENSO asymmetry due to underestimation of strong eastern Pacific El Niños. *Journal of Climate*, *37*(23), 6167–6182.

Bayr, T., Wengel, C., Latif, M., Dommenget, D., Lübbecke, J., & Park, W. (2019). Error compensation of ENSO atmospheric feedbacks in climate models and its influence on simulated ENSO dynamics. *Climate Dynamics*, *53*(1–2), 155–172. https://doi.org/10.1007/s00382-018-4575-7

Bellenger, H., Guilyardi, E., Leloup, J., Lengaigne, M., & Vialard, J. (2014). ENSO representation in climate models: From CMIP3 to CMIP5. *Climate Dynamics*, *42*(7–8), 1999–2018. https://doi.org/10.1007/s00382-013-1783-z

Bjerknes, J. (1966). A possible response of the atmospheric Hadley circulation to equatorial anomalies of ocean temperature. *Tellus*, *18*(4), 820–829. https://doi.org/10.1111/j.2153-3490.1966.tb00303.x

Bjerknes, J. (1969). Atmospheric teleconnections from the equatorial Pacific. *Monthly Weather Review*, *97*(3), 163–172. https://doi.org/10.1175/1520-0493(1969)097<0163:atftep>2.3.co;2

Boulanger, J. P., & Menkès, C. (1999). Long equatorial wave reflection in the Pacific Ocean from TOPEX/POSEIDON data during the 1992–1998 period. *Climate Dynamics*, *15*(3), 205–225. https://doi.org/10.1007/s003820050277

Burgers, G., Jin, F.-F., & Van Oldenborgh, G. J. (2005). The simplest ENSO recharge oscillator. *Geophysical Research Letters*, *32*(13), L13706. https://doi.org/10.1029/2005GL022951

Cai, W., Borlace, S., Lengaigne, M., van Rensch, P., Collins, M., Vecchi, G., et al. (2014). Increasing frequency of extreme El Niño events due to greenhouse warming. *Nature Climate Change*, *4*(2), 111–116. https://doi.org/10.1038/nclimate2100

Cai, W., Ng, B., Geng, T., Jia, F., Wu, L., Wang, G., et al. (2023). Anthropogenic impacts on twentieth-century ENSO variability changes. *Nature Reviews Earth & Environment*, *4*(6), 1–12. https://doi.org/10.1038/s43017-023-00427-8

Cai, W., Ng, B., Wang, G., Santoso, A., Wu, L., & Yang, K. (2022). Increased ENSO sea surface temperature variability under four IPCC emission scenarios. *Nature Climate Change*, *12*(3), 228–231. https://doi.org/10.1038/s41558-022-01282-z

Cai, W., Santoso, A., Collins, M., Dewitte, B., Karamperidou, C., Kug, J. S., et al. (2021). Changing El Niño–Southern Oscillation in a warming climate. *Nature Reviews Earth & Environment*, *2*(9), 628–644. https://doi.org/10.1038/s43017-021-00199-z

Cai, W., Wang, G., Santoso, A., McPhaden, M. J., Wu, L., Jin, F.-F., et al. (2015). Increasing frequency of extreme La Niña events induced by greenhouse warming. *Nature Climate Change*, *5*(2), 132–137. https://doi.org/10.1038/nclimate2492

Cai, W., Wu, L., Lengaigne, M., Li, T., McGregor, S., Kug, J. S., et al. (2019). Pantropical climate interactions. *Science*, *363*(6430), eeav4236. https://doi.org/10.1126/science.aav4236

Cane, M. A., & Zebiak, S. E. (1985). A theory for El Niño and the Southern Oscillation. *Science*, *228*(4703), 1085–1087. https://doi.org/10.1126/science.228.4703.1085

Capotondi, A., McGregor, S., McPhaden, M. J., Cravatte, S., Holbrook, N. J., Imada, Y., et al. (2023). Mechanisms of tropical Pacific decadal variability. *Nature Reviews Earth & Environment*, *4*(11), 1–16. https://doi.org/10.1038/s43017-023-00486-x

Capotondi, A., Sardeshmukh, P. D., & Ricciardulli, L. (2018). The nature of the stochastic wind forcing of ENSO. *Journal of Climate*, *31*(19), 8081–8099. https://doi.org/10.1175/jcli-d-17-0842.1

Capotondi, A., Wittenberg, A. T., Kug, J. S., Takahashi, K., & McPhaden, M. J. (2020). ENSO diversity. *El Niño Southern Oscillation in a Changing Climate*, 65–86. https://doi.org/10.1002/9781119548164.ch4

Capotondi, A., Wittenberg, A. T., Newman, M., Di Lorenzo, E., Yu, J. Y., Braconnot, P., et al. (2015). Understanding ENSO diversity. *Bulletin of the American Meteorological Society*, *96*(6), 921–938. https://doi.org/10.1175/BAMS-D-13-00117.1

Carréric, A., Dewitte, B., Cai, W., Capotondi, A., Takahashi, K., Yeh, S. W., et al. (2020). Change in strong Eastern Pacific El Niño events dynamics in the warming climate. *Climate Dynamics*, *54*(1–2), 901–918. https://doi.org/10.1007/s00382-019-05036-0

Chen, C., Cane, M. A., Wittenberg, A. T., & Chen, D. (2017). ENSO in the CMIP5 simulations: Life cycles, diversity, and responses to climate change. *Journal of Climate*, *30*(2), 775–801. https://doi.org/10.1175/jcli-d-15-0901.1

Chen, H. C., Fei-Fei-Jin, Zhao, S., Wittenberg, A. T., & Xie, S. (2021). ENSO dynamics in the E3SM-1-0, CESM2, and GFDL-CM4 climate models. *Journal of Climate*, *34*(23), 9365–9384.

Chen, H.-C., & Jin, F.-F. (2020). Fundamental behavior of ENSO phase locking. *Journal of Climate*, *33*(5), 1953–1968. https://doi.org/10.1175/JCLI-D-19-0264.1

Chen, H.-C., & Jin, F.-F. (2022). Dynamics of ENSO phase-locking and its biases in climate models. *Geophysical Research Letters*, *49*(3), e2021GL097603. https://doi.org/10.1029/2021GL097603

Chen, N., Fang, X., & Yu, J. Y. (2022). A multiscale model for El Niño complexity. *npj Climate and Atmospheric Science*, *5*(1), 16. https://doi.org/10.1038/s41612-022-00241-x

Chiang, J. C. H., & Vimont, D. J. (2004). Analogous Pacific and Atlantic meridional modes of tropical atmosphere–ocean variability. *Journal of Climate*, *17*(21), 4143–4158. https://doi.org/10.1175/jcli4953.1

Chikamoto, Y., Johnson, Z. F., Simon Wang, S.-Y., McPhaden, M. J., & Mochizuki, T. (2020). El Niño Southern Oscillation evolution modulated by Atlantic forcing. *Journal of Geophysical Research: Oceans*, *125*(8), e2020JC016318. https://doi.org/10.1029/2020JC016318

Choi, K. Y., Vecchi, G. A., & Wittenberg, A. T. (2013). ENSO transition, duration, & amplitude asymmetries: Role of the nonlinear wind stress coupling in a conceptual model. *Journal of Climate*, *26*(23), 9462–9476. https://doi.org/10.1175/JCLI-D-13-00045.1

Clarke, A. J. (2014). El Niño physics and El Niño predictability. *Annual Review of Marine Science*, *6*(1), 79–99. https://doi.org/10.1146/annurev-marine-010213-135026

Clarke, A. J., & Van Gorder, S. (2003). Improving El Niño prediction using a space-time integration of Indo-Pacific winds and equatorial Pacific upper ocean heat content. *Geophysical Research Letters*, *30*(7), 1399. https://doi.org/10.1029/2002GL016673

Clarke, A. J., & Zhang, X. (2019). On the physics of the warm water volume and El Niño/La Niña predictability. *Journal of Physical Oceanography*, *49*(6), 1541–1560. https://doi.org/10.1175/jpo-d-18-0144.1

Clement, A. C., Seager, R., Cane, M. A., & Zebiak, S. E. (1996). An ocean dynamical thermostat. *Journal of Climate*, *9*, 2190–2196. https://doi.org/10.1175/1520-0442(1996)009<2190:aodt>2.0.co;2

Collins, M., An, S. I., Cai, W., Ganachaud, A., Guilyardi, E., Jin, F. F., et al. (2010). The impact of global warming on the tropical Pacific Ocean and El Niño. *Nature Geoscience*, *3*(6), 391–397. https://doi.org/10.1038/ngeo868

Copernicus Climate Change Service, Climate Data Store. (2021). ORAS5 global ocean reanalysis monthly data from 1958 to present [Dataset]. *Copernicus Climate Change Service (C3S) Climate Data Store (CDS)*. https://doi.org/10.24381/cds.67e8eeb7

Dayan, H., Izumo, T., Vialard, J., Lengaigne, M., & Masson, S. (2015). Do regions outside the tropical Pacific influence ENSO through atmospheric teleconnections? *Climate Dynamics*, *45*(3–4), 583–601. https://doi.org/10.1007/s00382-014-2254-x

Delecluse, P., Davey, M. K., Kitamura, Y., Philander, S. G. H., Suarez, M., & Bengtsson, L. (1998). Coupled general circulation modeling of the tropical Pacific. *Journal of Geophysical Research*, *103*(C7), 14357–14373. https://doi.org/10.1029/97JC02546

Deser, C., & Wallace, J. M. (1987). El Niño events & their relation to the southern oscillation: 1925–1986. *Journal of Geophysical Research*, *92*, 14189–14196.

Ding, H., Newman, M., Alexander, M. A., & Wittenberg, A. T. (2018). Skillful climate forecasts of the tropical Indo-Pacific Ocean using model-analogs. *Journal of Climate*, *31*(14), 5437–5459. https://doi.org/10.1175/jcli-d-17-0661.1

Dommenget, B. D., & Al-Ansari, M. (2023). Asymmetries in the ENSO phase space. *Climate Dynamics*, *60*(7), 2147–2166. https://doi.org/10.1007/s00382-022-06392-0

Dommenget, D., Bayr, T., & Frauen, C. (2013). Analysis of the non-linearity in the pattern and time evolution of El Niño Southern Oscillation. *Climate Dynamics*, *40*(11–12), 2825–2847. https://doi.org/10.1007/s00382-012-1475-0

Dommenget, D., Priya, P., & Vijayeta, A. (2023). ENSO phase space dynamics with an improved estimate of the thermocline depth. *Climate Dynamics*, *61*(11), 5767–5783. https://doi.org/10.1007/s00382-023-06883-8

Dommenget, D., Semenov, V., & Latif, M. (2006). Impacts of the tropical Indian and Atlantic Oceans on ENSO. *Geophysical Research Letters*, *33*(11), L11701. https://doi.org/10.1029/2006GL025871

Dommenget, D., & Vijayeta, A. (2019). Simulated future changes in ENSO dynamics in the framework of the linear recharge oscillator model. *Climate Dynamics*, *53*(7–8), 4233–4248. https://doi.org/10.1007/s00382-019-04780-7

Dommenget, D., & Yu, Y. (2016). The seasonally changing cloud feedbacks contribution to the ENSO seasonal phase-locking. *Climate Dynamics*, *47*(12), 3661–3672. https://doi.org/10.1007/s00382-016-3034-6

Dommenget, D., & Yu, Y. (2017). The effects of remote SST forcings on ENSO dynamics, variability and diversity. *Climate Dynamics*, *49*(7–8), 2605–2624. https://doi.org/10.1007/s00382-016-3472-1

Eisenman, I., Yu, L., & Tziperman, E. (2005). Westerly wind bursts: ENSO's tail rather than the dog? *Journal of Climate*, *18*(24), 5224–5238. https://doi.org/10.1175/jcli3588.1

European Union-Copernicus Marine Service. (2023). Global Total (COPERNICUS-GLOBCURRENT), Ekman and Geostrophic currents at the surface and 15m [Dataset]. *Mercator Ocean International*. https://doi.org/10.48670/MDS-00327

Eyring, V., Bony, S., Meehl, G. A., Senior, C. A., Stevens, B., Stouffer, R. J., & Taylor, K. E. (2016). Overview of the Coupled Model Intercomparison Project Phase 6 (CMIP6) experimental design and organization [Dataset]. *Geoscientific Model Development*, *9*(5), 1937–1958. https://doi.org/10.5194/gmd-9-1937-2016

Fang, X., & Chen, N. (2023). Quantifying the predictability of ENSO complexity using a statistically accurate multiscale stochastic model and information theory. *Journal of Climate*, *36*(8), 2681–2702. https://doi.org/10.1175/jcli-d-22-0151.1

Fang, X., Dijkstra, H., Wieners, C., & Guardamagna, F. (2024). A nonlinear full-Field conceptual model for ENSO diversity. *Journal of Climate*, *37*(14), 3759–3774. https://doi.org/10.1175/JCLI-D-23-0382.1

Fang, X. H., & Mu, M. (2018). A three-region conceptual model for central Pacific El Niño including zonal advective feedback. *Journal of Climate*, *31*(13), 4965–4979. https://doi.org/10.1175/jcli-d-17-0633.1

Fedorov, A., Hu, S., Wittenberg, A. T., Levine, A., & Deser, C. (2020). ENSO low-frequency modulations and mean state interactions. In *Chapter 8 of: El Niño Southern Oscillation in a Changing Climate* (pp. 173–198). American Geophysical Union. https://doi.org/10.1002/9781119548164.ch8

Fedorov, A. V. (2010). Ocean response to wind variations, warm water volume, and simple models of ENSO in the low-frequency approximation. *Journal of Climate*, *23*(14), 3855–3873. https://doi.org/10.1175/2010JCLI3044.1

Fedorov, A. V., Hu, S., Lengaigne, M., & Guilyardi, E. (2015). The impact of westerly wind bursts and ocean initial state on the development, and diversity of El Niño events. *Climate Dynamics*, *44*(5–6), 1381–1401. https://doi.org/10.1007/s00382-014-2126-4

Ferrett, S., & Collins, M. (2019). ENSO feedbacks and their relationships with the mean state in a flux adjusted ensemble. *Climate Dynamics*, *52*(12), 7189–7208. https://doi.org/10.1007/s00382-016-3270-9

Frauen, C., & Dommenget, D. (2010). El Niño and La Niña amplitude asymmetry caused by atmospheric feedbacks. *Geophysical Research Letters*, *37*(18), L18801. https://doi.org/10.1029/2010GL044444

Frauen, C., & Dommenget, D. (2012). Influences of the tropical Indian and Atlantic Oceans on the predictability of ENSO. *Geophysical Research Letters*, *39*(2), L02706. https://doi.org/10.1029/2011gl050520

Fredriksen, H.-B., Berner, J., Subramanian, A. C., & Capotondi, A. (2020). How does El Niño–Southern Oscillation change under global warming—A first look at CMIP6. *Geophysical Research Letters*, *47*(22), e2020GL090640. https://doi.org/10.1029/2020GL090640

Fu, M., & Fedorov, A. (2023). The role of Bjerknes and shortwave feedbacks in the tropical Pacific SST response to global warming. *Geophysical Research Letters*, *50*(19), e2023GL105061. https://doi.org/10.1029/2023gl105061

Gadgil, S., Joseph, P. V., & Joshi, N. V. (1984). Ocean–atmosphere coupling over monsoon regions. *Nature*, *312*(5990), 141–143. https://doi.org/10.1038/312141a0

Gebbie, G., Eisenman, I., Wittenberg, A., & Tziperman, E. (2007). Modulation of westerly wind bursts by sea surface temperature: A semi-stochastic feedback of ENSO. *Journal of the Atmospheric Sciences*, *64*(9), 3281–3295. https://doi.org/10.1175/jas4029.1

Geng, L., & Jin, F. (2023a). Insights into ENSO diversity from an intermediate coupled model. Part I: Uniqueness and sensitivity of the ENSO mode. *Journal of Climate*, *36*(21), 7509–7525. https://doi.org/10.1175/JCLI-D-23-0043.1

Geng, L., & Jin, F. (2023b). Insights into ENSO diversity from an intermediate coupled model. Part II: Role of nonlinear dynamics and stochastic forcing. *Journal of Climate*, *36*(21), 7527–7547. https://doi.org/10.1175/JCLI-D-23-0044.1

Geng, T., Cai, W., & Wu, L. (2020). Two types of ENSO varying in tandem facilitated by nonlinear atmospheric convection. *Geophysical Research Letters*, *47*(15), e2020GL088784. https://doi.org/10.1029/2020GL088784

Geng, T., Cai, W., Wu, L., & Yang, Y. (2019). Atmospheric convection dominates genesis of ENSO asymmetry. *Geophysical Research Letters*, *46*(14), 8387–8396. https://doi.org/10.1029/2019GL083213

Gill, A. E. (1980). Some simple solutions for heat-induced tropical circulation. *Quarterly Journal of the Royal Meteorological Society*, *106*(449), 447–462. https://doi.org/10.1002/qj.49710644905

Gopika, S., Lengaigne, M., Suresh, I., Izumo, T., Kwatra, S., Neetu, S., & Vialard, J. (2024). Assessing CMIP models' ability to detect observed surface warming signals related to climate change. *Journal of Climate*, *37*(22), 6011–6027. https://doi.org/10.1175/JCLI-D-24-0102.1

Graham, N. E., & Barnett, T. P. (1987). Sea surface temperature, surface wind divergence, and convection over tropical oceans. *Science*, *238*(4827), 657–659. https://doi.org/10.1126/science.238.4827.657

Graham, N. E., & White, W. B. (1988). The El Niño cycle: A natural oscillator of the Pacific ocean-atmosphere system. *Science*, *240*(4857), 1293–1302. https://doi.org/10.1126/science.240.4857.1293

Guilyardi, E., Capotondi, A., Lengaigne, M., Thual, S., & Wittenberg, A. T. (2020). ENSO modeling: History, progress, and challenges. In *El Niño Southern Oscillation in a Changing Climate* (pp. 201–226). American Geophysical Union. https://doi.org/10.1002/9781119548164.ch9

Ham, Y. G., Kim, J. H., & Luo, J. J. (2019). Deep learning for multi-year ENSO forecasts. *Nature*, *573*(7775), 568–572. https://doi.org/10.1038/s41586-019-1559-7

Ham, Y.-G., Kug, J. S., & Park, J.-Y. (2013). Two distinct roles of Atlantic SSTs in ENSO variability: North Tropical Atlantic SST and Atlantic Niño. *Geophysical Research Letters*, *40*(15), 4012–4017. https://doi.org/10.1002/grl.50729

Harrison, D. E., & Giese, B. S. (1991). Episodes of surface westerly winds as observed from islands in the western tropical Pacific. *Journal of Geophysical Research*, *96*(S01), 3221–3237. https://doi.org/10.1029/90jc01775

Harrison, D. E., & Vecchi, G. A. (1997). Westerly wind events in the tropical Pacific, 1986–95. *Journal of Climate*, *10*(12), 3131–3156. https://doi.org/10.1175/1520-0442(1997)010<3131:wweitt>2.0.co;2

Hasselmann, K. (1976). Stochastic climate models part I. Theory. *Tellus*, *28*(6), 473–485. https://doi.org/10.1111/j.2153-3490.1976.tb00696.x

Heede, U. K., & Fedorov, A. V. (2021). Eastern equatorial Pacific warming delayed by aerosols and thermostat response to CO_2 increase. *Nature Climate Change*, *11*(8), 696–703. https://doi.org/10.1038/s41558-021-01101-x

Heede, U. K., & Fedorov, A. V. (2023a). A stronger Walker circulation and colder eastern equatorial Pacific in the early 21st century: Separating the forced response of the climate system from natural variability. *Geophysical Research Letters*, *50*(3), e2022GL101020. https://doi.org/10.1029/2022gl101020

Heede, U. K., & Fedorov, A. V. (2023b). Towards understanding the robust strengthening of ENSO and more frequent extreme El Niño events in CMIP6 global warming simulations. *Climate Dynamics*, *61*(5), 3047–3060.

Heede, U. K., Fedorov, A. V., & Burls, N. J. (2020). Timescales and mechanisms for the tropical Pacific response to global warming: A tug of war between the ocean thermostat and weaker Walker. *Journal of Climate*, *33*(14), 6101–6118. https://doi.org/10.1175/JCLI-D-19-0690.1

Hoerling, M. P., Kumar, A., & Zhong, M. (1997). El Niño, La Niña, and the nonlinearity of their teleconnections. *Journal of Climate*, *10*(8), 1769–1786. https://doi.org/10.1175/1520-0442(1997)010<1769:enolna>2.0.co;2

Hu, S., & Fedorov, A. V. (2018). Cross-equatorial winds control El Niño diversity and change. *Nature Climate Change*, *8*(9), 798–802. https://doi.org/10.1038/s41558-018-0248-0

Hu, S., Fedorov, A. V., Lengaigne, M., & Guilyardi, E. (2014). The impact of westerly wind bursts on the diversity and predictability of El Niño events: An ocean energetics perspective. *Geophysical Research Letters*, *41*(13), 4654–4663. https://doi.org/10.1002/2014gl059573

Im, S.-H., An, S.-I., Kim, S. T., & Jin, F.-F. (2015). Feedback processes responsible for El Niño-La Niña amplitude asymmetry. *Geophysical Research Letters*, *42*(13), 5556–5563. https://doi.org/10.1002/2015GL064853

Indian National Centre for Ocean Information Services. (2024). Tropflux wind stress and air-sea heat fluxes daily products: 1979 to present [Dataset]. *ESSO - Indian National Centre for Ocean Information Service*. Retrieved from https://incois.gov.in/tropflux/

Izumo, T., & Colin, M. (2022). Improving and harmonizing El Niño recharge indices. *Geophysical Research Letters*, *49*(23), e2022GL101003. https://doi.org/10.1029/2022GL101003

Izumo, T., Colin, M., Jin, F. F., & Pagli, B. (2024). The hybrid recharge delayed oscillator: A more realistic El Niño conceptual model. *Journal of Climate*, *37*(9), 2765–2787. https://doi.org/10.1175/jcli-d-23-0127.1

Izumo, T., Lengaigne, M., Vialard, J., Suresh, I., & Planton, Y. (2019). On the physical interpretation of the lead relation between warm water volume and the El Niño-Southern Oscillation. *Climate Dynamics*, *52*(5–6), 2923–2942. https://doi.org/10.1007/s00382-018-4313-1

Izumo, T., Vialard, J., Lengaigne, M., de Boyer Montegut, C., Behera, S. K., Luo, J. J., et al. (2010). Influence of the state of the Indian Ocean Dipole on the following years El Niño. *Nature Geoscience*, *3*, 168–172. https://doi.org/10.1038/ngeo760

Izumo, T., Vialard, J., Lengaigne, M., & Suresh, I. (2020). Relevance of relative sea surface temperature for tropical rainfall interannual variability. *Geophysical Research Letters*, *47*(3), e2019GL086182. https://doi.org/10.1029/2019GL086182

Jansen, M. F., Dommenget, D., & Keenlyside, N. (2009). Tropical atmosphere–ocean interactions in a conceptual framework. *Journal of Climate*, *22*(3), 550–567. https://doi.org/10.1175/2008jcli2243.1

Jiang, F., Zhang, W., Jin, F.-F., Stuecker, M. F., & Allan, R. (2021). El Niño pacing orchestrates inter-basin Pacific-Indian Ocean interannual connections. *Geophysical Research Letters*, *48*(19), e2021GL095242. https://doi.org/10.1029/2021GL095242

Jin, F.-F. (1996). Tropical ocean-atmosphere interaction, the Pacific cold tongue, and the El Niño-Southern Oscillation. *Science*, *274*(5284), 76–78. https://doi.org/10.1126/science.274.5284.76

Jin, F.-F. (1997a). An equatorial ocean recharge paradigm for ENSO. Part I: Conceptual model. *Journal of the Atmospheric Sciences*, *54*(7), 811–829. https://doi.org/10.1175/1520-0469(1997)054<0811:aeorpf>2.0.co;2

Jin, F. F. (1997b). An equatorial ocean recharge paradigm for ENSO. Part II: A stripped-down coupled model. *Journal of the Atmospheric Sciences*, *54*(7), 830–847. https://doi.org/10.1175/1520-0469(1997)054<0830:aeorpf>2.0.co;2

Jin, F. F., & An, S. I. (1999). Thermocline and zonal advective feedbacks within the equatorial ocean recharge oscillator model for ENSO. *Geophysical Research Letters*, *26*(19), 2989–2992. https://doi.org/10.1029/1999gl002297

Jin, F. F., An, S. I., Timmermann, A., & Zhao, J. (2003). Strong El Niño events and nonlinear dynamical heating. *Geophysical Research Letters*, *30*(3). 20-1–20-1. https://doi.org/10.1029/2002gl016356

Jin, F. F., Chen, H. C., Zhao, S., Hayashi, M., Karamperidou, C., Stuecker, M. F., et al. (2020). Simple ENSO models. In M. J. McPhaden, A. Santoso, & W. Cai (Eds.), *El Niño Southern Oscillation in a Changing Climate*, *Geophysical Monograph Series* (pp. 119–151). AGU.

Jin, F.-F., Kim, S. T., & Bejarano, L. (2006). A coupled-stability index for ENSO. *Geophysical Research Letters*, *33*(23), L23708. https://doi.org/10.1029/2006GL027221

Jin, F.-F., Lin, L., Timmermann, A., & Zhao, J. (2007). Ensemble-mean dynamics of the ENSO recharge oscillator under state-dependent stochastic forcing. *Geophysical Research Letters*, *34*(3), L03807. https://doi.org/10.1029/2006GL027372

Jin, F.-F., & Neelin, J. D. (1993). Modes of interannual tropical ocean atmosphere interaction—A unified view. Part I: Numerical results. *Journal of the Atmospheric Sciences*, *50*(21), 3477–3503. https://doi.org/10.1175/1520-0469(1993)050<3477:moitoi>2.0.co;2

Johnson, N., & Xie, S.-P. (2010). Changes in the sea surface temperature threshold for tropical convection. *Nature Geoscience*, *3*(12), 842–845. https://doi.org/10.1038/ngeo1008

Jourdain, N. C., Lengaigne, M., Vialard, J., Izumo, T., & Gupta, A. S. (2016). Further insights on the influence of the Indian Ocean dipole on the following year's ENSO from observations and CMIP5 models. *Journal of Climate*, *29*(2), 637–658. https://doi.org/10.1175/jcli-d-15-0481.1

Kang, I.-S., & Kug, J.-S. (2002). El Niño and La Niña sea surface temperature anomalies: Asymmetry characteristics associated with their wind stress anomalies. *Journal of Geophysical Research*, *107*(D19). ACL 1-1–ACL 1-10. https://doi.org/10.1029/2001JD000393

Kessler, W. S. (2002). Is ENSO a cycle or a series of events? *Geophysical Research Letters*, *29*(23). 40-1–40-4. https://doi.org/10.1029/2002gl015924

Kessler, W. S., McPhaden, M. J., & Weickmann, K. M. (1995). Forcing of intraseasonal Kelvin waves in the equatorial Pacific. *Journal of Geophysical Research*, *100*(C6), 10613–10631. https://doi.org/10.1029/95JC00382

Kim, S.-K., & An, S.-I. (2020). Untangling El Nino-La Nina asymmetries using a nonlinear coupled dynamics index. *Geophysical Research Letters*, *47*(4), e2019GL085881. https://doi.org/10.1029/2019GL085881
Kim, S.-K., & An, S.-I. (2021). Seasonal Gap theory for ENSO phase locking. *Journal of Climate*, *34*(14), 5621–5634. https://doi.org/10.1175/jcli-d-20-0495.1
Kim, S. T., Cai, W., Jin, F. F., & Yu, J. Y. (2014). ENSO stability in coupled climate models and its association with mean state. *Climate Dynamics*, *42*(11–12), 3313–3321. https://doi.org/10.1007/s00382-013-1833-6
Kim, S. T., & Jin, F. F. (2011). An ENSO stability analysis. Part II: Results from the twentieth and twenty-first century simulations of the CMIP3 models. *Climate Dynamics*, *36*(7–8), 1609–1627. https://doi.org/10.1007/s00382-010-0872-5
Kleeman, R. (2008). Stochastic theories for the irregularity of ENSO. *Philosophical Transactions of the Royal Society A: Mathematical, Physical and Engineering Sciences*, *366*(1875), 2509–2524. https://doi.org/10.1098/rsta.2008.0048
Knutson, T. R., & Manabe, S. (1995). Time-mean response over the tropical Pacific to increased CO_2 in a coupled ocean-atmosphere model. *Journal of Climate*, *8*(9), 2181–2199. https://doi.org/10.1175/1520-0442(1995)008<2181:tmrott>2.0.co;2
Kug, J. S., Jin, F. F., & An, S. I. (2009). Two types of El Niño events: Cold tongue El Niño and warm pool El Niño. *Journal of Climate*, *22*(6), 1499–1515. https://doi.org/10.1175/2008jcli2624.1
Kug, J.-S., Jin, F.-F., Sooraj, K. P., & Kang, I.-S. (2008). State-dependent atmospheric noise associated with ENSO. *Geophysical Research Letters*, *35*(5), L05701. https://doi.org/10.1029/2007GL032017
Kug, J. S., & Kang, I. S. (2006). Interactive feedback between ENSO and the Indian Ocean. *Journal of Climate*, *19*(9), 1784–1801. https://doi.org/10.1175/jcli3660.1
Kug, J. S., Li, T., An, S. I., Kang, I., Luo, J., Masson, S., & Yamagata, T. (2006). Role of the ENSO-Indian Ocean coupling on ENSO variability in a coupled GCM. *Geophysical Research Letters*, *33*(9), L09710. https://doi.org/10.1029/2005gl024916
Kug, J. S., Vialard, J., Ham, Y. G., Yu, J. Y., & Lengaigne, M. (2020). ENSO remote forcing: Influence of climate variability outside the tropical Pacific. *El Niño Southern Oscillation in a Changing Climate*, 247–265.
Larkin, N. K., & Harrison, D. E. (2002). ENSO warm (El Niño) and cold (La Niña) event life cycles: Ocean surface anomaly patterns, their symmetries, asymmetries, and implications. *Journal of Climate*, *15*, 1118–1140. https://doi.org/10.1175/1520-0442(2002)015<1118:EWENOA>2.0.CO;2
Latif, M., Anderson, D., Barnett, T., Cane, M., Kleeman, R., Leetmaa, A., et al. (1998). A review of the predictability and prediction of ENSO. *Journal of Geophysical Research*, *103*(C7), 14375–14393. https://doi.org/10.1029/97jc03413
Lee, S., L'Heureux, M., Wittenberg, A. T., Seager, R., O'Gorman, P. A., & Johnson, N. C. (2022). On the future zonal contrasts of equatorial Pacific climate: Perspectives from observations, simulations, and theories. *Npj Climate and Atmospheric Science*, *5*(1), 82. https://doi.org/10.1038/s41612-022-00301-2
Lengaigne, M., Boulanger, J. P., Menkes, C., Delecluse, P., & Slingo, J. (2004). Westerly wind events in the tropical Pacific and their influence on the coupled ocean-atmosphere system. In *Earth climate: The ocean-atmosphere interaction*. *Geophysical Monograph Series* (Vol. 147, pp. 49–69).
Levine, A. F., & Jin, F. F. (2017). A simple approach to quantifying the noise–ENSO interaction. Part I: Deducing the state-dependency of the windstress forcing using monthly mean data. *Climate Dynamics*, *48*(1–2), 1–18. https://doi.org/10.1007/s00382-015-2748-1
Levine, A. F., & McPhaden, M. J. (2015). The annual cycle in ENSO growth rate as a cause of the spring predictability barrier. *Geophysical Research Letters*, *42*(12), 5034–5041. https://doi.org/10.1002/2015gl064309
Levine, A. F. Z., Jin, F. F., & McPhaden, M. J. (2016). Extreme noise-extreme El Niño: How state-dependent noise forcing creates El Niño-La Niña asymmetry. *Journal of Climate*, *29*(15), 5483–5499. https://doi.org/10.1175/JCLI-D-16-0091.1
L'Heureux, M. L., Levine, A. F. Z., Newman, M., Ganter, C., Luo, J.-J., Tippett, M. K., & Stockdale, T. N. (2020). ENSO prediction. In M. J. McPhaden, A. Santoso, & W. Cai (Eds.), *El Niño Southern Oscillation in a changing climate*. https://doi.org/10.1002/9781119548164.ch10
Lian, T., Chen, D., Tang, Y., Liu, X., Feng, J., & Zhou, L. (2018). Linkage between westerly wind bursts and tropical cyclones. *Geophysical Research Letters*, *45*(20), 11431–11438. https://doi.org/10.1029/2018GL079745
Liang, Y., & Fedorov, A. V. (2021). Linking the Madden–Julian Oscillation, tropical cyclones and westerly wind bursts as part of El Niño development. *Climate Dynamics*, *57*(3), 1039–1060. https://doi.org/10.1007/s00382-021-05757-1
Liang, Y., & Fedorov, A. V. (2024). Stronger westerly wind bursts in a warming climate: The effects of the Pacific warming pattern, the Madden–Julian Oscillation, and tropical cyclones. *Journal of Climate*, *37*(22), 6029–6045. https://doi.org/10.1175/jcli-d-23-0681.1
Liu, F., Vialard, J., Fedorov, A. V., Éthé, C., Person, R., Zhang, W., & Lengaigne, M. (2024). Why do oceanic nonlinearities contribute only weakly to extreme El Niño events? *Geophysical Research Letters*, *51*(11), e2024GL108813. https://doi.org/10.1029/2024GL108813
Liu, Z., & Huang, B. (1997). A coupled theory of tropical climatology: Warm pool, cold tongue, and Walker circulation. *Journal of Climate*, *10*(7), 1662–1679. https://doi.org/10.1175/1520-0442(1997)010<1662:actotc>2.0.co;2
Lopez, H., Lee, S.-K., Kim, D., Wittenberg, A. T., & Yeh, S.-W. (2022). Projections of faster onset and slower decay of El Niño in the 21st century. *Nature Communications*, *13*(1), 1915. https://doi.org/10.1038/s41467-022-29519-7
Lu, B., Jin, F. F., & Ren, H. L. (2018). A coupled dynamic index for ENSO periodicity. *Journal of Climate*, *31*(6), 2361–2376. https://doi.org/10.1175/jcli-d-17-0466.1
Luo, J. J., Wang, G., & Dommenget, D. (2018). May common model biases reduce CMIP5's ability to simulate the recent Pacific La Niña-like cooling? *Climate Dynamics*, *50*(3–4), 1335–1351. https://doi.org/10.1007/s00382-017-3688-8
Maher, N., Wills, R. C. J., DiNezio, P., Klavans, J., Milinski, S., Sanchez, S. C., et al. (2022). The future of the El Niño-Southern Oscillation: Using large ensembles to illuminate time-varying responses and inter-model differences. *Earth System Dynamics Discussions*, *2022*, 1–28.
McCreary, J. P., Jr., & Anderson, D. L. T. (1991). An overview of coupled ocean-atmosphere models of El Niño and the Southern Oscillation. *Journal of Geophysical Research*, *96*(S01), 3125–3150. https://doi.org/10.1029/90JC01979
McGregor, S., Dommenget, D., & Neske, S. (2022). Distinct off-equatorial zonal wind stress and oceanic responses for EP-and CP-type ENSO events. *Journal of Climate*, *35*(5), 1423–1440. https://doi.org/10.1175/jcli-d-21-0473.1
McGregor, S., Stuecker, M. F., Kajtar, J. B., England, M. H., & Collins, M. (2018). Model tropical Atlantic biases underpin diminished Pacific decadal variability. *Nature Climate Change*, *8*(6), 493–498. https://doi.org/10.1038/s41558-018-0163-4
McGregor, S., Timmermann, A., Schneider, N., Stuecker, M. F., & England, M. H. (2012). The effect of the South Pacific convergence zone on the termination of El Niño events and the meridional asymmetry of ENSO. *Journal of Climate*, *25*(16), 5566–5586. https://doi.org/10.1175/JCLI-D-11-00332.1
McGregor, S., Timmermann, A., Stuecker, M., England, M. H., Merrifield, M., Jin, F. F., & Chikamoto, Y. (2014). Recent Walker circulation strengthening and Pacific cooling amplified by Atlantic warming. *Nature Clim Change*, *4*(10), 888–892. https://doi.org/10.1038/nclimate2330
McPhaden, M. J. (2003). Tropical Pacific Ocean heat content variations and ENSO persistence barriers. *Geophysical Research Letters*, *30*(9), 1480. https://doi.org/10.1029/2003GL016872

McPhaden, M. J. (2015). Playing hide and seek with El Niño. *Nature Climate Change*, *5*(9), 791–795. https://doi.org/10.1038/nclimate2775
McPhaden, M. J., Busalacchi, A. J., Cheney, R., Donguy, J., Gage, K. S., Halpern, D., et al. (1998). The tropical ocean-global atmosphere observing system: A decade of progress. *Journal of Geophysical Research*, *103*(C7), 14169–14240. https://doi.org/10.1029/97JC02906
McPhaden, M. J., Lee, T., Fournier, S., & Balmaseda, M. A. (2020). ENSO observations. *El Niño Southern Oscillation in a Changing Climate*, 39–63.
McPhaden, M. J., Santoso, A., & Cai, W. (2020). Introduction to El Niño Southern Oscillation in a changing climate. In M. J. McPhaden, A. Santoso, & W. Cai (Eds.), *El Niño Southern Oscillation in a Changing Climate*. AGU Monograph. https://doi.org/10.1002/9781119548164.ch1
McPhaden, M. J., & Yu, X. (1999). Equatorial waves and the 1997–98 El Niño. *Geophysical Research Letters*, *26*(19), 2961–2964. https://doi.org/10.1029/1999gl004901
McPhaden, M. J., Zebiak, S. E., & Glantz, M. H. (2006). ENSO as an integrating concept in Earth science. *Science*, *314*(5806), 1740–1745. https://doi.org/10.1126/science.1132588
Meinen, C. S., & McPhaden, M. J. (2000). Observations of warm water volume changes in the equatorial Pacific and their relationship to El Niño and La Niña. *Journal of Climate*, *13*(20), 3551–3559. https://doi.org/10.1175/1520-0442(2000)013<3551:oowwvc>2.0.co;2
Met Office Hadley Centre. (2021). Hadley Centre Sea Ice and Sea Surface Temperature data set (HadISST) version 4 dataset [Dataset]. *Met Office Hadley Centre*. Retrieved from https://www.metoffice.gov.uk/hadobs/hadisst/data/download.html
Mu, B., Qin, B., & Yuan, S. J. (2021). ENSO-ASC 1.0.0: ENSO deep learning forecast model with a multivariate air-sea coupler. *Geoscientific Model Development*, *14*(11), 6977–6999. https://doi.org/10.5194/gmd-14-6977-2021
Neelin, J. D., Battisti, D. S., Hirst, A. C., Jin, F.-F., Wakata, Y., Yamagata, T., & Zebiak, S. E. (1998). ENSO theory. *Journal of Geophysical Research*, *103*(C7), 14261–14290. https://doi.org/10.1029/97JC03424
Neelin, J. D., & Held, I. M. (1987). Modeling tropical convergence based on the moist static energy budget. *Monthly Weather Review*, *115*(1), 3–12. https://doi.org/10.1175/1520-0493(1987)115<0003:mtcbot>2.0.co;2
Neske, S., & McGregor, S. (2018). Understanding the warm water volume precursor of ENSO events and its interdecadal variation. *Geophysical Research Letters*, *45*(3), 1577–1585. https://doi.org/10.1002/2017GL076439
Ohba, M., & Ueda, H. (2007). An impact of SST anomalies in the Indian Ocean in acceleration of the El Niño to La Niña transition. *Journal of the Meteorological Society of Japan*, *85*(3), 335–348. https://doi.org/10.2151/jmsj.85.335
Okumura, Y. M., & Deser, C. (2010). Asymmetry in the duration of El Niño and La Niña. *Journal of Climate*, *23*(21), 5826–5843. https://doi.org/10.1175/2010JCLI3592.1
O'Neill, B. C., Tebaldi, C., van Vuuren, D. P., Eyring, V., Friedlingstein, P., Hurtt, G., et al. (2016). The Scenario Model Intercomparison Project (ScenarioMIP) for CMIP6. *Geoscientific Model Development*, *9*, 3461–3482. https://doi.org/10.5194/gmd-9-3461-2016
Philander, S. G., & Fedorov, A. (2003). Is El Niño sporadic or cyclic? *Annual Review of Earth and Planetary Sciences*, *31*(1), 579–594. https://doi.org/10.1146/annurev.earth.31.100901.141255
Picaut, J., Masia, F., & du Penhoat, Y. (1997). An advective-reflective conceptual model for the oscillatory nature of the ENSO. *Science*, *277*(5326), 663–666. https://doi.org/10.1126/science.277.5326.663
Planton, Y. Y., Guilyardi, E., Wittenberg, A. T., Lee, J., Gleckler, P. J., Bayr, T., et al. (2021). Evaluating climate models with the CLIVAR 2020 ENSO metrics package [Software]. *Bulletin of the American Meteorological Society*, *102*(2), E193–E217. https://doi.org/10.1175/BAMS-D-19-0337.1
Planton, Y. Y., Vialard, J., Guilyardi, E., Lengaigne, M., & Izumo, T. (2018). Western Pacific oceanic heat content: A better predictor of La Niña than of El Niño. *Geophysical Research Letters*, *45*(18), 9824–9833. https://doi.org/10.1029/2018GL079341
Planton, Y. Y., Vialard, J., Guilyardi, E., Lengaigne, M., & Mcphaden, M. J. (2021). The asymmetric influence of ocean heat content on ENSO predictability in the CNRM-CM5 coupled general circulation model. *Journal of Climate*, *34*(14), 5775–5793. https://doi.org/10.1175/JCLI-D-20-0633.1
Power, S., Delage, F., Wang, G., Smith, I., & Kociuba, G. (2017). Apparent limitations in the ability of CMIP5 climate models to simulate recent multi-decadal change in surface temperature: Implications for global temperature projections. *Climate Dynamics*, *49*(1–2), 53–69. https://doi.org/10.1007/s00382-016-3326-x
Power, S., Lengaigne, M., Capotondi, A., Khodri, M., Vialard, J., Jebri, B., et al. (2021). Decadal climate variability in the tropical Pacific: Characteristics, causes, predictability, and prospects. *Science*, *374*(6563), eaay9165. https://doi.org/10.1126/science.aay9165
Praveen Kumar, B., Vialard, J., Lengaigne, M., Murty, V. S. N., & McPhaden, M. J. (2012). TropFlux: Air–sea fluxes for the global tropical oceans—Description and evaluation [Dataset]. *Climate Dynamics*, *38*(7–8), 1521–1543. https://doi.org/10.1007/s00382-011-1115-0
Praveen Kumar, B., Vialard, J., Lengaigne, M., Murty, V. S. N., McPhaden, M. J., Cronin, M. F., et al. (2013). TropFlux wind stresses over the tropical oceans: Evaluation and comparison with other products [Dataset]. *Climate Dynamics*, *40*(7–8), 2049–2071. https://doi.org/10.1007/s00382-012-1455-4
Program for Climate Model Diagnosis and Intercomparison, Lawrence Livermore National Laboratory. (2024a). CLIVAR ENSO metrics package [Software]. *GitHub*. Retrieved from https://github.com/CLIVAR-PRP/enso_metrics
Program for Climate Model Diagnosis and Intercomparison, Lawrence Livermore National Laboratory. (2024b). CMIP6 dataset [Dataset]. *Earth Systems Grid Federation Project US Node*. Retrieved from https://aims2.llnl.gov/search/cmip6/
Puy, M., Vialard, J., Lengaigne, M., & Guilyardi, E. (2016). Modulation of equatorial Pacific westerly/easterly wind events by the Madden–Julian Oscillation and convectively-coupled Rossby waves. *Climate Dynamics*, *46*(7–8), 2155–2178. https://doi.org/10.1007/s00382-015-2695-x
Puy, M., Vialard, J., Lengaigne, M., Guilyardi, E., DiNezio, P. N., Voldoire, A., et al. (2019). Influence of westerly wind events stochasticity on El Niño amplitude: The case of 2014 vs. 2015. *Climate Dynamics*, *52*(12), 7435–7454. https://doi.org/10.1007/s00382-017-3938-9
Rashid, H. A., & Hirst, A. C. (2016). Investigating the mechanisms of seasonal ENSO phase locking bias in the ACCESS coupled model. *Climate Dynamics*, *46*(3–4), 1075–1090. https://doi.org/10.1007/s00382-015-2633-y
Ray, S., Wittenberg, A. T., Griffies, S. M., & Zeng, F. (2018). Understanding the equatorial Pacific cold tongue time-mean heat budget. Part II: Evaluation of the GFDL-FLOR coupled GCM. *Journal of Climate*, *31*(24), 9987–10011. https://doi.org/10.1175/JCLI-D-18-0153.1
Rayner, N. A., Parker, D. E., Horton, E. B., Folland, C. K., Alexander, L. V., Rowell, D. P., et al. (2003). Global analyses of sea surface temperature, sea ice, and night marine air temperature since the late nineteenth century [Dataset]. *Journal of Geophysical Research*, *108*(D14), 4407. https://doi.org/10.1029/2002JD002670
Ren, H. L., & Jin, F. F. (2013). Recharge oscillator mechanisms in two types of ENSO. *Journal of Climate*, *26*(17), 6506–6523. https://doi.org/10.1175/jcli-d-12-00601.1
Rio, M. H., Mulet, S., & Picot, N. (2014). Beyond GOCE for the ocean circulation estimate: Synergetic use of altimetry, gravimetry, and in situ data provides new insight into geostrophic and Ekman currents [Dataset]. *Geophysical Research Letters*, *41*(24), 8918–8925. https://doi.org/10.48670/mds-00327

Santoso, A., Mcphaden, M. J., & Cai, W. (2017). The defining characteristics of ENSO extremes and the strong 2015/2016 El Niño. *Reviews of Geophysics*, *55*(4), 1079–1129. https://doi.org/10.1002/2017rg000560

Seager, R., Henderson, N., & Cane, M. (2022). Persistent discrepancies between observed and modeled trends in the tropical Pacific Ocean. *Journal of Climate*, *35*(14), 4571–4584. https://doi.org/10.1175/jcli-d-21-0648.1

Shin, N. Y., Kug, J. S., Stuecker, M. F., Jin, F. F., Timmermann, A., & Kim, G. I. (2022). More frequent central Pacific El Niño and stronger eastern Pacific El Niño in a warmer climate. *npj Climate and Atmospheric Science*, *5*(1), 101. https://doi.org/10.1038/s41612-022-00324-9

Srinivas, G., Vialard, J., Liu, F., Voldoire, A., Izumo, T., Guilyardi, E., & Lengaigne, M. (2024). Dominant contribution of atmospheric non-linearities to ENSO asymmetry and extreme El Niño events. *Scientific Reports*, *14*(1), 8122. https://doi.org/10.1038/s41598-024-58803-3

Stein, K., Schneider, N., Timmermann, A., & Jin, F. F. (2010). Seasonal synchronization of ENSO events in a linear stochastic model. *Journal of Climate*, *23*(21), 5629–5643. https://doi.org/10.1175/2010JCLI3292.1

Stein, K., Timmermann, A., Schneider, N., Jin, F. F., & Stuecker, M. F. (2014). ENSO seasonal synchronization theory. *Journal of Climate*, *27*(14), 5285–5310. https://doi.org/10.1175/JCLI-D-13-00525.1

Stuecker, M. F. (2018). Revisiting the Pacific meridional mode. *Scientific Reports*, *8*(1), 3216. https://doi.org/10.1038/s41598-018-21537-0

Stuecker, M. F. (2023). The climate variability trio: Stochastic fluctuations, El Niño, and the seasonal cycle. *Geoscience Letters*, *10*(1), 51. https://doi.org/10.1186/s40562-023-00305-7

Stuecker, M. F., Timmermann, A., Jin, F.-F., Chikamoto, Y., Zhang, W., Wittenberg, A. T., et al. (2017). Revisiting ENSO/Indian Ocean Dipole phase relationships. *Geophysical Research Letters*, *44*(5), 2481–2492. https://doi.org/10.1002/2016GL072308

Stuecker, M. F., Timmermann, A., Jin, F. F., McGregor, S., & Ren, H. L. (2013). A combination mode of the annual cycle and the El Niño/Southern Oscillation. *Nature Geoscience*, *6*(7), 540–544. https://doi.org/10.1038/ngeo1826

Stuivenvolt-Allen, J., Fedorov, A. V., Fu, M., & Heede, U. (2024). Widening of wind-stress anomalies amplifies ENSO in a warming climate. *Journal of Climate*, *38*(2), 497–512. https://doi.org/10.1175/JCLI-D-24-0126.1

Suarez, M. J., & Schopf, P. S. (1988). A delayed action oscillator for ENSO. *Journal of the Atmospheric Sciences*, *45*(21), 3283–3287. https://doi.org/10.1175/1520-0469(1988)045<3283:adaofe>2.0.co;2

Sun, D.-Z., & Liu, Z. (1996). Dynamic ocean-atmosphere coupling: A thermostat for the tropics. *Science*, *272*(5265), 1148–1150. https://doi.org/10.1126/science.272.5265.1148

Takahashi, K., Karamperidou, C., & Dewitte, B. (2019). A theoretical model of strong and moderate El Niño regimes. *Climate Dynamics*, *52*(12), 7477–7493. https://doi.org/10.1007/s00382-018-4100-z

Takahashi, K., Montecinos, A., Goubanova, K., & Dewitte, B. (2011). ENSO regimes: Reinterpreting the canonical and Modoki El Niño. *Geophysical Research Letters*, *38*(10), L10704. https://doi.org/10.1029/2011GL047364

Taschetto, A. S., Ummenhofer, C. C., Stuecker, M. F., Dommenget, D., Ashok, K., Rodrigues, R. R., & Yeh, S. W. (2020). ENSO atmospheric teleconnections. *El Niño Southern Oscillation in a Changing Climate*, 309–335. https://doi.org/10.1002/9781119548164.ch14

Thual, S., & Dewitte, B. (2023). ENSO complexity controlled by zonal shifts in the Walker circulation. *Nature Geoscience*, *16*(4), 328–332. https://doi.org/10.1038/s41561-023-01154-x

Thual, S., Dewitte, B., An, S.-I., & Ayoub, N. (2011). Sensitivity of ENSO to stratification in a recharge–discharge conceptual model. *Journal of Climate*, *4*, 4331–4348.

Tian, F., Zhang, R.-H., & Wang, X. (2019). A positive feedback onto ENSO due to tropical instability wave (TIW)-induced chlorophyll effects in the Pacific. *Geophysical Research Letters*, *46*(2), 889–897. https://doi.org/10.1029/2018GL081275

Timmermann, A., An, S. I., Kug, J. S., Jin, F. F., Cai, W., Capotondi, A., et al. (2018). El Niño–Southern Oscillation complexity. *Nature*, *559*(7715), 535–545. https://doi.org/10.1038/s41586-018-0252-6

Timmermann, A., Jin, F.-F., & Abshagen, J. (2003). A nonlinear theory for El Niño bursting. *Journal of the Atmospheric Sciences*, *60*(1), 152–165. https://doi.org/10.1175/1520-0469(2003)060<0152:antfen>2.0.co;2

Trenberth, K. E. (2020). ENSO in the global climate system. *El Niño Southern Oscillation in a Changing Climate*, 21–37. https://doi.org/10.1002/9781119548164.ch2

Tziperman, E., Cane, M. A., & Zebiak, S. E. (1995). Irregularity and locking to the seasonal cycle in an ENSO prediction model as explained by the quasi-periodicity route to chaos. *Journal of the Atmospheric Sciences*, *52*(3), 293–306. https://doi.org/10.1175/1520-0469(1995)052<0293:ialtts>2.0.co;2

Tziperman, E., Cane, M. A., Zebiak, S. E., Xue, Y., & Blumenthal, B. (1998). Locking of El Nino's peak time to the end of the calendar year in the delayed oscillator picture of ENSO. *Journal of Climate*, *11*(9), 2191–2199. https://doi.org/10.1175/1520-0442(1998)011<2191:loenos>2.0.co;2

Vallis, G. K. (1986). El Niño: A chaotic dynamical system? *Science*, *232*(4747), 243–245. https://doi.org/10.1126/science.232.4747.243

Vecchi, G. A., Soden, B. J., Wittenberg, A. T., Held, I. M., Leetmaa, A., & Harrison, M. J. (2006). Weakening of tropical Pacific atmospheric circulation due to anthropogenic forcing. *Nature*, *441*(7089), 73–76. https://doi.org/10.1038/nature04744

Vecchi, G. A., & Wittenberg, A. T. (2010). El Niño and our future climate: Where do we stand? *Wiley Interdisciplinary Reviews: Climate Change*, *1*(2), 260–270. https://doi.org/10.1002/wcc.33

Vialard, J., Menkes, C., Boulanger, J. P., Delecluse, P., Guilyardi, E., McPhaden, M. J., & Madec, G. (2001). A model study of oceanic mechanisms affecting equatorial Pacific sea surface temperature during the 1997–98 El Niño. *Journal of Physical Oceanography*, *31*(7), 1649–1675. https://doi.org/10.1175/1520-0485(2001)031<1649:amsoom>2.0.co;2

Vijayeta, A., & Dommenget, D. (2018). An evaluation of ENSO dynamics in CMIP simulations in the framework of the recharge oscillator model. *Climate Dynamics*, *51*(5), 1753–1771. https://doi.org/10.1007/s00382-017-3981-6

Vimont, D., Battisti, D., & Hirst, A. (2001). Footprinting: A seasonal connection between the tropics and mid-latitudes. *Geophysical Research Letters*, *28*(20), 3923–3926. https://doi.org/10.1029/2001gl013435

Walker, G. T. (1924). Correlations in seasonal variations of weather. VIII, A further study of world weather. *Memoirs of India Meteorological Department*, *24*, 275–332.

Wang, C. (2001). A unified oscillator model for the El Niño-Southern Oscillation. *Journal of Climate*, *14*(1), 98–115. https://doi.org/10.1175/1520-0442(2001)014<0098:auomft>2.0.co;2

Wang, C. (2018). A review of ENSO theories. *National Science Review*, *5*(6), 813–825. https://doi.org/10.1093/nsr/nwy104

Wang, C., & Fiedler, P. C. (2006). ENSO variability and the eastern tropical Pacific: A review. *Progress in Oceanography*, *69*(2–4), 239–266. https://doi.org/10.1016/j.pocean.2006.03.004

Wang, C., Weisberg, R. H., & Virmani, J. I. (1999). Western Pacific interannual variability associated with the El Niño-Southern Oscillation. *Journal of Geophysical Research*, *104*(C3), 5131–5149. https://doi.org/10.1029/1998jc900090

Wang, W., & McPhaden, M. J. (2000). The surface layer heat balance in the equatorial Pacific Ocean. Part II: Interannual variability. *Journal of Physical Oceanography*, *30*(11), 2989–3008. https://doi.org/10.1175/1520-0485(2001)031<2989:tslhbi>2.0.co;2

Watanabe, M., Kang, S. M., Collins, M., Hwang, Y. T., McGregor, S., & Stuecker, M. F. (2024). Possible shift in controls of the tropical Pacific surface warming pattern. *Nature*, *630*(8016), 315–324. https://doi.org/10.1038/s41586-024-07452-7

Weisberg, R. H., & Wang, C. (1997). A western Pacific oscillator paradigm for the El Niño-Southern Oscillation. *Geophysical Research Letters*, *24*(7), 779–782. https://doi.org/10.1029/97gl00689

Wengel, C., Dommenget, D., Latif, M., Bayr, T., & Vijayeta, A. (2018). What controls ENSO-amplitude diversity in climate models? *Geophysical Research Letters*, *45*(4), 1989–1996. https://doi.org/10.1002/2017gl076849

Wengel, C., Lee, S. S., Stuecker, M. F., Timmermann, A., Chu, J. E., & Schloesser, F. (2021). Future high-resolution El Niño/Southern Oscillation dynamics. *Nature Climate Change*, *11*(9), 758–765. https://doi.org/10.1038/s41558-021-01132-4

Willett, C. S., Leben, R. R., & Lavín, M. F. (2006). Eddies and tropical instability waves in the eastern tropical Pacific: A review. *Progress in Oceanography*, *69*(2–4), 218–238. https://doi.org/10.1016/j.pocean.2006.03.010

Williams, I. N., & Patricola, C. M. (2018). Diversity of ENSO events unified by convective threshold sea surface temperature: A nonlinear ENSO index. *Geophysical Research Letters*, *45*(17), 9236–9244. https://doi.org/10.1029/2018gl079203

Wills, R. C. J., Dong, Y., Proistosecu, C., Armour, K. C., & Battisti, D. S. (2022). Systematic climate model biases in the large-scale patterns of recent sea-surface temperature and sea-level pressure change. *Geophysical Research Letters*, *49*(17), e2022GL100011. https://doi.org/10.1029/2022GL100011

Wittenberg, A. T. (2009). Are historical records sufficient to constrain ENSO simulations? *Geophysical Research Letters*, *36*(12), L12702. https://doi.org/10.1029/2009GL038710

Wittenberg, A. T., Rosati, A., Delworth, T. L., Vecchi, G. A., & Zeng, F. (2014). ENSO modulation: Is it decadally predictable? *Journal of Climate*, *27*(7), 2667–2681. https://doi.org/10.1175/JCLI-D-13-00577.1

Wyrtki, K. (1975). El Niño—The dynamic response of the equatorial Pacific Oceanto atmospheric forcing. *Journal of Physical Oceanography*, *5*(4), 572–584. https://doi.org/10.1175/1520-0485(1975)005<0572:entdro>2.0.co;2

Wyrtki, K. (1985). Water displacements in the Pacific and the genesis of El Niño cycles. *Journal of Geophysical Research*, *90*(C4), 7129–7132. https://doi.org/10.1029/jc090ic04p07129

Xie, S. P., Deser, C., Vecchi, G. A., Ma, J., Teng, H., & Wittenberg, A. T. (2010). Global warming pattern formation: Sea surface temperature and rainfall. *Journal of Climate*, *23*(4), 966–986. https://doi.org/10.1175/2009jcli3329.1

Xie, S. P., Hu, K., Hafner, J., Tokinaga, H., Du, Y., Huang, G., & Sampe, T. (2009). Indian Ocean capacitor effect on Indo-Western Pacific climate during the summer following El Niño. *Journal of Climate*, *22*(3), 730–747. https://doi.org/10.1175/2008jcli2544.1

Yu, J.-Y., Mechoso, C. R., McWilliams, J. C., & Arakawa, A. (2002). Impacts of the Indian Ocean on the ENSO cycle. *Geophysical Research Letters*, *29*(8), 1204. https://doi.org/10.1029/2001GL014098

Yu, S., & Fedorov, A. V. (2022). The essential role of westerly wind bursts in shaping ENSO characteristics and extreme events in model "wind stress shaving" experiments. *Journal of Climate*, 7519–7538.

Zebiak, S. E., & Cane, M. A. (1987). A model El Niño–Southern Oscillation. *Monthly Weather Review*, *115*(10), 2262–2278. https://doi.org/10.1175/1520-0493(1987)115<2262:AMENO>2.0.CO;2

Zhang, L., & Li, T. (2014). A simple analytical model for understanding the formation of sea surface temperature patterns under global warming. *Journal of Climate*, *27*(22), 8413–8421. https://doi.org/10.1175/jcli-d-14-00346.1

Zhang, R.-H., Zhou, L., Gao, C., & Tao, L. (2024). A transformer-based coupled ocean-atmosphere model for ENSO studies. *Science Bulletin*, *69*(15), 2323–2327. https://doi.org/10.1016/j.scib.2024.04.048

Zhang, W., Jiang, F., Stuecker, M. F., Jin, F. F., & Timmermann, A. (2021). Spurious North Tropical Atlantic precursors to El Niño. *Nature Communications*, *12*(1), 3096. https://doi.org/10.1038/s41467-021-23411-6

Zhang, Y., Chen, N., Vialard, J., & Fang, X. (2024). A physics-informed auto-learning framework for developing stochastic conceptual models for ENSO diversity. *Journal of Climate*, *37*(23), 6323–6347. https://doi.org/10.1175/jcli-d-24-0092.1

Zhao, B., & Fedorov, A. (2020). The effects of background zonal and meridional winds on ENSO in a coupled GCM. *Journal of Climate*, *33*(6), 2075–2091. https://doi.org/10.1175/jcli-d-18-0822.1

Zhao, S., Jin, F.-F., & Stuecker, M. F. (2021). Understanding lead times of warm water volumes to ENSO sea surface temperature anomalies. *Geophysical Research Letters*, *48*(19), e2021GL094366. https://doi.org/10.1029/2021GL094366

Zhao, S., Jin, F. F., Stuecker, M. F., Thompson, P. R., Kug, J. S., McPhaden, M. J., et al. (2024). Explainable El Niño predictability from climate mode interactions. *Nature*, *630*(8018), 891–898. https://doi.org/10.1038/s41586-024-07534-6

Zheng, X. T., Xie, S. P., Lv, L. H., & Zhou, Z. Q. (2016). Intermodel uncertainty in ENSO amplitude change tied to Pacific Ocean warming pattern. *Journal of Climate*, *29*(20), 7265–7279. https://doi.org/10.1175/jcli-d-16-0039.1

Zuo, H., Balmaseda, M. A., Tietsche, S., Mogensen, K., & Mayer, M. (2019). The ECMWF operational ensemble reanalysis–analysis system for ocean and sea ice: A description of the system and assessment [Dataset]. *Ocean Science*, *15*(3), 779–808. https://doi.org/10.24381/cds.67e8eeb7